

Technische Hochschule Deggendorf

Hochschule für angewandte Wissenschaften

Fakultät Angewandte Naturwissenschaften und Wirtschaftsingenieurwesen

Studiengang: Master of Mechatronic and Cyber-Physical Systems

**Entwicklung einer mechanischen Antriebseinheit am Kniegelenk
mit Gelenkviereck-kinematik**

**Development of a belt-driven knee exoskeleton with four bar
mechanism actuation**

Betreut von

Peter Landstorfer, M.Sc
THD - Technologie Campus Cham

Wiss. Mitarbeiter

Peter Landstorfer, M.Sc
THD - Technologie Campus Cham

Vorgelegt von

Chandra Yuvesh, Aubeeluck
00811273,
Cham

Prüfer

Peter Landstorfer, M.Sc
THD - Technologie Campus Cham

Eingereicht am

Cham, 01.11.2021

EHRENWÖRTLICHE ERKLÄRUNG

Name des Studierenden: Chandra Yuvesh Aubeeluck

Name des Betreuers: Peter Landstorfer

Thema der Arbeit:

Entwicklung einer mechanischen Antriebseinheit am Kniegelenk
mit Gelenkviereck-kinematik

1. Ich erkläre hiermit, dass ich die Bachelorarbeit selbstständig verfasst, noch nicht anderweitig für Prüfungszwecke vorgelegt, keine anderen als die angegebenen Quellen oder Hilfsmittel benutzt sowie wörtliche und sinngemäße Zitate als solche gekennzeichnet habe.

Deggendorf, den 01.11.2021 Unterschrift des Studierenden: 

2. Ich bin damit einverstanden, dass die von mir angefertigte Arbeit über die Bibliothek der Hochschule einer breiteren Öffentlichkeit zugänglich gemacht wird.

Ja Nein

Deggendorf, den 01.11.2021 Unterschrift des Studierenden: 

Ich erkläre und stehe dafür ein, dass ich alleiniger Inhaber aller Rechte an der Bachelorarbeit, einschließlich des Verfügungsrrechts über Vorlagen an beigefügten Abbildungen, Plänen o.ä., bin und durch deren öffentliche Zugänglichmachung weder Rechte und Ansprüche Dritter noch gesetzliche Bestimmungen verletzt werden.

Bei Einverständnis des Verfassers mit einer Zugänglichmachung der Bachelorarbeit vom Betreuer auszufüllen:

3. Eine Aufnahme eines Exemplars der Bachelorarbeit in den Bestand der Bibliothek und die Ausleihe des Exemplars wird

befürwortet nicht befürwortet

Ort, Datum
Cham, 01.11.2021 Unterschrift des Studierenden: 

Acknowledgements

Throughout the process of writing my Master Thesis, I have received a lot of support and assistance.

First and foremost, I would like to thank my supervisor, Mr. Peter Landstorfer, whose knowledge and expertise during the course of the project played an important role in the development of my prototype. His guidance at every step of the thesis sparked ingenious ideas in my mind which can be seen in the outcome of my work.

I would also like to thank the staff at the Technologie Campus Cham, who ensured that I complete my task within the time frame that I had set. More specifically, I would like to thank Claudia, Christina and Thomas, the supervisors of the project and my professors.

The project and my thesis would not have been complete without the collaboration of the brilliant team working together on the knee exoskeleton. For this I am grateful for and proud of the work that my fellow team members have accomplished.

Last but not least, my immense gratitude goes to my family and friends. More specifically my parents who taught me the proper balance persevering and also enjoying what I do, my brother and sister who will never stop believing in me, and Ella for her relentless and everlasting support.

Overview

This master thesis was written as part of a project led by the Technische Hochschule Deggendorf. The aim of the project was to create an exoskeleton for the lower-limb support, with the focus being on the knee. Different campuses were involved, each having a specific role for the completion of the project. The Technologie Campus Cham was responsible for the development of a first actuator model and the interface between the actuator, the control unit and subsequently the sensing element.

The Technologie Campus Hütthurm was responsible for the development of the prosthetic frame, the backplate to hold the components as well as the hip support. Furthermore, the campus had for aim to develop a multibody simulation for the analysis of the lower-limb active exoskeleton. The first phase of the project was to create the basis of the actuator, together with the supporting exoskeleton frame which was successfully achieved through the coordinated collaboration of all the campuses.

Abstract

The aim of this master thesis was to select an appropriate actuating method to create an active knee exoskeleton for the purpose of rehabilitation. Research was conducted to analyze the state-of-the-art actuators for exoskeleton systems. Furthermore, the knee joint was analyzed to learn more about the improvements which could be brought about in newer knee exoskeletons. The actuating element chosen was a brushless DC motor (BLDC) which was powered by a Lithium Polymer battery to make the system portable. BLDC's provide higher power to weight ratio, as in this case a 369g motor which could provide 2 Nm of torque and 1550 W of power. To increase the torque and reduce the speed, a belt-and-pulley system with a High Torque Drive (HTD) profile was used and a ratio of 1:27 was achieved, using two consecutive belt and pulley sets. Owing to the limits in the tensile forces of the belt, the projected peak torque of 54 Nm was reduced to 36.3 Nm. As for the biomechanics, research showed that the knee rotation is not about a monocentric joint. Anatomically, the ACL (Anterior Cruciate Ligament) and PCL (Posterior Cruciate ligament) influence the rotation of the knee since they form a crossed four-bar-linkage inside the knee joint which connects the thigh and shank parts of the lower-limbs. Hence, a four-bar-linkage mechanism was designed to match the knee rotation. The lengths of the ACL and PCL chosen were 35.5 mm and 46.15 mm respectively. A smooth rotation profile was obtained which was comfortable, despite the torque variations due to the four-bar-linkage. The actuator torque is about 60% of the peak torque at 0° extension of the knee. Thus, an actual peak torque of 21.78 Nm was achieved by the actuator, which satisfies the up to 60% assistance to the torque requirement of 36 Nm knee torque during slow walking and up to 30% assistance for the 71 Nm of knee torque required during stair climbing. With an unpowered motor, the detent torque was low enough to allow backdrivability. The parts for the actuator case were designed using Autodesk AutoCAD and Inventor and were made with additive manufacturing using SLS (PA 2200) and MJF (PA 12) which resulted in an aesthetic and form-fitting model which adapts well to the wearer's leg and knee.

Contents

Acknowledgements	ii
Overview	iii
Abstract	iii
1 Introduction	1
1.1 Motivation	1
1.2 Research question.....	2
2 Literature Review	2
2.1 Actuators	2
2.1.1 Rotary Motion.....	3
2.1.2 Linear Motion	5
2.1.3 Other actuating principles	6
2.2 Actuator comparison	7
2.3 Human biomechanics	9
2.3.1 Kinematic design of the human body and exoskeleton	9
2.3.2 Average human height ratios	13
2.3.3 Speed, power, and torque of the knee	14
2.3.4 Summary of the peak static/dynamic knee torques.....	17
2.3.5 Dynamic properties of the knee	17
3 Conceptual Design.....	17
3.1 Requirements for the knee-exoskeleton	17
3.1.1 User operation requirements	18
3.1.2 Kinematic and kinetic requirements:	18
3.1.3 Technical requirements	19
3.2 Conceptual design steps	19
3.2.1 Non-linear alignment of the femur and tibia (thigh and shank).....	19
3.2.2 Roll and slide motion of the knee	20
3.2.3 Compliant actuator.....	21
3.2.4 Motor controller system.....	22
3.2.5 Feedback and control system	22
3.3 Chosen concept	23

4	Detailed Design	24
4.1	Mechanical Design.....	25
4.1.1	Motor selection	25
4.1.2	Servo Motors.....	25
4.1.3	Stepper Motors.....	26
4.1.4	Outrunner brushless DC Motors	26
4.2	Parameters and selection of outrunner brushless DC motors.....	27
4.3	Speed reduction	29
4.3.1	Detailed speed reduction calculations.....	32
4.3.2	Required torques	42
4.4	Four bar mechanism force calculation	49
4.4.2	Freudenstein's Equations for the variation in angle	55
4.5	Actuator Case	57
4.6	Electrical and Electronics Design	63
4.6.1	Electrical schematic	63
4.6.2	Power requirements	64
4.6.3	Microcontroller	65
4.6.4	Bourns ACE Absolute Encoder and AS5048A Angle sensor	66
4.6.5	ODrive Controller	67
4.6.6	AMT102-V CUI Motor encoder.....	68
4.7	Software Design	69
4.7.1	ODrive parameter setup	69
4.7.2	ODrive Motor tuning	71
4.7.3	Arduino Coding	71
4.8	Overall final actuator.....	75
5	Implementation, Testing and Evaluation.....	76
5.1	Implementation and testing	76
5.1.1	List of components.....	76
5.1.2	Knee model	78
5.1.3	ODrive and Arduino setup	78
5.1.4	Layer based actuator	79

5.1.5	ODrive and actuator testing	82
5.1.6	Inclined closed actuator	88
5.2	Evaluation.....	97
5.2.1	Angular displacement range	97
5.2.2	Peak torque range.....	97
5.2.3	Peak angular speed.....	98
5.2.4	Maximum weight.....	98
5.2.5	Overall actuator.....	99
6	Conclusion and further works.....	100
7	Bibliography	i
8	Appendix	v
	Appendix I - List of Figures and Tables	v
	Appendix II - List of Abbreviations.....	viii
	Appendix III - Detailed comparison of available actuating methods.....	ix
	Appendix IV - Comparison between different BLDC Motors.....	xi
	Appendix V - Electrical Connection Schematic	xii
	Appendix VI - Exploded View of final prototype model	xiii

Nomenclature:

Formula Symbol	Unit	Description
W	kg force or N	Weight
l	m or mm	Length
T	Nm or Nm/kg	Torque
P	W or W/kg	Power
ω	rad/s	Angular speed
K_v	rpm/V	Motor speed constant
K_T	Nm/A	Motor torque constant
d_n	mm	Pulley 'n' diameter
l_{bn}	mm	Belt 'n' length
C_n	mm	Centre distance
N	-	Pulley ratio
z_n	-	Number of teeth in pulley 'n'
F_n	N	Force acting at point 'n'
α	rad/s ²	Angular acceleration
SF	-	Safety Factor
I	kg m ²	Moment of Inertia

1 Introduction

Exoskeletons have been present since the 1960's and the primary use was solely for the military due to their bulky design. Since then, there has been a multitude of improvements which allowed their use to be extended to the general public. Besides the military, exoskeletons are still however limited to a small number of people such as people doing repetitive menial jobs in assembly lines. This serves the purpose of alleviating the pain from the consistent muscle strain that their bodies are subjected to. Furthermore, they also assist in heavy load lifting which could not be possible without, or in rehabilitating motions such as after a broken bone or torn ligament in the arms. [1]

They are further subdivided into active or passive exoskeletons which provide assistance while powered and unpowered respectively. An exoskeleton aids a person in his/her mobility and is present as an outer shell outside of the body, which assists a certain body part, by reinforcing, augmenting, or rehabilitating the strength of that body part. To achieve this, an actuation method is primordial in active exoskeletons. Actuation is simply described as the physical motion that is generated from energy conversion. Electromechanical, pneumatics and hydraulics are some examples of actuation means, in comparison to the human body, which utilizes muscles that contract and relax so as to provide force and thus, motion. An actuator in an exoskeleton is constantly assisting that muscular contraction and relaxation, at the body joints, which can effectively be measured to know the extent of force that has to be applied.

With the advent of additive manufacturing, wearable technologies follow the F3 framework (form, fit, function) to a better extent, as it allows complex designs to be created which will match the wearer's specifications. With 3D scanners, the form of the body can be copied, however, to precisely replicate the inner elements, such as the bones and muscles is a challenging matter. These data can be obtained from anatomical studies and in the recent decades, both prosthetic and orthotic devices are adapting to the inner mechanics of the human body.

The knee, being a major load bearing joint in the body, is highly susceptible to a variety of ailments that render it weak which can result in its failure. Thus, this thesis focuses on the rehabilitation of the human knee by the means of an active exoskeleton which is created by additive manufacturing, and which is driven by a compliant actuating mechanism.

1.1 Motivation

The one degree of freedom of the human knee joint does not consist of a monocentric joint type, but of a polycentric joint type. This polycentric rotation can be broken down into two distinct motions, namely a roll and a slide of the femur when the knee undergoes extension. With a conventional one-axis joint, the same roll and slide motions cannot be replicated, although the knee itself is a one-axis hinge joint. For this purpose, conventional knee exoskeletons require an additional linear variable element to cope with the discomfort that this might bring to the wearer. This will make wearing and using exoskeletons less painful as the knee is allowed to heal.

Motors alone cannot provide high enough torques to assist the knee in an exoskeleton. As a result, speed reduction is required and depending on the motor used, higher speed reduction ratios might be required. Worm gears, planetary gears setup and harmonic drives provide high speed reduction, however, they lack backdrivability. The latter is important as the exoskeleton becomes more compliant, such that the application of force is tolerated from both the machine's side, and the user's side. This makes the exoskeleton more suitable for rehabilitation purposes [13].

1.2 Research question

What improvements, such as a mechanism or specific material or form, can be implemented in a conventional knee exoskeleton to increase its acceptability and compliance in users, particularly for the purpose of rehabilitation?

2 Literature Review

2.1 Actuators

Before an appropriate actuator can be selected, the different actuation methods are laid out based on the latest state-of-the-art machines or research papers. For this purpose, research is to be conducted to analyze the existing models of exoskeletons. While the project itself is concerned with the knee, all actuation principles are considered which are derived from exoskeletons acting at various parts of the body. A systematic approach is required to compare and analyze the actuators.

As a brief summary, the schematic in Figure 2.1 shows all the available actuators which are classified in terms of their driving mechanism.

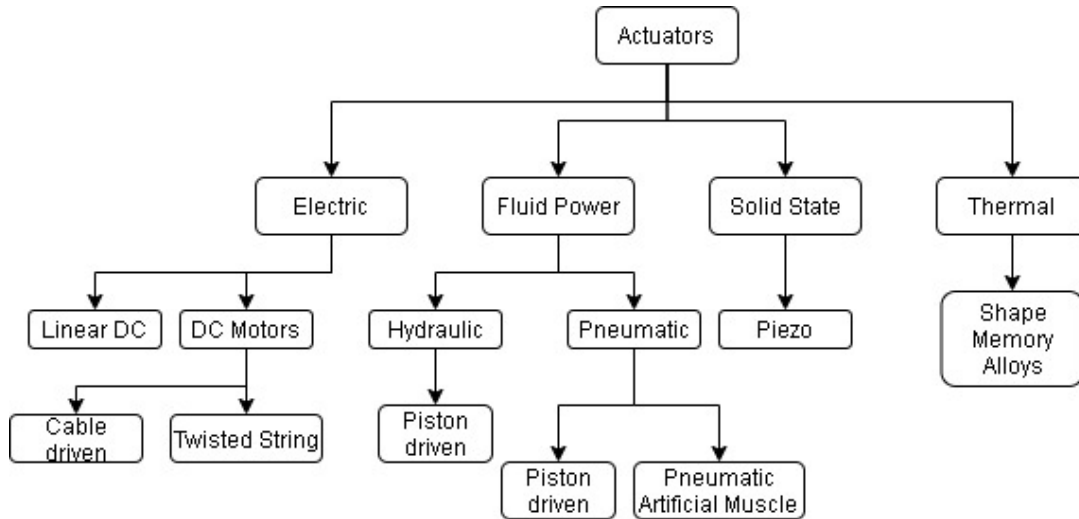


Figure 2.1: Classification of Actuators

A comparison for each was carried out to showcase their actuation principle and energy conversion. For this, two different motions: rotary and linear motion mechanisms are considered in

exoskeletons. Other motions which do not conform with rotation or linear movement are described afterwards.

2.1.1 Rotary Motion

Rotary actuators provide a torque directly at the human joint which requires assistance.

2.1.1.1 Electromagnetic Actuators

This comprises most DC Motors and stepper motors that provide angular motion. DC Motors can be also classified into brushless and brushed DC Motors. EC (Electronically Commutated) motors work with the similar principle to AC motors. Servo motors used servomechanism for closed-loop control. Stepper Motors form part of a special classification of brushless DC Motors, and they provide angular motion in steps. The input quantity is electrical power.

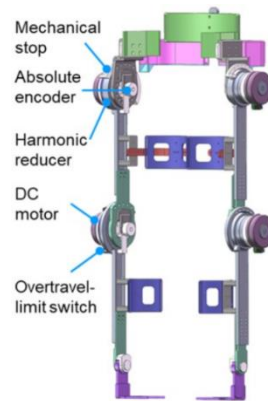


Figure 2.2: DC Motor powered lower limb exoskeleton with Harmonic Reducer [2]

2.1.1.2 Fluid power rotary actuators

These consist of mechanisms such as the vane mechanism and cylinders which follow a circular or curved extension. Further examples are geared pistons, such as one fitted with a rack and pinion or a double acting cylinder which drives a pulley.

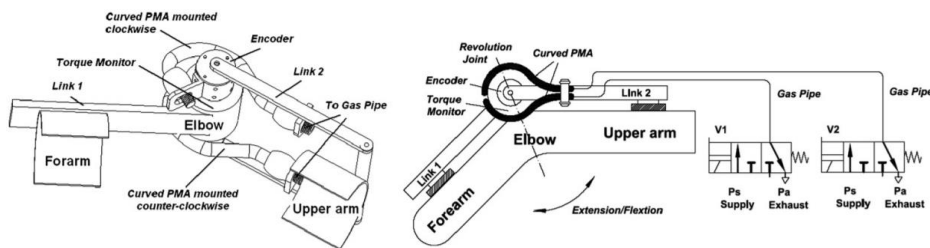


Figure 2.3: Fluid power actuator with curved cylinder [4]

In Figure 2.3, the two pneumatic cylinders, being curved, allow for a better two directional control of the forearm which is connected as the piston of the pneumatic system [4]. Since air is compressible, it provides damping and a slightly elastic behaviour of the joint.



Figure 2.4: Fluid power linear to rotation motion [5]

Figure 2.4 illustrates a pneumatic-driven pulley mechanism for a lower limb exoskeleton. A total flexion of 60 degrees is possible with this setup with a stroke length of 40mm. The pressure supplied is variable from 0.5 to 10 bar, which makes the speed and torque variable as well. Peak torque is stated to be at 25 Nm, with a maximum velocity of 10 rad/s (or 573 degrees/s). This setup is comparable with the belt-and-pulley driven system due to its compliance, with the difference being the input is a linear motion which is converted to a rotary motion [5].

2.1.1.3 Bowden cable or belt-drive system

A Bowden cable driven actuator operates by applying tension on a particular point through a cable that is rotating about a pulley mechanism at the motor axis. The rotary motion of the motor is transmitted via tensile force in the Bowden cable to the actuating point. The Bowden cable can be replaced by a belt-drive system and would operate in the same principle, with higher power transmission capability and higher precision. The advantage is that the wearer can rotate or backdrive the motor due to the lower back drivable torque required.

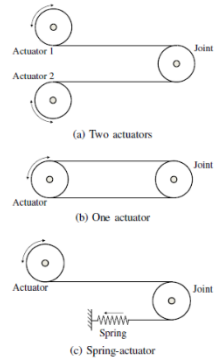


Figure 2.5: Principles of rotation of belt and Bowden cable [9]

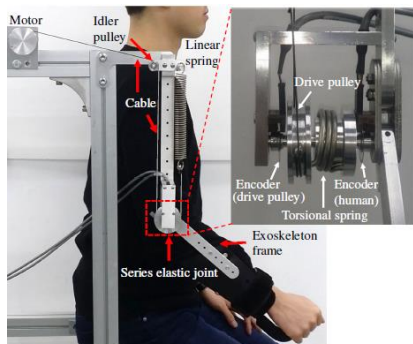


Figure 2.6: Bowden Cable upper-limb actuator setup [9]

Usually a combination of spring-return force is required for a cable driven actuator, where only one motor is used. In a mechanism with two pulleys, a belt can be used instead of a cable. To increase compliance, and shock tolerance, SEA's (Series Elastic Actuators) are used. Springs replace the cables in this case [9]. This is demonstrated in Figure 2.5. A belt has the same effect as an elastic element.



Figure 2.7: Belt driven knee exoskeleton

Figure 2.7 shows a belt driven system which consists of belts and toothed pulleys to efficiently transmit a peak torque of 16 Nm, which is stated to be 40% of the wearer's requirement. With lightweight pulleys, this type of torque increase mechanism also eliminates shear forces which are present with gears or harmonic reducers, as well as reduces the effects of inertia. They are more lightweight. One downside is the relative reduced torque output due to the force limit on the belt [28].

2.1.2 Linear Motion

In linear actuators, the torque around the joint is applied indirectly as a force parallel to the limb connected to the joint. A free-spinning joint is used to create the rotary motion.

2.1.2.1 Fluid power pistons

This is achieved via a common piston that is driven by fluid pressure inside a cylinder. Both pneumatic and hydraulic pistons are available, with different source requirements: for pneumatic systems, pressurized air is required which can be provided by a compressor or stored in an air receiver. As for a hydraulic system, a pump provides the required pressure through a viscous fluid, such as oil. An oil reservoir stores the oil. An additional linkage is required to apply the force directly to the limb, which results in an indirect torque in the joints.

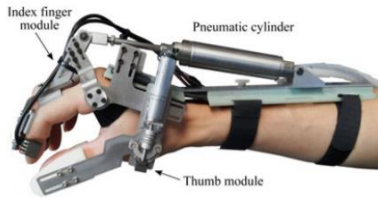


Figure 2.8: Pneumatic pistons for articulate hand motions [6]

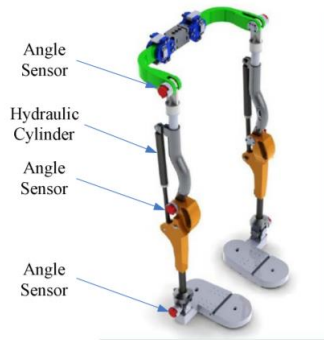


Figure 2.9: Hydraulic pistons for lower limb knee actuation [7]

In Figure 2.8, pneumatic cylinders use a compressible fluid such as air which allows for an elastic actuator. They are best suited for finer applications such as a wrist-finger exoskeleton or low torque applications for portable systems due to an air tank requirement [6].

Hydraulic systems are usually combined with servo valve control such as this example for a lower limb exoskeleton [3]. Another hydraulic lower limb exoskeleton uses a compact onboard hydraulic power unit to make it portable [8]. The weight of a hydraulic supply still stays higher than that of an electric supply, such as a battery. For the linear cylinders, a moment is created by connecting the actuating rod to a free-moving pivot point as shown in Figure 2.9.

2.1.2.2 Pneumatic Artificial Muscles (PAM's)

Pneumatic drive can also be of the force of artificial muscles, referred to as Pneumatic Artificial Muscles (PAM's) or Pneumatic Muscle Actuators (PMA's). By pressurizing and depressurizing a pneumatic bladder, linear extension and contraction is possible. An increase in pressure causes the braided shell to extend laterally and contract longitudinally as shown in Figure 2.10. Rotation of the joint is achieved by means of a pulley and two tensile elements connected to the PAM's.

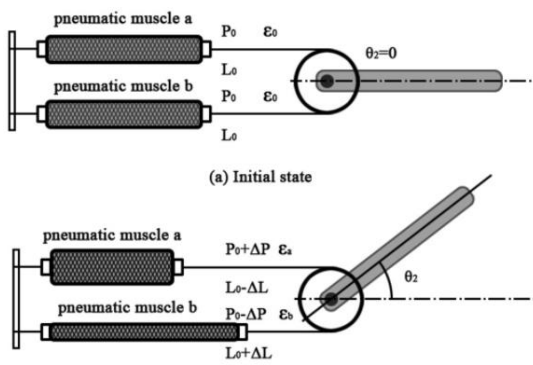


Figure 2.10: Principle of operation of PAM [3]

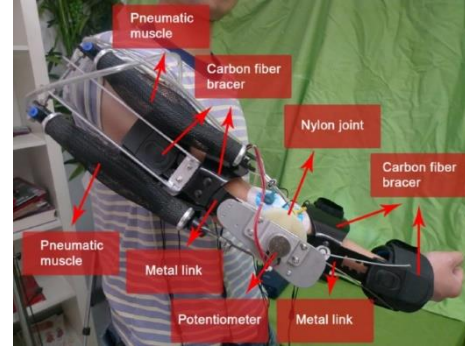


Figure 2.11: Pneumatic Artificial Muscle (PAM) for upper-limb exoskeleton [3]

2.1.2.3 Shape Memory Alloys

They offer a very lightweight solution, given the actuator itself is not bulky and weighs much less. A heating element is required to activate the states. In this paper [11], nitinol wires are used to control a wrist exoskeleton for rehabilitation. It allowed for a range of 40 degrees flexion, which can be covered in about 16 seconds. The only downside is the slow reaction time of the nitinol under load conditions. The device was made with additive manufacturing and the exoskeleton frame is shown in Figure 2.12.

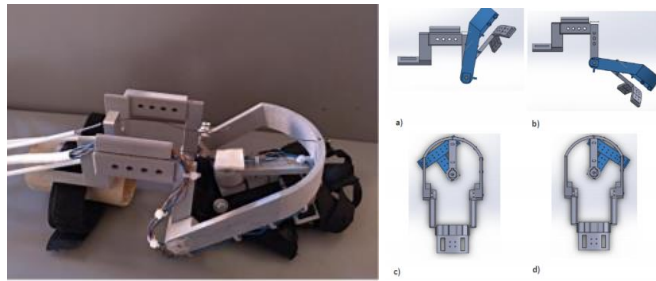


Figure 2.12: Shape Memory Alloy (SMA) for wrist movements [11]

2.1.3 Other actuating principles

There is limited research in exoskeletons for these methods of transmitting power.

- A spherical actuator is a multi DOF actuator, that is the motion is not limited to a single plane. It can be driven by several ways, namely cable, electromagnetic or piezoelectric. This actuation method is most suitable for multi DOF joints such as the hip or the shoulder.
- Mechanisms driven by electromagnetic principles such as cams and gears, as well as screw mechanisms. These rely on a rotary electromagnetic motor or similar rotary actuation to be driven. It can be seen as a simple rotary to linear conversion.
- Moving coil and solenoid actuators which use electromagnetic principles to generate linear motion.
- Piezo electric actuators which use the piezo-electric effect of crystals to provide expansion of the material at high voltages.

2.2 Actuator comparison

A review of the most current and state of the art research and type of actuator used is summarized in the bar-graphs in Figure 2.13 and Figure 2.14. This gives a deeper insight into the frequency of the type actuators which are present in the lower limb exoskeletons. These include upper-limb exoskeleton actuation for shoulder, elbow and wrist combined. The areas of application include motion assistance and medical rehabilitation. For the lower limb exoskeletons, they include hip, knee and ankle-foot exoskeleton support. The numbers were gathered from papers similar to [37].

Upper-limb exoskeletons:

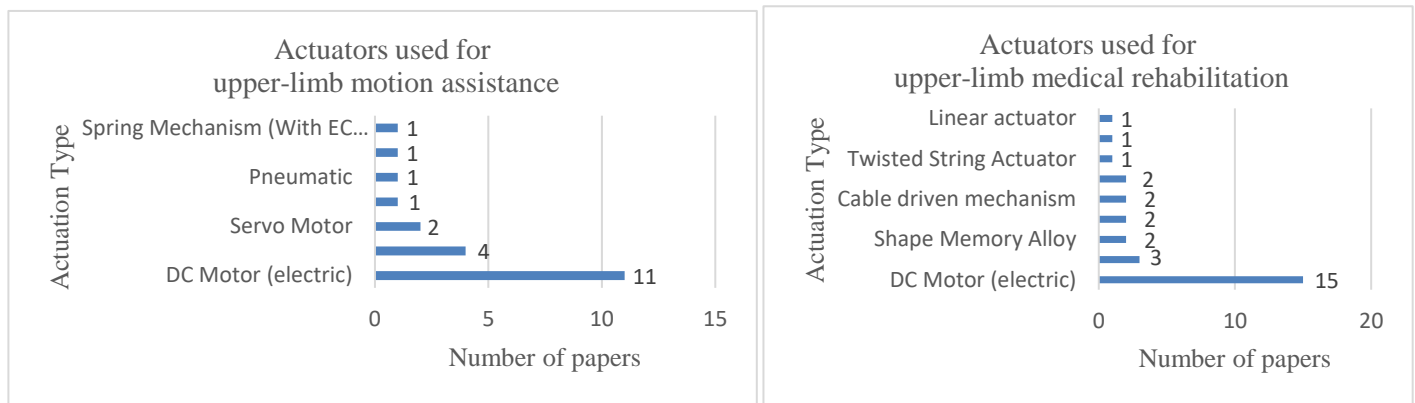


Figure 2.13: Review list of actuators for upper-limb exoskeletons

Lower-limb exoskeletons:

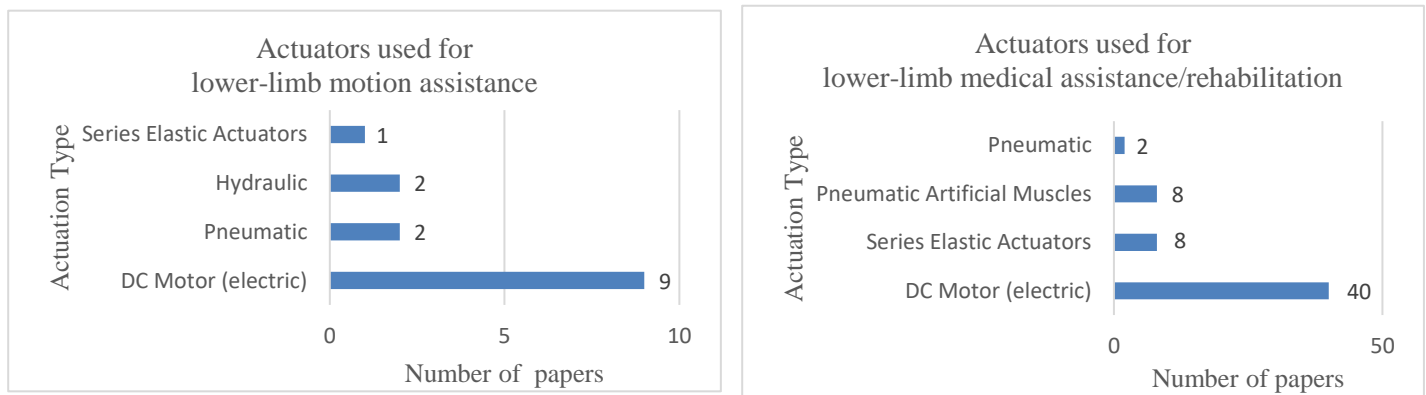


Figure 2.14: Review list of actuators for lower-limb exoskeletons

From the review, in the majority of cases, the actuation type is electric, that is, DC Motor for a successful active and partially passive exoskeleton control. The motors typically used are stepper, servo, brushed and brushless motors.

Each of the actuation type caters specifically for a defined purpose, and, hence, is suitable for that application. Several examples have been shown in Section 2.1. For example, Shape Memory Alloy as an actuator is mostly fit for hand exoskeleton actuation given its lightweight and high strength-

to-weight ratio properties. Additionally, while for rehabilitation purpose, SEA's are much more adapted, DC Motor with harmonic drives can cater for an application for human strength augmentation and low compliance rehabilitation. Certain actuators have not been considered, such as piezo-electric actuator since they do not appear in any of previous full-body existing exoskeleton models.

General properties of the actuators are summarized in Table 2.1.

Actuators	Input Quantity	Mechanical requirements	Source	Control Method
DC Motor	Electricity	gear reduction and gear housing,	Power supply, battery	Motor drivers
Linear actuator	Electricity	pivot points on links		
Pneumatic cylinder	Fluid pressure	Cylinder, pipes, Solenoid valves, air tank, air compressor, pivot points on links	Power supply, Air compressor, air tank	Solenoid valves
Pneumatic artificial muscle (PAM) or McKibben Artificial Muscle	Fluid pressure	PAM (Pneumatic bladder), pipes, Solenoid valves, air tank, air compressor		
Hydraulic cylinder	Fluid pressure	Cylinders, pipes, Solenoid valves, pump, oil reservoir,	Power supply, Pump, oil reservoir	
Cable driven actuator (Bowden cable) or belt-drive system	Electromechanical	Stiff cable, pulley mechanism, possible gear reduction, belts	Power supply, battery	Motor drivers
Series elastic actuator (SEA)	Electromechanical	Elastic element, pulley mechanism, possible gear reduction		
Shape memory alloy (SMA)	Temperature	Nitinol, fixtures	Power supply, battery	Temperature element

Table 2.1: Summary of the general properties of actuators

A detailed comparison of different important properties of the actuators is also summarized in Table 8.1 in Appendix III. The comparison is relative to the actuators and considers the application of a portable lightweight exoskeleton. This entails that a higher power-to-weight ratio is desirable.

The torque requirements for each actuator type varies, and for linear actuators, a performance index chart can be used to compare their maximum stress that they can exert. The human muscle has been included as well. This is included in the details' column. This is a primary comparison to narrow down the list of actuators. The actual selection is based on the performance characteristics of the actuator, such as the torque and speed requirements, with respect to the requirements and design of the system. The data has been gathered from the performance index charts [13, p. 33] and from the papers that have been reviewed.

2.3 Human biomechanics

2.3.1 Kinematic design of the human body and exoskeleton

Prior to the development of an actuator concept, the kinematic design of the exoskeleton is analyzed. Different motions such as flexion and extension are also discussed later in this chapter, as well as the respective degrees of freedom, angular speed, and angular ranges.

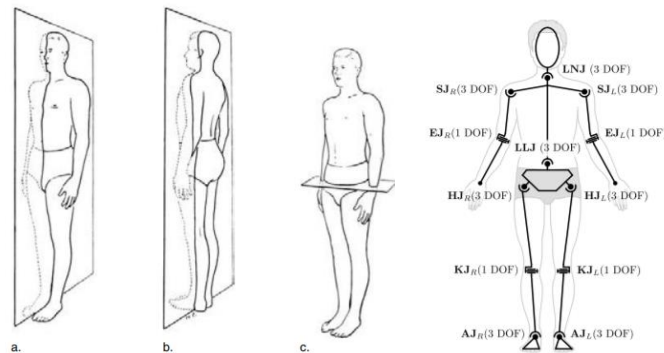


Figure 2.15: Planes of motion in the body: a) Sagittal/median, b) frontal/coronal and c) transverse/horizontal planes [14]

Figure 2.16: Description of the Degrees of Freedom (DoF) in the body [15]

Referring to Figure 2.15 and Figure 2.16, the body can be represented by the specific Degree of Freedom (DoF) at each joint, as well as with the planes. Most important ones include Shoulder (SJ), elbow (EJ), wrist, hip (HJ), knee (KJ), and ankle (AJ). The three planes are: a) sagittal or median, b) frontal or coronal, c) transverse or horizontal planes. For this case, the different possibilities of the hip and knee motion are described.

Hip and knee motions:

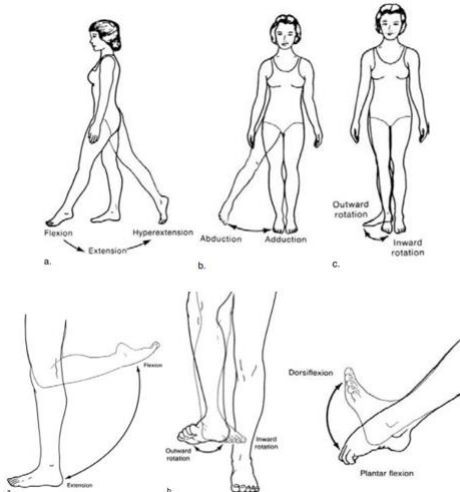


Figure 2.17: Rotation limits of the lower limbs (Hip, Knee and Ankle) [15]

As illustrated in the images in Figure 2.17, in the sagittal plane, there is flexion, extension, circumduction, hyperextension. In the frontal plane, there is abduction and adduction. In the horizontal plane, there is outward/inward rotation and pronation/ supination. The actuator motion directions should correspond to those motions. The focus is laid on the Sagittal or median plane, and on the flexion and extension of the knee.

The extent to which the joints can be moved is summarized in Table 2.2 below. An average was taken from the multiple sources provided. This is due to the fact that different human bodies have different physiologies. The range of motion of the joint starts at 0° to the maximum rotation angle. The data for the range of motion was confirmed by the book ‘Kinesiology: a scientific basis of human motion’ [15].

Joint	Motion	Range of maximum rotation (degrees)	Average(degrees)
Hip	Flexion	100 – 125	116.25
	Hyperextension	10 – 30	20
	Abduction	40 – 45	43.75
	Adduction	10 – 25	18.5
	Inward rotation	35 – 45	41.25
	Outward rotation	45 – 50	46.25
Knee	Flexion	120 - 150	135
Ankle	Plantar flexion	20 – 50	40
	Dorsiflexion	15 – 30	21.25

Table 2.2: Range of limits of motion of the hip, knee and ankle

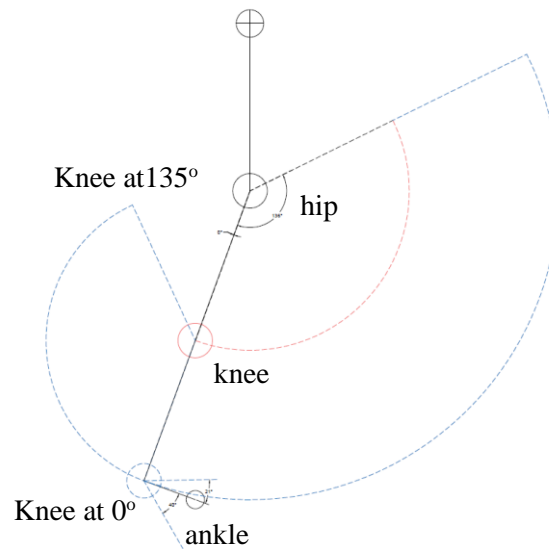


Figure 2.18: Possible positions of the knee

This will set the base for later development of the exoskeleton kinematics and kinetics. Based on the gathered data about the human body, a kinematic diagram can be created which facilitates the description of joints with respect to each other. In addition, the placement or positioning of actuators can be determined this way. Figure 2.19 shows the kinematic model of the human body, from which the kinematic model for the exoskeleton was obtained.

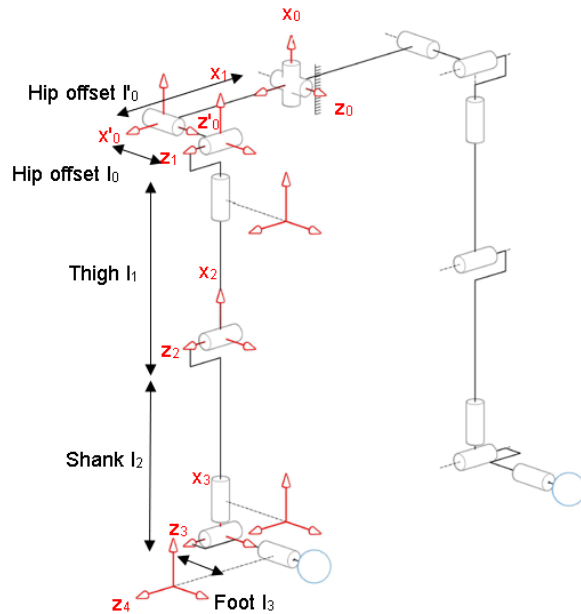


Figure 2.19: Kinematic diagram of the lower limbs showing 1 DoF of the knee

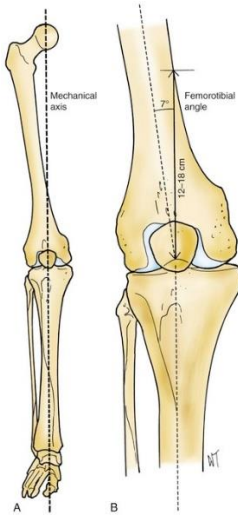


Figure 2.20: Inclination of the femur with respect to the tibia [16]

The knee consists of a single 1 DOF joint which rotates in the sagittal plane (flexion and extension). There is the possibility for a slight adduction (movement towards the interior), however, this is not regarded as an additional DOF for the knee joint, but as an added flexibility feature, as this angle does not exceed 10°. It is involved in the locking mechanism of the knee when standing and when knee is flexed beyond 90°. Additionally, in a standing human, the femur and tibia are not perfectly aligned. There is an angular offset which ranges between 6° to 9°. This is illustrated in Figure 2.20. The axis of rotation of the knee remains horizontal.

The knee moves with a roll and a glide motion. While a similar joint can be created by using the same form of the knee bone parts such as the femoral condyles, the meniscus in the tibia and the patella, there are two other crucial elements which can be realized. These are the cruciate ligaments. These ligaments ensure that the knee rotates along a specific profile and upon analysis of the ligament's attachment points, a four-bar-linkage mechanism can be derived from that setup.

This makes the motion of the actuator match that of the knee joint more appropriately, as the knee is not a simple hinge joint. Figure 2.21 shows the four-bar-linkage in the knee. The arrow indicates the change in the Instantaneous Centre of Rotation (ICR). Figure 2.22 shows the roll and glide motion.

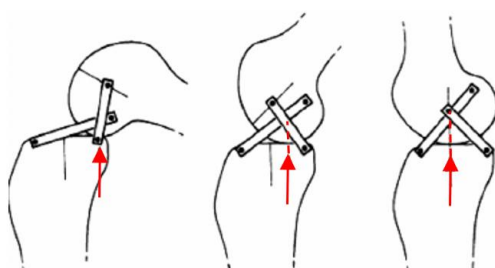


Figure 2.22: Four-bar-linkage in knee

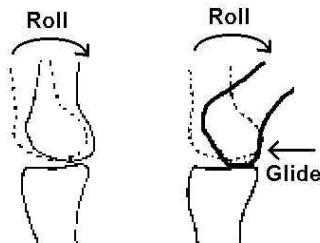


Figure 2.21: Roll and glide motion of the knee

2.3.1.1 Dimension specifications:

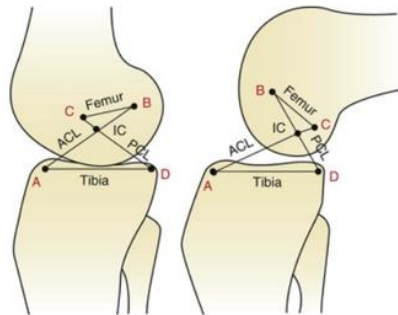


Figure 2.23: ACL and PCL with instantaneous centre of rotation (IC) [29]

Figure 2.23: According to Mitchell [30], the measured lengths of the ACL and the PCL were stated to be

$$\text{ACL: } 32.9 - 42.5 \text{ mm}$$

$$\text{PCL: } 28 - 48.3 \text{ mm}$$

Figure 2.23 shows the links which are ligaments with their respective names ACL (Anterior Cruciate Ligament) and PCL (Posterior Cruciate Ligament). To obtain final design of the four-bar linkage based on the cruciate ligaments, the data in [25] was used. From this, the angular offsets between the links also were obtained. The chosen lengths and angles are later discussed in section 4.3.3.

2.3.2 Average human height ratios

A vital factor to be considered when designing the exoskeletons is the dimensioning. The human body varies greatly and for this reason, the link sizes, as well as the straps around the body should be adjustable. A standard for the body parts ratios were provided by [17] and this is illustrated in the Figure 2.24.

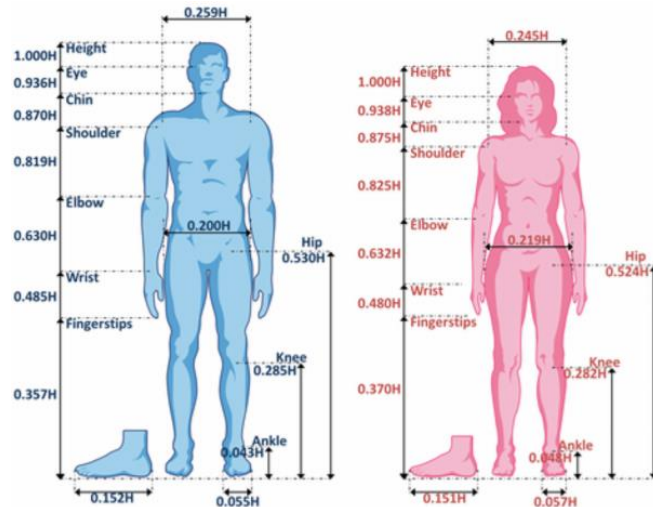


Figure 2.24: Approximate ratio of body parts [17]

For this work, the average heights for Germany have been considered, where the average male height is 175.4 cm, and the average female height is 162.8 cm. Data collected about the human anatomy and physiology will set the base for further development of the exoskeleton kinematics and kinetics.

2.3.3 Speed, power, and torque of the knee

To consider the motions of the knee, the following schematic model is used. The body is viewed in the sagittal/median plane as the 1 DoF motion of the knee occurs in that plane alone. The following motions are considered:

- Static knee flexion
- Sit-to-stand (STS)
- Walking (Gait Analysis)
- Running (Gait Analysis)
- Climbing stairs, uphill motion, jumping and ground impact

2.3.3.1 Static knee flexion

The segmental body weight, and centre of gravity of the human body has been documented in [17] and [35] and can be used to determine an average of the torque values for specific positions of the leg. The centre of gravity was obtained as a percentage of the lengths from the proximal ends, such that for the foot, it is the ankle; for the shank, it is the knee. The following shows the basis for peak static torque calculation for the knee.

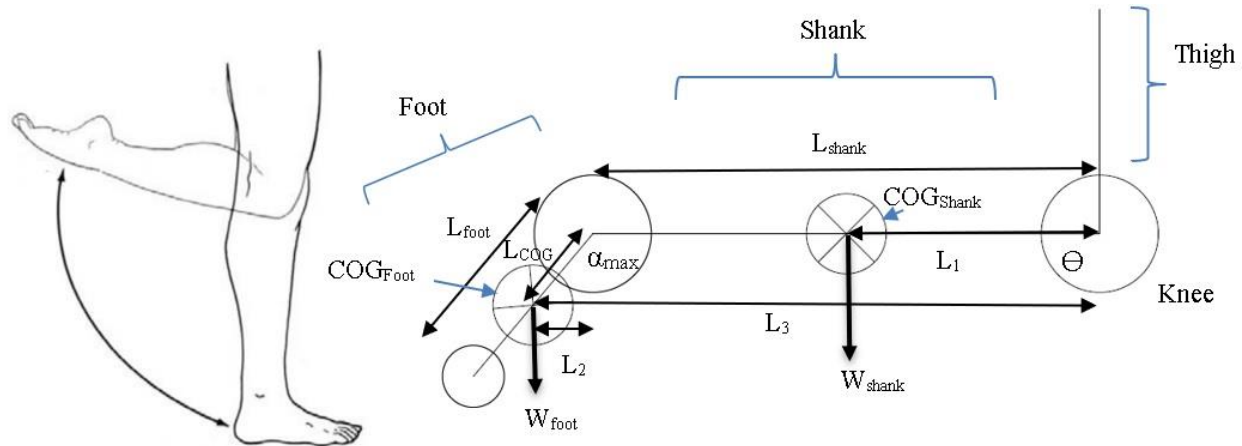


Figure 2.25: Force diagram for static knee flexion torque calculation

For a person standing at a height H , weighing W , and for a flexion of the ankle $\alpha_{\max} = 40^\circ$ and a knee flexion of $\Theta = 90^\circ$, the maximum static torque exerted on the knee joint is calculated as shown:

From [35],

$$\begin{aligned}
 L_{COG} &= 0.42 * L_{foot} [\text{m}] \\
 L_1 &= L_{COGShank} = 0.44 * L_{shank} [\text{m}] \\
 W_{foot} &= 0.0133 * W [\text{kg}] \\
 W_{shank} &= 0.0457 * W [\text{kg}]
 \end{aligned}$$

From [17],

$$\begin{aligned}
 L_{foot} &= 0.15 * H [\text{m}] \\
 L_{shank} &= 0.238 * H [\text{m}] \\
 L_2 &= \sin(40^\circ) * L_{foot} * 0.42 [\text{m}] \\
 L_3 &= L_{shank} + L_2 [\text{m}]
 \end{aligned}$$

The peak static knee torque is

$$T_{knee} = W_{foot} * L_3 + W_{shank} * L_1 [\text{Nm}]$$

For a person weighing 80 kg and with a height of 1.75m:

$$\begin{aligned}
 L_{shank} &= 0.4165 \text{ m} \\
 L_2 &= 0.07 \text{ m} \\
 L_3 &= 0.25387 \text{ m} \\
 T_{knee} &= (9.1331 * 0.4865) + (31.3812 * 0.183) = 10.186 \text{ Nm} \\
 \text{Torque per body weight} &= \frac{10.186 \text{ [Nm]}}{80 \text{ [kg]}} = 0.1273 \text{ Nm/kg}
 \end{aligned}$$

2.3.3.2 Sit-to-stand (STS) motion

From [19], the nominal knee torque required for sit-to-stand motion was determined using a rotary potentiometer, an IMU and multi-body simulation approach. A peak value of 1.34 Nm/kg knee torque was required for the sit-to-stand motion. Previous research has shown that a range of 0.92 to 2.2 Nm/kg knee torque is required, depending on the health of the person and the speed of motion. There was no significant difference between the knee torques for natural speed and fast speed STS motion from the two papers [18] and [19]. Figure 2.26 illustrates the change in knee torque and the respective body motion.

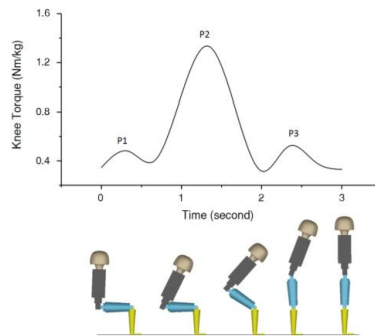


Figure 2.26: Basic Sit-to-Stand motion [19]

2.3.3.3 Gait analysis (Walking and running)

The knee-torque profile was obtained from [22] and [33]. The gait cycle is represented in terms of percentages, which shows the stance phase and the swing phase in Figure 2.27. During the stance phase, the knee torque is maximum as it is used to push the body forward. It generally starts between 0% to 10% and ends at 50% of the walking cycle.

Figure 2.28 shows the result obtained from a test subject walking in the range 0.5 – 2.6 m/s and running in the range of 0.5 – 4 m/s. The darker line represents higher speeds [22, p 4- 5]. The peak knee angular speed was estimated to be in the range of 360 to 400 degrees/s during a gait cycle [41]. The maximum unrestrained knee angular speed is about 680 degrees/s [34] which can occur during the swing phase.

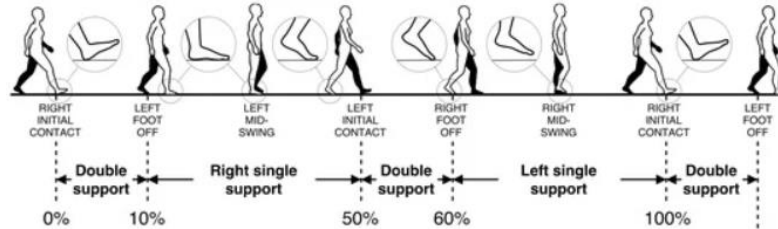


Figure 2.27: Different phases of gait cycle [20]

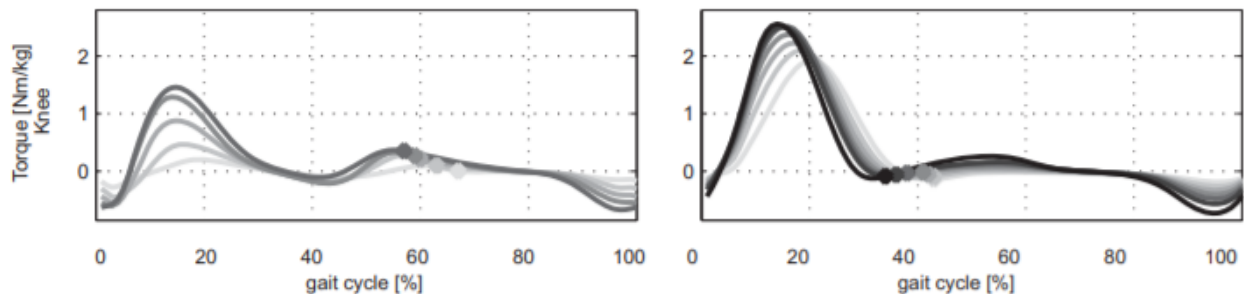


Figure 2.28: Torque requirements per kilogram of body weight for walking and running [22]

2.3.3.4 Ascent/descent on stairs, jumping and ground impact

This takes into account both the torque exerted by the extensor and flexor at the knee, as well as the shock absorbed by the human tissues such as the skin, tendons, ligaments, and the muscle itself. The ground impacts on the knee are present during walking and the higher the speed, the higher the impacted reaction force, to a point where the force exceeds the human biomechanical damping system. Such forces will be reflected in the mechanical actuator system such as gears or belts and must be accounted for. This was discussed in [23]. One possibility is to reduce the number of moving parts and to ensure sturdier connections between moving elements, however since the scope of operation is limited to low-speed rehabilitation purposes, this will not have a great adverse effect on the exoskeleton actuator. The torque requirements for stair-climbing and jumping were obtained from [40].

2.3.4 Summary of the peak static/dynamic knee torques

The weight of an adult male is taken as 80 kg which lies in the 95th percentile based on the data gathered. Torques from different motions mentioned previously are summarized in Table 2.3.

Motion	Phase	Torque per kg of body mass [Nm/kg]	Torque (avg. 80 kg adult)
Knee flexion/extension	Flexion at 90°	0.127	10.2
Sit-to-stand (STS)	Sit to stand position	0.900 – 2.20	72 – 176
Walking (0.5 – 2.6 m/s)	Stance phase	0.450 – 1.50	36 – 120
Running (2.6 – 4 m/s)	Stance phase	1.50 – 2.70	120 – 216
Stair climbing	Ascent	0.890	71.2
	Descent	1.55	124
Vertical Jumping	Push	2.77	221.6

Table 2.3: Summary of the torque requirements for different motions

2.3.5 Dynamic properties of the knee

To determine the torque exerted by the knee, several methods were used such as exoskeletons built specifically for the purpose of measuring the isometric torque at different angles. Isometric torque is caused by the reaction against an external resistance. However, to determine power and acceleration requirements, it is important to know the dynamic properties of the knee. These include the angular speed and dynamic torques.

Using the relation for instantaneous power $P = T * \omega$, the angular velocity of the knee can be determined. For example, the peak knee power per kilogram of body mass during jumping is 10.7 W/kg [40]. Hence, the peak knee angular velocity is $(\frac{10.7}{2.77})$ 3.86 rad/s or 221.2 degrees/s, given that the peak knee torque is 2.77 Nm/kg from Table 2.3.

3 Conceptual Design

3.1 Requirements for the knee-exoskeleton

For the use-case of rehabilitation, assistance or therapeutic exoskeletons, certain requirements are to be met. A general idea can be obtained on how to categorize those modes as stated in this paper [27]. These include passive assistance, active correction, and resistance modes.

Passive assistance: if mobility impairment is at an early stage, the person still has the capacity to move the limbs, hence, the actuator will serve as directing the limb in the proper pathway or a so-called reference trajectory.

Active correction: the person's limb has to be both guided and made sure that the limbs move in the correct path as there can be an error in the calculated trajectory.

Resistance mode: the joints of the patient have to overcome mechanical rotational resistance so as to self-correct the calculated trajectory.

Considering the different kinds of assistance, the following user and operation requirements are set for the prototype. These will be used to choose an appropriate design which includes different sub parts that match the requirements.

3.1.1 User operation requirements

No.	Requirement
1	Ease of use, cost effective, portability, gather feedback data, safe to use
2	Good level of acceptability in terms of comfortability
3	Proper delivery of power from the actuator to the patient's limb
4	Actuation compliant with the knee rotation
5	Actuator is back drivable up to a certain acceptable level
6	Provision of enough torque dependent on the mode of use
7	Making the system portable which will allow displacement of the user within a certain speed limit
8	Control of the actuator with a sensor such that there is dynamic feedback and operation

Table 3.1: Numbered list of requirements for the knee exoskeleton

For rehabilitation modes such as passive assistance and active correction, a lower percentage of the knee torque requirement is provided by the actuator. In resistance mode, a torque equal to or higher than the researched value has to be provided.

3.1.2 Kinematic and kinetic requirements:

The following numerical parameters are to be respected while designing the actuator.

Angular displacement: 0 to 135°

Angular speed: Given that the peak angular speed is in the range 360 to 680 degrees/s, the chosen angular limit was set at 500 degrees/s as it is the peak angular during the swing phase. This value should be modifiable through the controller and is dependent on the walking speed of the user.

Maximum weight of the actuator: Based on the review on lower-limb exoskeletons [37, p.3], the recorded untethered exoskeletons' weights range from 2.7 kg to 5 kg. The knee exoskeleton counts as an additional weight cuffed to the wearer's knee, as discussed in [38]. There is no optimal weight, and the lower the actuator is, the lower is the effects due to inertia during walking. Additional weight also leads to a lower change in the gait cycle. It was thus decided that optimally the actuators should not exceed 2.5 kg combined (left and right knees), excluding the peripheral components which are present on the backplate and at the hip. Considering other parts such as the controllers and the battery, the weight for the whole exoskeleton's actuator should ideally not exceed 5 kg, given that this value is also the upper limit of the additional weight to be considered for torque and power measurements.

Torque: Based on the 95th percentile data for human weight and an additional 5 kg for the exoskeleton weight, the required assistive peak torque values:

Motion	Torque per kg of body mass [Nm/kg]	Torque (85 kg) [Nm]	30% Torque [Nm]
Knee flexion/extension	0.146	10.8	3.25
Sit-to-stand (STS)	0.900 - 2.20	76.5 - 187	23.0 - 56.1
Walking (0.5 – 2.6 m/s)	0.450 - 1.50	38.3 - 127.5	11.5 - 38.3
Running (2.6 – 4 m/s)	1.50 - 2.70	127.5 - 229.5	38.3 - 68.9
Stair climbing	0.890	75.6	22.7
	1.55	131.8	39.5
Vertical Jumping	2.77	235.5	70.6

Table 3.2: Torque requirements based on 30% assistance

Power: Given that the angular speed limit is 500 degs^{-1} and the peak achievable torque that is required is 70.6 Nm from vertical jumping, the upper-limit of the motor power is within 616.4 W.
*(Calculation: $70.6 * 500 * \frac{\pi}{180}$)*

3.1.3 Technical requirements

No.	Parameter	Value	Unit [Symbol]
1	Angular displacement range	0 to 135	degrees [$^{\circ}$]
2	Peak unrestrained angular Speed (swing phase)	500	degrees/s
3	Peak Torque range at 30% assistance	11.5 - 56.1	Nm
4	Peak power at 30% assistance	184.9 - 616.4	W
5	Maximum weight	5	kg
6	Peak angular acceleration (stance - swing)	2000 - 8000	degrees/s ²

Table 3.3: Parameters for the technical requirements of the knee exoskeleton

The peak angular acceleration was taken from [26, p. 11]. This value is coherent with the peak unrestrained knee angular velocity of about 500 degrees/s during the swing phase. The angular acceleration time during walking is determined by observing the gait cycle from Figure 2.26. Considering 20% of the gait cycle, the knee has about 0.2 s from the left mid swing to the right foot off to accelerate to its peak angular speed. The peak acceleration during the stance phase of the walking cycle from the graph can be observed to be about 2000 deg/s². For the swing phase, it is at most 8000 deg/s².

3.2 Conceptual design steps

There are certain specific guidelines or design rules for the selection of the appropriate actuator design. The actuator component is broken down into sub-elements (1A, 1B, 2A, 2B, etc.) and each represent a specific concept which will be combined to form the chosen concept. The concepts were chosen by considering to what extent the related requirements were fulfilled by the particular sub element.

3.2.1 Non-linear alignment of the femur and tibia (thigh and shank)

The tibia and femur are at an angle of 6 to 9 degrees. Additionally, the measured angle taking into consideration additional organs like the muscles amount to 18°. To create a comfortable and

compliant actuator, the axis of rotation should lie on the plane of rotation of the knee which falls in between the two angular offset that exists between the shank and the thigh.

3.2.1.1 Concept 1A: Inclined actuator design

In this concept, the components of the actuator and the axis of rotation do not lie on the same plane. This is achieved by shifting the components or by rotating them along a specific plane.

3.2.1.2 Concept 1B: Hinge design

In this concept, a hinge like mechanism is implemented at the axis of rotation, so the shank can be at any angle with respect to the thigh and the knee itself.

Since the offset angle does not vary, with room for adjustments with padded supports, the concept 1A of using an inclined actuator is used. In addition, a hinge mechanism will require compensation for additional twisting forces which may arise, as well as a misalignment of the rotation axis of the knee.

3.2.2 Roll and slide motion of the knee

The roll and slide motion of the knee which is naturally made possible by the ligaments in the joint can be replicated using the four bar mechanism, as well as a double gear system. This introduces a polycentric joint design. With the monocentric joint, there is a translation as the shift in the rotation axis results in a displacement of the shank link due to the mismatch between the polycentric and monocentric joints. Thus, the polycentric joint is more favorable.

3.2.2.1 Concept 2A: Double pulley or gear design

Two gears whereby each rotates about an eccentric centre are used to simulate the roll and slide movements. This is achieved by having two different sets of varying pitch radii and will thus allow monocentric rotation.

3.2.2.2 Concept 2B: Four-bar-linkage design

Four bars which corresponds to four elements inside the knee are replicated and are described as such in terms of mechanism: the ground, the crank, the follower, and the coupler. Each of those are present inside the knee and have specific dimensions, angular separations as well as ratios which are known. There is an apparent or instantaneous centre of rotation which exists, and this is constantly changing so as to provide the roll and slide motion.

The double-gear with varying pitch radii design provides a compact solution where there is a reliable transmission at all times. However, there is no proper function which can be derived from the knee to obtain the varying pitch radius for each of the gears. Even if the shape of the tibia and femur are replicated, this will require and additional tensioning or spring element to ensure that the two gears are constantly in contact. On the other hand, the known dimensions of the four bar mechanism which is present inside the knee can be scaled up to be fitted inside the actuator component. Thus, concept 2B is chosen.

3.2.3 Compliant actuator

Owing to its lower weight and higher power to mass ratio, a DC motor has been chosen as the most appropriate actuating part. Furthermore, this includes the peripherals such as the power source and the control elements. A DC motor requires a battery and a board controller without any additional relays or valves. The battery as a power source can last for several hours, as opposed to, for example, an air receiver tank for a pneumatic system. [Refer to the Table 2.1 in section 2.2 Actuator Comparison.](#)

DC motors are further divided into brushed and brushless motors. Brushed motors are more compact, have higher power outputs and are easier to control with H-Bridges. However, since a commutator is present for the unidirectional rotation, it is prone to wear and cannot be used without maintenance or replacement for long periods of time. Additionally, there is the tendency of sparks with brushed motors. These problems are not present in brushless DC motors, and they are more efficient both at high and low speeds and create lower levels of noise. They are thus ideal for the use in exoskeletons.

The increased power to weight ratio of brushless DC motors is, however, not adequate enough to provide the required torques. As a result, speed-reduction techniques are required to increase the torque output of the actuator.

3.2.3.1 Concept 3A: Belt and pulley actuation

Pulleys are coupled to the motor shaft, and to the output shaft and belts are used for transmitting the mechanical power, with a set reduction ratio so as to increase the torque and decrease the motor speed. A system with intermediate pulleys allows higher reductions to be achieved, while maintaining backdrivability of the actuator. As for the pulley design, various profiles are available, mainly flat belts, V-belts, ribbed belts, and toothed belts. For this application, toothed belts provide a much higher accuracy and power transmission.

3.2.3.2 Concept 3B: Harmonic drive with clutch

Harmonic drives are compact gear reduction parts which consist of a wave generator coupled to the driving unit or the motor, a flexible toothed spline which is oval in shape and a rigid circular toothed spline. The wave generator causes the flexible spline to displace and touch with the rigid spline, offsetting the rotation one tooth at a time, hence the interaction is to that of a toothed belt and a toothed pulley. The main downside is that harmonic drives are not easily back drivable with a reduced torque from the knee. For this reason, a clutch mechanism could be implemented which disengages the actuation of the motor with that of the output link, hence, allowing the person to also move their leg when the motor is inactive.

There are other gear reduction components such as cycloidal drives or planetary gear boxes, but these are closely similar to the two described concepts, even though the working principles are not precisely the same. Additionally, the described speed reduction mechanisms can be implemented without much experimental tests to improve or eliminate issues such as backlash, mechanical noise

and wear and tear. The number of rotating components as well are to be kept at a minimum to reduce the risk of failures that would happen. As a result, a belt-and-pulley is preferable as it eliminates the use of a clutch system to make the actuator back drivable, while at the same time, it can transmit the increased torque. Thus, concept 3A is chosen.

3.2.4 Motor controller system

Most brushless DC Motor controllers consist of transistors, typically MOSFET bridges, used to control the position and speed of the brushless motor, which usually consist of three phases, thus three wires. Each phase voltage is varied in a sinusoidal waveform. At each step of the motion, one transistor is activated to allow current flow, based on the feedback of the encoder. The motor controller system consists of the motor drivers which monitor the position of the motor and thus, facilitates the motor control in terms of position, velocity, or torque change. It is a crucial element of the actuator part as without the controller, sensor data fed into the microcontroller cannot be used to allow any kind of motion.

3.2.4.1 Concept 4A: Field-Oriented Control (FOC)

In FOC, the motor driver uses the back-emf generated by each phase which is sinusoidal in nature and phased at an angle of 120° apart to determine the position of the motor. This is referred to as sensor-less control. It is generated by the motion of the motor and requires a complex algorithm and a powerful processor. However, since there is no encoder attached to the shaft, and the measurement is made directly from the motor's rotor, there is low noise and high torque efficiency.

3.2.4.2 Concept 4B: Brushless motor controllers

In the conventional controllers, for position control, an encoder is required. However, there are additional sensing elements such as a current sensor which can provide motor torque feedback as well. Similar to FOC, some controllers are equipped with the capability of sensor-less control.

For motor control, it is optimal to have both the position and current control loop present. This depends on the controller being used and thus, the available controllers on the market. FOC provides a good solution, however, it can be complex to program and troubleshoot in case of errors as there are no external encoders. If there is an error for example, where the system cannot determine the position, it might not be able to determine the source of the error easily. It is crucial considering the safety aspect of the exoskeleton actuator that a controller with an external encoder attached to the motor is used. Concept 4B is thus chosen.

3.2.5 Feedback and control system

Feedback is required to monitor the position of the motor. This is present as a loop for DC motors which primarily loops back the position, the derivative of which is the velocity from which the acceleration can be derived. A current sensor allows current feedback, which is proportional to the torque of the motor. Hence, there is more than one method of controlling the brushless DC motor.

3.2.5.1 Concept 5A: Admittance control (Force)

In admittance control, force feedback is used to control the motor. Additional to motor current, which is proportional to the torque, a torque sensing element can be implemented to receive more accurate feedback.

3.2.5.2 Concept 5B: Impedance control (Position)

In impedance control, the position of the actuator is used to control the motor. An angle sensor or an absolute encoder with an accurate enough resolution can be used to provide position feedback.

An optimal concept could include both forms of admittance and impedance control. For the initial test prototype, Concept 5B is chosen.

3.3 Chosen concept

A combination of each sub elements of the actuator component yields the final chosen concept which is summarized in the chart in Figure 3.1.

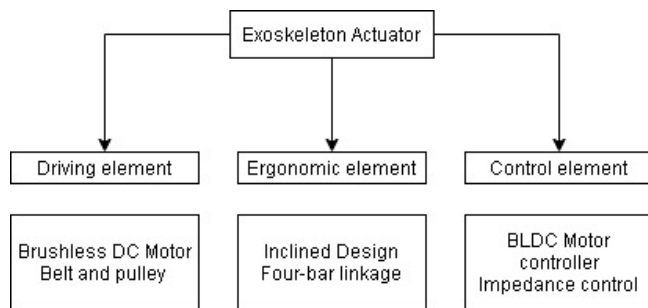
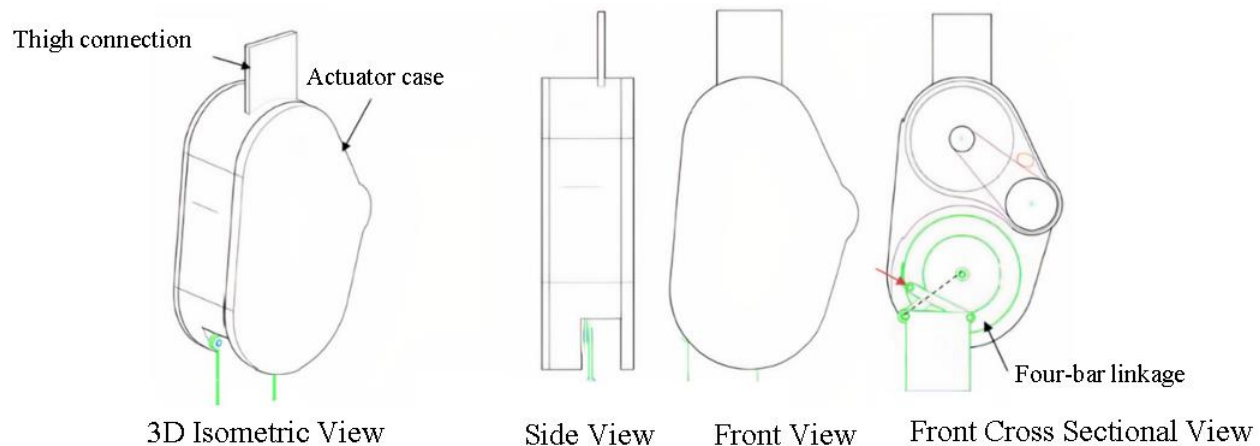


Figure 3.1: Classification of the sub-sections of the knee exoskeleton

The chosen concept is illustrated as a whole element in Figure 3.2.



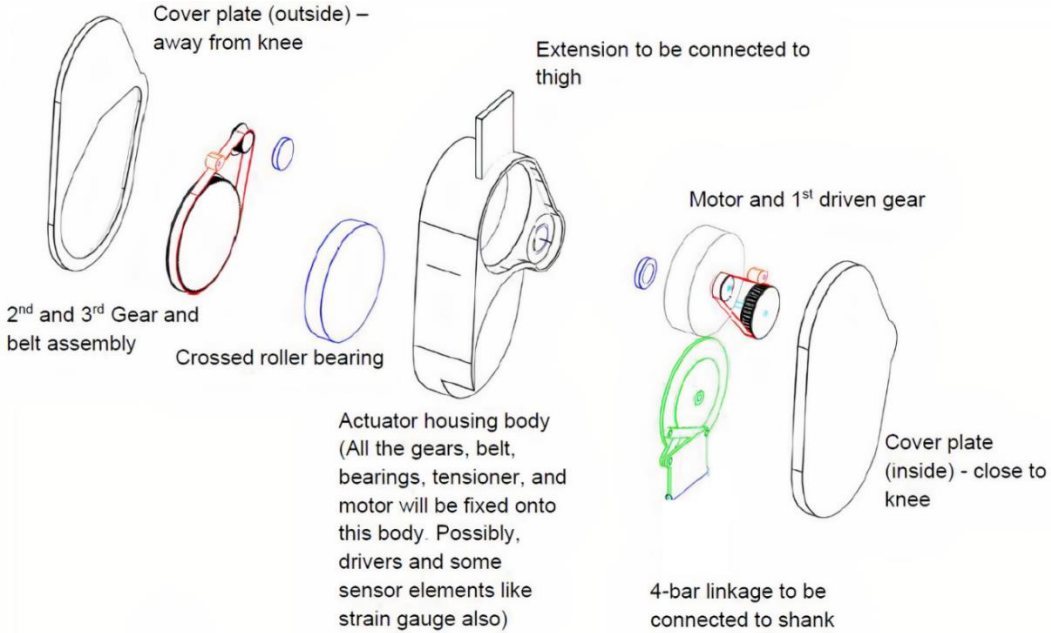


Figure 3.2: Description of the chosen concept of the knee exoskeleton

An initial concept was created with the motor and the actuating output being on the same plane so as to facilitate the testing of the belt and pulley mechanism, and the four bar mechanism. The inclined design, together with the four-bar linkage design were included during the detailed design and implementation phase.

4 Detailed Design

Based on the concept generated so far, it can be concluded that there will be a system of 4 interconnected gears via synchronous belts. The gears' shafts are supported on the main actuator housing using ball bearings. Ideally crossed roller bearing would be used, as it would support the radial load, however this is distributed amongst the different axles or shafts in the system.

Synchronous belts and gears serve the purpose of speed reduction, and also allows backdrivability of the actuator, which makes it more compliant. Furthermore, to properly match the knee motion profile, a four-bar mechanism is used which has a polycentric motion about the knee joint. A brushless DC Motor is used to supply the driving torque, which could be monitored via current sensing or strain gauge sensors. The angle of rotation is measured using an absolute encoder.

With the requirements of the actuator obtained, a more detailed design of the actuator was design. It is broken down into four main topics, namely

- Mechanical Design
- Electrical and Electronics Design
- Software Design

Safety design is included in each section.

4.1 Mechanical Design

This section comprises the mechanical aspect of the actuator which involves the forces acting on the different components, such as the motor torque, frictional forces, and inertia. Additionally, the steps to design the gear reduction are discussed, as well as the four-bar-linkage mechanism.

Mechanical Design is broken down into:

- Motor selection
- Speed reduction
- Four-bar-linkage mechanism
- Actuator case

4.1.1 Motor selection

The main driving unit of the exoskeleton actuator is a brushless DC motor. *Servo motors, stepper motors* and *outrunner-type motors* form part of the brushless DC motor class, and they are commonly used in robotics and exoskeleton applications. There are further classifications of brushless motors such as depending on the number of poles. However, these fall under subcategories of the three main types of brushless DC motors and makes the selection process more focused. Each have their own advantage and characteristics that make them more suited for the knee exoskeleton application as compared to the rest.

The internal build of a brushless DC motor follows the same principle. Brushless DC motors consists of a fixed stator and a rotor which. The stator consists of a energized coil, while the rotor is made up of alternating magnet poles. The number of coils and wires coming out of the motor depends on the type of the motor. This also affects the control strategy, as well as the resolution and parameters such as the torque and power of the motor.

The main focus will be on the disc shape motor (also referred to as *pancake dc motor*) which implies that the diameter of the base is greater than the length of the motor. This fits the form of the actuator better as it does not extend too far from the exoskeleton frame. Additional gearing is not required as well to swap the position of the rotation axes.

4.1.2 Servo Motors

Servo motors operate with an integrated circuit (IC) or a servo drive which drives the position of the motor based on the inbuilt encoder position. They are the easiest to control given that there is a brushless motor which only requires the target command to be controlled. The target command can be a position, velocity, or torque. A multi-turn absolute encoder provides the feedback for the position. Since the servo drive provides a tuned control algorithm, the output has high accuracy and resolution. Generally, servo motors are pre-equipped with a compact and fixed high gear reduction to provide a higher torque. This results in high output power to weight ratios, while maintaining a low noise level.

The downsides of servo motors include the requirement of a servo drive which can support the particular servo motor being used. Consequently, there is a high cost both for the installation and maintenance of the motor and drives. And while servo drives and motors provide a high level of accuracy that may not be required for the knee exoskeleton, the most important part is that the peak torque is only provided at least at 1-2% of the duty cycle, hence, the servo motor is not ideal for sustained overload. This can occur if there is an opposing reaction torque from the wearer's knee. There is also only a limited number of servo motors which are manufactured in a disc-shape that could cater for the torque requirements of the exoskeleton, as generally they are lengthier and have a cuboidal shape. The result is a bulkier and heavier motor design which does not suit the requirements of the knee exoskeleton actuator.

4.1.3 Stepper Motors

The cheapest and most common type of brushless motors is the stepper motor. The most widely used are hybrid stepper motors which have a magnetized rotor and electromagnetically energized stator. The phases are energized such that the motor moves from one step to another, by a combination of each pair of magnetized poles attracting and repelling each other. Additional functions such as half step and micro-stepping allow the motor to move in a smoother way. Stepper motors provide high torques, however at higher speeds, this torque is not efficient enough, causing the motor to overheat as it has to overcome the higher detent torque as well. The downside is that this will not be ideal for a dynamic system which has to operate at both high and low speeds, while maintaining a proper torque and power output. Furthermore, stepper motors are much bulkier than servo motors due to the broader magnets in the rotor.

4.1.4 Outrunner brushless DC Motors

When it comes to disc-shaped or pancake motors, outrunner type brushless motors provide the best solution. They are also referred to as 'external rotor motors'. Most brushless disc DC motors are three-phase, with the rotor consisting of thin neodymium magnets which are usually placed on the surface lining (circumference) of the motor and the stator consisting of coils which are energized to drive the rotor. There is usually a very thin air gap between the coil and the magnet, which is maintained by a high tolerance bearing. A controller is used to excite the respective coils so as to actuate the motor. They are analogous to servo motors, however, in this case, there is the possibility to decide which specific motor, encoder and motor controller to use.

Outrunner Brushless DC Motors are frequently used in quadcopters or electric airplanes and have a specific pole-magnet pole configuration as a means of identifying their capabilities. This also entails that they are lightweight for the application in the knee exoskeleton and can provide a dynamically changing output in terms of torque and rotational speed.

Table 4.1 summarizes the comparison between the three brushless motor types. Remarks are provided to help understand the selection process better.

No.	Motor	Torque	Form	Remark (+/-)
1	Stepper Motor	Moderate to high torque. Flat steppers have lower torque.	Mostly cuboidal.	Motion in steps which require high current. High precision, low top speed, and high holding torque. High noise.
2	Servo Motor	Low to moderate. Bulky industrial servos have higher torques.	Cuboidal and disc shape. Disc shaped servos are high priced.	High precision, low noise, and good repeatability. However, at high torques, not ideal for sustained loads. Expensive and complex installation. Mostly operate in a small speed range.
3	BLDC external rotor motor	Low to moderate. Gearbox required.	Mostly cylindrical and disc shaped.	Good precision, low noise, and good ability to provide smooth motion. Good speed and torque balance. Overheating can be an issue. Requires a proper motor controller.

Table 4.1: Summary and comparison of motor types

4.2 Parameters and selection of outrunner brushless DC motors

Outrunner type brushless motors have the following parameters which allow them to be distinguished from one another:

- **Pole-magnet pole configuration:** higher pole-magnet pole implies higher torque
- **Motor speed constant:** to estimate torque constant and maximum speed
- **Motor torque constant:** to obtain a linear relationship between current and torque
- **Motor peak current:** to estimate peak torque
- **Nominal current:** to estimate nominal torque
- **Nominal voltage:** to estimate nominal speed
- **Peak voltage:** to estimate peak speed
- **Peak power:** to estimate peak torque at high speed (not stall torque)
- **Motor winding resistance:** to estimate heating of motor
- **Nominal torque:** running torque without overheating motor
- **Nominal speed:** running speed at nominal voltage based on pulse width

Research of the available motors on the market was carried out and the outcome is summarized in Table 4.2 below. The peak power, peak current and torque constant are important factors, as well as the weight. Additionally, all the prices are listed based at the time of the research so as to allow a fair comparison. Table 8.2 in Appendix IV provides a more detailed comparison. The available online links are also included.

No.	Motor	Nominal Voltage [V]	Speed Constant Kv [rpm/V]	Torque Constant K _T [Nm/A]	Peak Current [A]	Peak Power [W]	Weight [g]	Price [EUR]	Remark (+/-)
1	Maxon EC 90 Flat	18	118	0.0807	183	260	985	217	Requires Maxon controller and lead time ~ 6 to 14 weeks
2	GARTT ML 8318	22.2 - 44.4	100	0.0955	62	3000	635	179	Unconfirmed manufacturer and lead time ~ 8 weeks
3	T-Motor P60	22.2 - 30	340	0.0308	65	1550	347	75	Compact moderate torque motor, lead time ~ 1 to 3 days
4	T-Motor P80 III	22.2 - 44.4	120	0.0795	70	3600	635	200	Compact high power motor, lead time ~ 2 to 4 weeks

Table 4.2: Comparison of commercially available motors

The three important equations governing DC motors can be used interchangeably to determine the required parameters.

$$Torque T = I_{motor} * K_T [Nm] \quad (4-1)$$

$$Speed \omega = V_{motor} * K_V [rad/s] \quad (4-2)$$

$$Output Power P = T * \omega [W] \quad (4-3)$$

and $Power loss P_{loss} = I^2 * R_{winding} [W] \quad (4-4)$

To drive the brushless DC motor, a motor controller is required. The motor controller in this case should allow position control based on feedback from an encoder, thus, generic Electronic Speed Controllers (ESC's) which are used to control brushless DC motors' speed were not considered. Based on the motor parameters in Table 4.2 above, the controller has to cater for requirements such as the peak current of the motor. Table 4.3 below summarizes the research carried out on available brushless DC motor controllers.

No.	Motor controller	Peak voltage [V]	Peak Current [A]	Price [EUR]	Remark (+/-)
1	ODrive Controller (dual motor control)	24 - 56	120 A (60A per motor)	150	Offers a wide range of built-in control options, including FOC and encoder position control, current sensing and built in PID.
2	Trinamic FOC controller with TMC6200 Development Board	60	100	67	Very good motor controller in given price range. Development board available. No standalone encoder control.

3	Maxon Motor controller	10 - 50	Motor dependent	> 200	Highly motor specific. Position control reserved for industrial applications only.
4	Generic Brushless Motor controller	12 - 36	15 A peak	30	Limited supply current. Ideal for low current motors.

Table 4.3: Comparison of commercially available motor controllers

The selection of the motor based on the listed parameters was done alongside the design of the speed reduction mechanism. This is because, as the motor power increases, the speed reduction ratio decreases, and the opposite holds true as well.

Hence, initially, a suitable speed reduction with belt and pulley design was determined. To perform the initial calculations for the prototype, the T-Motor P60 was chosen. Since the ODrive controller provides both dual motor control and position control, it was chosen over the Trinamic FOC controller.

4.3 Speed reduction

A relation is to be determined between the output torque and the input torque, as well as the output power relative to the input power. In this case, the input torque is provided by the motor and there is the assumption that the input power by the motor is equal to the output power of the actuator. Since from the requirements, the peak required torque for 30% assistance which will both help a person get up and walk at fastest speed of 2.6 m/s was set at 56.1 Nm.

Based on the peak input torque of the motor which is stated to be $\sim 2\text{Nm}$, the ratio required is $\frac{56.1}{2} = 28.05$. Hence, a ratio of 1:28 is desired. With a belt and pulley design, this ratio cannot be achieved without using two consecutive pulley sets, as the difference in pulley diameters will be too high. Additionally, the backdrivability of the system should be assessed.

The principle of speed reduction with a belt and pulley design is rather straight-forward. The basic equation states that the ratio N of speed reduction is

$$N = \frac{d_{n+1}}{d_n} \quad (4-5)$$

Where d_n is the diameter of the n^{th} pulley, starting with $n = 1$.

If there are four consecutive pulleys, with pulleys 2 and 3 on the same shaft, the equation (4-5) then becomes:

$$N = \frac{d_{n+1} * d_{n+3}}{d_n * d_{n+2}} \quad (4-6)$$

The required ratio can be determined by varying the effective diameter of the pulleys and using equation (4-6). An iterative process was carried out to determine the proper ration, which was

achieved using a set of pulleys with the following number of teeth: 20, 90, 15, 90 and a total gear reduction of 1:27.

The final actuator torque $T_{actuator}$ can then be calculated using:

$$T_{actuator} = T_{motor} * N [Nm] \quad (4-7)$$

$$T_{actuator} = 2 * 27 = 54 [Nm]$$

The final actuator rotational speed $\omega_{actuator}$:

$$\omega_{actuator} = \frac{\omega_{motor}}{N} [rad/s] \quad (4-8)$$

For a speed of 2700 rpm (282.74 rad/s) by the T-Motor P60:

$$\omega_{actuator} = \frac{282.74}{27} = 10.47 [rad/s] \sim 600 [deg/s]$$

Assuming no frictional losses, the actuator power $P_{actuator}$:

$$P_{actuator} = P_{motor} = T_{motor} * \omega_{motor} [W]$$

Figure 4.1 describes the belt-and-pulley mechanism schematic, with the initial parameters. The belt length l_b and centre distance C_n selection is discussed later in [Section 4.3.1](#).

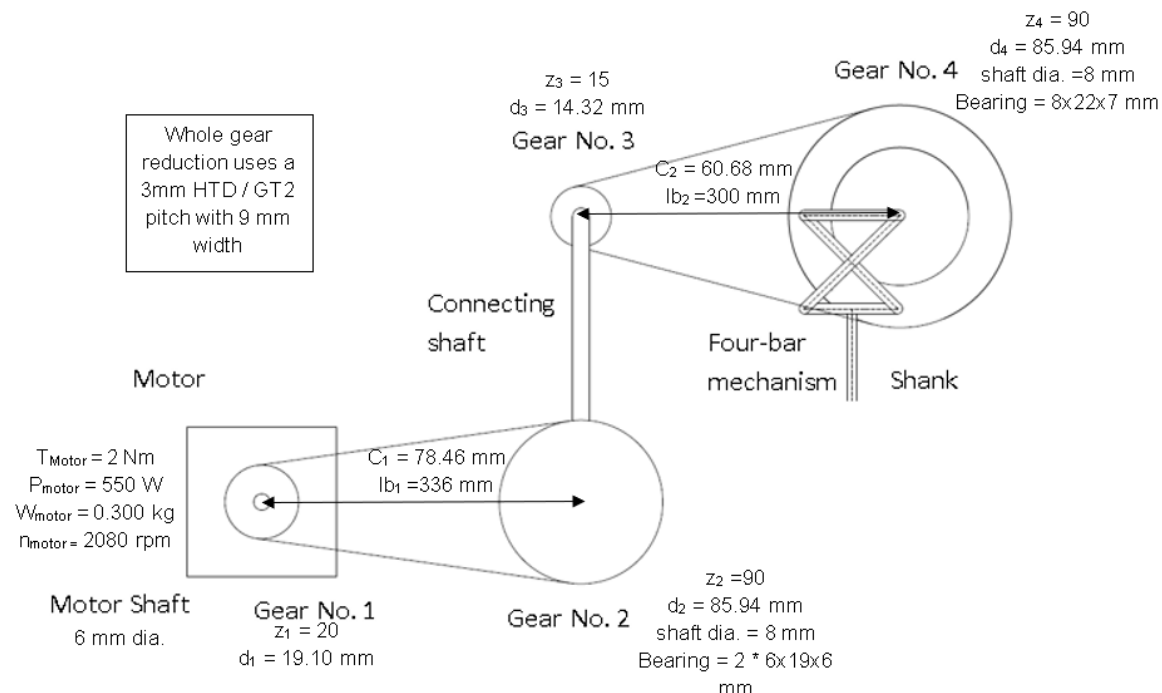


Figure 4.1: Mechanical schematic of the actuator

The peripheral forces in the belts and torques at the shaft are described in Figure 4.2.

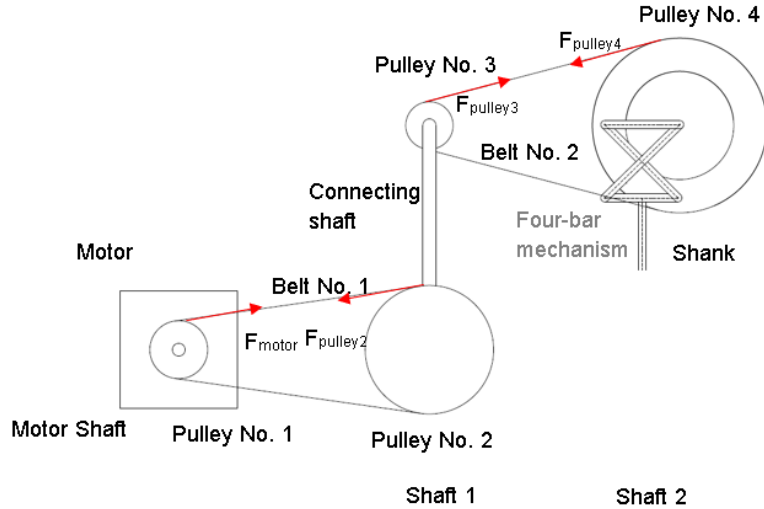


Figure 4.2: Description of belt tensile forces

The peripheral force at each pulley, acting as tensile force on the belt is represented as F_{motor} , $F_{pulley2}$, $F_{pulley3}$ and $F_{pulley4}$, whereby

$$F_{motor} = F_{pulley2} \text{ and}$$

$$F_{pulley3} = F_{pulley4}$$

Given d is in mm, the relation with the torque of the driver pulley is

$$F_{peripheral} = \frac{T_{driver}}{\frac{d_{driver}}{2 * 1000}} [N] \quad (4-9)$$

The belt has to be able to withstand the peripheral force due to the high torques at the last pulley. Consequently, the designed maximum torque output of the actuator has to be adjusted.

The torques inside the actuator can be broken down into:

- T_{motor} : Torque produced by the energized motor
- T_{detent} : Detent torque present in the unenergized motor
- T_{shaft1} : Torque present at shaft 1
- T_{shaft2} : Torque present at shaft 2 (equal to the crank torque (T_{input}) in four-bar-linkage)
- $T_{actuator}$: Torque output from the crank of the four-bar-linkage

An accelerative torque and angular displacement at the motor shaft will result in an accelerative torque and angular displacement at the four-bar mechanism. This is modelled by the rotational inertia of the motor and that of the pulleys, together with the inertia of the shank link.

The above equations (4-7) and (4-8) give a simple relation between the motor and the actuator output, and do not include frictional forces, motor detent torque and effects of the four-bar-linkage on the torque. The set of equations are used to determine the speed reduction that is required based on the selected motor and required assistance from the knee exoskeleton actuator.

Additionally, there are dimensional constraints that are to be applied to the actuator case, hence, the pulleys have an upper-limit in their diameter sizes, and consequently, the belt length also is to be monitored. This is discussed as well in the next subtopic.

4.3.1 Detailed speed reduction calculations

4.3.1.1 Type of belt and pulley

There are different equations to determine specific properties of the belt such as the length based on the centre distance. Initially, known or values that can be set are used. Given there are various types of belt shape profiles, the most suitable one chosen is the HTD (High Torque Drive) belt profile, as it has advantages such as high torque transmission and low vibration and noise. Alternatively, AT series (trapezoidal tooth profile) provide higher backlash control and stronger tension members. In case peripheral force in the belt is too high, AT is more suitable, but it loses precision. For this application, an HTD profile from ‘Maedler’ was chosen.

4.3.1.2 Dimensional and force constraints

Based on the human lower-limb dimensions, the part of the actuator which is connected to the thigh should not exceed 30 cm, and the height from the back of the thigh to the kneecap is about 15 cm, thus the width of the actuator should not exceed that length also.

The proposed dimension of the actuator was achieved as follows:

1. Initially, by setting the diameter upper-limit for the motor and the pulley at 90 mm, and estimating the centre distances, a schematic was obtained. The lower limit of the pulley was set at 10 mm to maximize the speed reduction ratio. The offset angle represents the angle between the vertical alignment of the pulleys and that of the offset position of the pulleys. This was created using AutoCAD program.

The minimum centre distance C between the pulleys was determined using

$$C = \frac{b + \sqrt{b^2 - 32 * (d_2 - d_1)^2}}{16} \quad (4-10)$$

where:

$$b = 4 * l_b - 6.28 * (d_2 + d_1)$$

l_b is the known belt length connecting the two pulleys.

This method was used since the belt length are available only at certain specific lengths and is used as the limiting factor during calculations. Conversely, using an iterative process, the centre distance could be set based on other design dimensional constraints, and the belt length is determined using CAD program. Then the closest available belt length on the market is found, and the centre distance is re-calculated.

The equation to determine the belt length from the centre distance is

$$l_b = 2 * C + 1.57 * (d_2 + d_1) + \frac{(d_2 - d_1)^2}{4 * C} \quad (4-11)$$

This ensures that there is no belt slipping and appropriate teeth meshing, as well as a sufficient arc-of-contact. This is discussed later in subtopic 4.3.1.4.

2. The offset angle was adjusted until a compact design was achieved in which the width of the actuator is close to the required width limit, while leaving enough space for the actuator case thickness. This entails that the length is as minimal as possible.
3. A preliminary actuator case was laid over the components with a general overall thickness of 5 mm. This step was iterated with step 2 so as to obtain an appropriate actuator design.

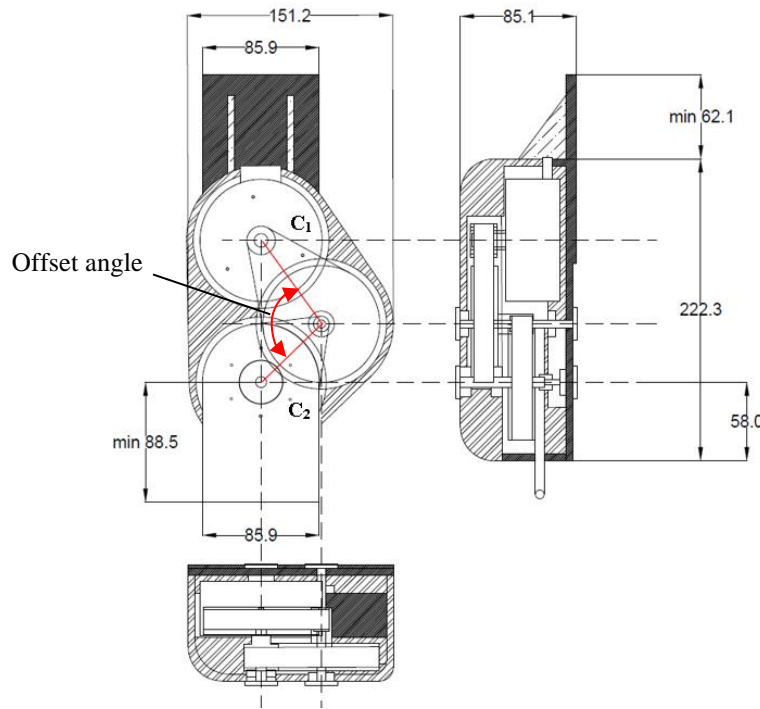


Figure 4.3: Primary dimensions from concept model

Thus, using the upper-limit for the diameter of the pulleys and that of the motor which has been set at 90 mm, and the lower-limit for the pulley diameter which has been set at 10mm, based on the configuration of the pulleys, the CAD model in Figure 4.3 was obtained.

This allows an adequately lengthy centre distance between the small and large pulleys. Ideally, the lower limits of the centre distances were used. The chosen centre distances C_1 and C_2 were 76.1 mm and 61.7 mm respectively.

By using smaller offset angles, the pulleys and the motor are brought closer to each other and results in a more compact design for the actuator. Additionally, if a more powerful motor is used, the speed reduction can be adjusted which would result in a smaller diameter of the larger pulley and this would still lie within the requirements of the actuator dimensions.

As for the height of the actuator, there are two factors that were considered:

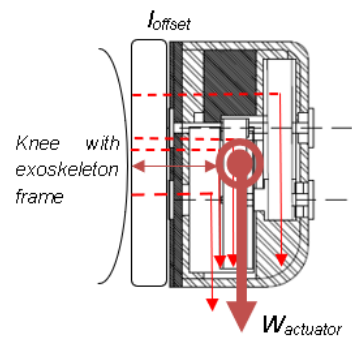
- Allowing enough space for the user to walk through doors and in tight spaces
- Low reaction torques so that it is comfortable when being worn

The minimum clearance varies based on where the person is moving or sitting. Doors usually have an interior width of 800 mm (Germany), and since the average width of a person is about 420 mm (Germany), this would imply that the maximum height of the actuator and the exoskeleton frame should be within 95 mm to allow proper passage through doorways at least. Other situations, such as the leg room available under a desk when the person is sitting could affect the usage.

4.3.1.2.1 Force constraints:

The defining factor for the height is the components such as the motor height and the pulley width. Ideally, a motor with a low height and a pulley with a smaller width would result in an actuator of smaller height.

The further away heavier components are from the exoskeleton support frame, the higher is the reaction moment. This is reflected as a lateral force along the thigh where the wristbands are attached. Thus, the goal is to ensure that all substantially heavy components are placed as closed as possible to the prosthesis, and the leg surface, to keep the moment as low as possible. The centre-of-gravity of each component and that of the actuator are determined by a CAD software. Longitudinally, the forces are resolved and distributed through the hip support.



The total moment about the support due to the centre of mass:

$$M_{actuator} = W_{actuator} * l_{offset}$$

Where $W_{actuator}$ is the effective weight of the actuator at the centre of mass and l_{offset} is the distance of the centre of mass from the exoskeleton frame support.

Figure 4.4: Lateral force due to actuator weight

The total height of the initial design was estimated at 80 mm, excluding the exoskeleton prosthesis. This includes the 5 mm wall thickness of the actuator case. By using a smaller belt width and a motor with a lower height, the average height of the actuator alone has been reduced to 75 mm in the final design.

4.3.1.3 Frictional and resistive forces

For an improved determination of force transmission from the motor to the output link at the shank, the frictional forces are analyzed at the following:

- Motor detent torque
- Bearing frictional forces
- Belt and pulley frictional force
- Pulley inertia

To obtain a standardized method of calculating the resistive forces, the friction torque has been used. The friction torque is the torque resultant from frictional forces about rotating objects. Thus, the effective torque at each rotating axis in the actuator is the resultant torque or in terms of the required torque which are

$$\text{Resultant torque} = \text{required torque} - \text{friction torque}$$

4.3.1.3.1 Motor detent torque:

The detent torque is present when the motor is not energized only, hence it is also referred to as “open-circuit torque” or “cogging torque”. When the actuator is in passive mode, the person wearing the exoskeleton has to do work against the motor detent torque. For brushless DC motors, the detent torque is generally lower as opposed to stepper or servo motors. It is position-dependent and is due to the force needed to break the attraction between the magnet pole and the stator slots. Thus, it is practically not ideal to calculate the detent torque for a BLDC motor with more than 6 pole-pairs unless more coefficients are known [39].

To obtain an estimate of the detent torque, a spring balance or a dynamometer can be used to measure the force when the motor is starting to spin freely. In this case, the detent torque of the T-Motor P60 340 KV was estimated to be

$$T_{\text{detent}} = 0.05 \text{ Nm}$$

4.3.1.3.2 Bearing frictional force:

The friction torque in the bearing and the cylindrical bushes are calculated using the coefficient of friction μ and the known load force. This value is an estimate as the frictional forces depend also on the type and amount of lubricant used. Furthermore, temperature affects the viscosity of the lubricant and hence, the friction. Given the low coefficient of friction, the single friction torques are low. The general equation for the frictional force is

$$F_{bearing} = F_{load} * \mu \quad (4-12)$$

With the pitch diameter known, the resistive torque can be measured as well:

$$T_{bearing/bushing} = \frac{F_{load} * \mu * d_{bearing}}{2} \quad (4-13)$$

Where $d_{bearing}$ is the average pitch diameter of the bearing.

From the '*Maedler.de*' web shop, the coefficient of friction for a deep-groove ball bearing is stated to be 0.0015 and that for a cylindrical slotted bush is at most 0.10 to 0.20. The coefficient of friction between the encoder bushing and the encoder itself is 0.25 to 0.40.

In this case, the F_{load} is the peripheral force acting on the pulley, by the belt tension. At shaft 1 and shaft 2, the load is shared between two bearings. Table 4.4 below summarizes the friction torque in the actuator:

Bearing and bush position	Coefficient of Friction
Motor (19 mm dia.)	0.0015
Motor encoder (15mm dia.)	0.25
Shaft 1 bearing	0.0015
Shaft 2 bearing	0.0015
Shaft 2 slotted bush	0.10

Table 4.4: Coefficients of friction

Coefficient of friction of PA2200 parts with a bearing pressure of 1N/mm² ranges from 0.375 to 0.625 as stated by EOS GmbH.

4.3.1.3.3 Belt and pulley frictional force:

For the belt, the peripheral force is considered. The peripheral force at the driver gear is simply the forces which are resisting the belt motion. The forces have been previously illustrated in Figure 4.2.

In a synchronous gear, the frictional forces at the belt teeth and gear are negligible. Since there is a flange on pulley 1 and pulley 3, the frictional force due to the flanges is determined using the same equation (4-11). However, since there is adequate spacing between the flange and the belt, greater than 1 mm, this value is set to zero.

$$F_{flange} = F_{load} * \mu_{flange} = 0$$

Including an idler pulley to create a jockey belt and pulley design, where the idler pulley acts as a tensioner, will increase the frictional forces due to the idler pulley.

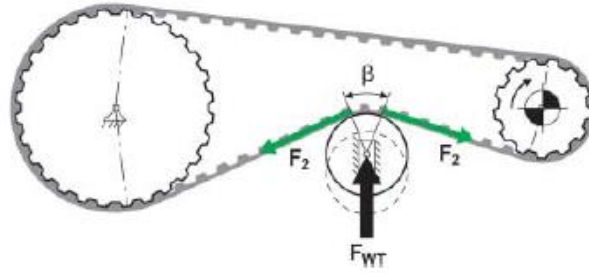


Figure 4.5: Belt tensioning forces

The tensioning force $F_{tensioner}$ (F_{WT}) can be determined thus:

$$F_{tensioner} = 0.4 * F_{load} * \sin\left(\frac{\beta_{tensioner}}{2}\right)$$

The angle of the tensioner arc of contact can be determined by the CAD model. To determine the force in the belt F_{belt} (F_2):

$$F_{belt} = \frac{F_{tensioner}}{2 * \sin\left(\frac{\beta_{tensioner}}{2}\right)}$$

The new value F_{belt} represents the new peripheral force on the now tight side with the tensioner.

4.3.1.3.4 Pulley inertia:

The pulley inertia affects the angular acceleration and deceleration of the actuator. The inertia in the smaller driver pulleys and that of the belt can be neglected due to their infinitesimally small values. However, with the larger pulleys, there is a substantial effect on how the actuator rotates, due to their larger radius and mass. The peripheral forces acting on the pulley has to be known to determine the angular acceleration and the inertia represents an opposing torque in this case. This torque is present when the pulley starts and stops moving. The angular acceleration and speed of the pulley are the same along the shaft.

The acceleration of the pulley if the angular speed and acceleration time t_{acc} is known is

$$\alpha_{shaft} = \frac{\omega_{shaft}}{t_{acc}} \quad (4-14)$$

The torque to accelerate the pulley to the desired angular speed is:

$$\tau_{acc} = I_{pulley} * \alpha_{shaft} \quad (4-15)$$

The effective diameter of the fourth pulley is 85.9 mm, and it has a mass of about 197.7 g. Hence, the moment of inertia of the fourth pulley is determined using

$$I_{pulley} = \frac{m_{pulley} * r_{pulley}^2}{2} \quad (4-16)$$

$$I_{pulley4} = \frac{0.1977 * \left(\frac{85.94}{2 * 1000}\right)^2}{2}$$

$$I_{pulley4} = 0.1825 * 10^{-3} [kg m^2]$$

The torque required for an acceleration time of $t = 0.2$ s to a peak speed of 500 degrees/s:

$$\tau_{pulley4} = I_{pulley4} * \alpha_{peak} * \frac{\pi}{180} = 0.1825 * 10^{-3} * 2500 * \frac{\pi}{180}$$

$$\tau_{pulley4} = 7.96 * 10^{-3} [Nm]$$

This represents the torque required to accelerate the pulley to a full output speed of 500 degrees/s at the output link. Work has to be done to overcome this inertia and thus, the torque required is included in the total resistance torque.

Table 4.5 below gives a summary of the moments of inertia of the pulleys, assuming they have a closed centre since the shafts will run through it. The moment of inertia of the motor is included since it is an outrunner type where the whole rotor with the magnet moves. The mass was measured using an electronic scale to be 138.8g. The moment of inertia was calculated assuming a hollow cylinder.

$$I_{motor} = \frac{m_{motor} * (r_1^2 + r_2^2)}{2} = \frac{0.1388 * \left(\left(\frac{69}{2 * 1000}\right)^2 + \left(\frac{59}{2 * 1000}\right)^2\right)}{2}$$

$$I_{motor} = 1.43 * 10^{-4} [kg m^2]$$

Pulley	Moment of Inertia [Kg m ²]
Motor	$1.43 * 10^{-4}$
Pulley 1	$4.128 * 10^{-7}$
Pulley 2	0.000207
Pulley 3	$1.687 * 10^{-7}$
Pulley 4	0.0001825

Table 4.5: Moment of inertia of motor and pulley

In active mode, with the peripheral force acting on the pulley being known; the acceleration can also be determined. The torque required for that acceleration can also be determined to obtain a better estimate of the efficiency of the system and the actual motor torque required.

Using peripheral force F_{pulley} ,

$$\alpha_{peak} = \frac{\tau_{pulley}}{I_{pulley}} = \frac{F_{pulley} * \frac{d_n}{2 * 1000}}{I_{pulley}}$$

The inertias of the pulleys are mostly used during the tuning phase of the motor where this parameter is input in the motor controller which is integrated with PID tuning. They are also used to determine the backdrivable torque required by the user.

Considering the shank as point mass rotating about the knee, the values from Section 2.3.3.1 are used, with a radius equal to the length till the centre of gravity as the point of contact, and moment of inertia of the shank is calculated.

$$I_{shank} = m_{shank+foot} * r_{COG}^2$$

$$I_{shank} = (0.951 + 3.20) * 0.183^2 = 0.139 \text{ kg m}^2$$

4.3.1.4 Teeth meshing, belt slipping and safety

To determine the safety of the system and if the belt and pulley can truly transmit the required torque, several factors are considered: the teeth-in-mesh factor, total power transfer and the maximum belt tensile forces.

The number of teeth in mesh on the gears can be defined as the number of teeth which are transmitting torque at any instant on pulley. It is calculated using the known arc of contact:

$$z_m = \frac{z_a * \beta}{360} \quad (4-17)$$

where z_m is the number of teeth in mesh, z_a is the total number of driver teeth and β is the arc of contact on the driver pulley. The arc of contact is determined during the design on AutoCAD. Referring to Figure 4.6, t is determined by measuring the angle from the first pulley tooth till the last pulley tooth which is fully meshed. Similarly, the number of teeth can be measured too.

The number of teeth in the driven pulley:

$$z_m = z_1 * \left(0.5 - \frac{d_2 - d_1}{2 * \pi * C}\right) \quad (4-18)$$

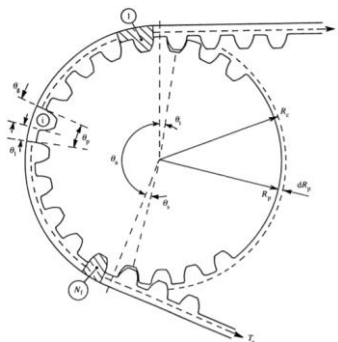


Figure 4.6: Description of teeth-in-mesh

The *tooth-in-mesh factor* can be determined from the provided manufacturer's table or if the type and pitch of the pulley and belt are known. The teeth-in-mesh factor is inherent of the belt used and can be determined. Referring to datasheet from Maedler [31]:

For belt 1, teeth in mesh for pulley 1(smaller pulley):

$$z_m = \frac{z_a * \beta}{360}$$

$$z_{m1} = \frac{20 * 130}{360} = 7.22 \sim 7$$

For belt 2, teeth in mesh for pulley 3(smaller pulley):

$$z_{m3} = \frac{14.32 * 108}{360} = 4.296 \sim 4$$

The effective transmission power required for the belt, which also serves the purpose of selecting the appropriate belt width and belt profile can be determined using the equation (4-19).

$$P_{effective} = P_{driver} * (K_1 + K_2 + K_3 + C_1) \quad (4-19)$$

Where

P_{driver}: the power of the driver pulley

K₁: Corrective factor for the load type

K₂: Corrective factor for the tensioner pulley

K₃: Corrective factor for the transmission ratio (Gear ratio)

C₁: Teeth in mesh factor

Since there are two consecutive belts, there are two driver pulleys, and the calculation is performed for each. The maximum power by the *T-Motor P60* motor is 1500 W or 1.5 kW. Coefficient K₁ is set at 1.8 since a brushless DC motor is used for reciprocating and intermittent motion for a maximum period of up to 12 hours daily. The power is multiplied by a factor of 0.29 for 10 mm width 3M belts.

Coefficients	Belt 1
K₁	1.8
K₂	0
K₃	0
C₁	0
P_{driver}	1500 W

Table 4.6: Coefficients for permissible belt power 1

Using a 9mm belt width, the correction factor is 0.29, hence, the effective power:

$$P_{effective1} = [1.5 * (1.8 + 0 + 0 + 0)] * 0.29 = 0.783 kW$$

From the chart, for a maximum speed of 2400 rpm from the small pulley at the motor shaft, a power of 0.76 kW can be applied from a driver pulley of 20 teeth, for a period of up to 12 hours daily with minimum decrease to the service life of the belt.

The speed on shaft 1 is then $2400 \div \frac{90}{20} = 533.33 \text{ rpm}$ while the effective power for the driver pulley is 760 W. Since there are only 4 teeth in mesh, the teeth-in-mesh factor C_1 from the table is 0.7.

Hence, the table of coefficients for the second belt is:

Coefficients	Belt 1
K_1	1.8
K_2	0
K_3	0
C_1	0.7
P_{driver}	760 W

Table 4.7: Coefficients for permissible belt power 2

$$P_{\text{effective2}} = [0.760 * (1.8 + 0 + 0 + 0.7)] * 0.29 = 0.551 \text{ kW}$$

The effective power transmitted by belt 2 is 0.551 kW at a speed of 533.33 rpm of the driver pulley. The speed of the driven pulley is then $533.33 \div \frac{90}{15} = 88.88 \text{ rpm}$. The speed of the driver pulley is lower than that in the manufacturer's table, hence, the belt can safely transmit the power required. Nevertheless, since this power is lower than the 783 W transmitted by belt 1, the total permissible transmission power is limited to 551 W. Hence, the motor will operate by transmitting a maximum power of 551 W, which is within the technical requirements range in [Table 3.3](#).

4.3.1.4.1 Maximum belt tensile force

It is important to obtain a safety value of the belt and pulley in terms of the maximum permissible tensile force. The HTD belt is made with neoprene with only 25% fiberglass reinforcement which has a minimum yield stress of 45 N/mm^2 , with a maximum strain of 1.2%. However, non-linear elastic deformation occurs after 28 N/mm^2 , but is still in the range of 0 to 0.4% strain [32].

The cross-sectional area of the neoprene with fiberglass tensile member is $1.18 * 10 = 11.8 \text{ mm}^2$ for the 10 mm belt width, and $1.18 * 16 = 18.88 \text{ mm}^2$ for the 16 mm belt width. Hence, the maximum tensile force that can be sustained by the HTD 3M belt is 531 N for the 10 mm belt width and 849.6 N for the 16 belt width. If a linear elastic deformation only is desired, then the maximum permissible tensile force is 330.4 N and 528.64 N respectively.

The maximum torque at the fourth pulley is thus:

$$T_{\text{maximum}} = 22.63 \text{ Nm}, \text{ for the 10 mm belt width and}$$

$$T_{\text{maximum}} = 36.30 \text{ Nm}, \text{ for the 16 mm belt width}$$

Hence, using a 15mm wide belt for the second belt, the peak torque is reduced to 36.40 Nm from the previously calculated 54 Nm. The torque requirements are still fulfilled based on the purpose of the actuator, as it is higher than the torque assistance for slow walking (11.5 Nm).

Given that the effective actuator torque at its minimum is about 60% of the output due to the four-bar-linkage, as calculated in [Section 4.3.3](#),

$$T_{maximum} = 36.30 * 0.6 = 21.96 \text{ Nm}$$

With a safety factor, SF, being 1.5, the torque requirements for 30% assistance during slow walking is still satisfied.

$$T_{maximum} = \frac{21.96}{1.5} = 14.64 \text{ Nm}$$

4.3.2 Required torques

When considering the forces from the motor to the shank output link (active drive system), the peripheral force will also include the force required to move the shank. This is directly affected by the percentage of assistance provided by the actuator as a whole. Hence, the percentage of the force being provided by the actuator is counted as the resistive force on the leg.

For example, if the knee requires 20 Nm of torque for flexion, but the actuator provides 30% assistance, then, the biological force of the knee is only equivalent to 14 Nm, which then equals to a resistance of 6 Nm from the knee in terms of magnitude. However, since the direction of the forces are the same, this adds up to the actuator torque and eventually the peripheral forces on the belts. There are two modes, namely active mode where the actuator exerts an assisting torque, and passive, where the actuator does not exert any torque.

4.3.2.1 Active Mode

The motor provides the assistance torque, hence, the external torque provided by the wearer and the actuator torque should amount to the total required knee torque for the motion. At its peak, the torque provided is 30% of the user's knee torque. An estimation of the actual required torque after the resistive forces is evaluated in this section.

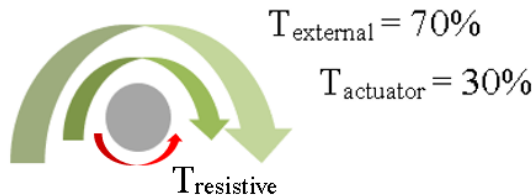


Figure 4.7: Actuator and external torque representation

$$T_{actual} = T_{actuator} + T_{external} - T_{resistive}$$

The total forces required to calculate the actual peripheral force at any point starts from the knee is worked towards the motor. The peripheral forces are the forces acting on the belts are:

$$F_{\text{peripheral}} = -F_{\text{external}} + F_{\text{bearing}} + F_{\text{belt}} + F_{\text{flange}} + F_{\text{friction}} + F_{\text{required}} + F_{\text{inertia}}$$

Since the combined friction of the flange and between the belt and pulley is negligible and no tensioner is being used, the peripheral force is described in Equation (4-29).

$$F_{\text{peripheral}} = -F_{\text{external}} + F_{\text{bearing}} + F_{\text{required}} + F_{\text{inertia}} \quad (4-20)$$

From section 1.3.1.4, the peak transmissible torque is 36.30 Nm. Consider the safety factor with the notation SF . Hence, the actual torque is $\frac{36.30}{SF}$ for the second belt with width 16 mm. With a SF of 1, the peak torque will result in failure of the belt.

Thus, at the fourth pulley, using the relation from Equation (4-9),

$$\begin{aligned} F_{\text{pulley4}} &= \frac{\frac{T_{\text{maximum}}}{SF}}{\frac{d_4}{2 * 1000}} [N] \\ F_{\text{pulley4}} &= \frac{\frac{36.30}{SF}}{\frac{d_4}{2 * 1000}} = \frac{\frac{36.30}{SF}}{\frac{85.94}{2 * 1000}} = \frac{844.775}{SF} [N] \end{aligned}$$

Since $d_4 = 85.94$ mm.

Given that no tensioner is used,

$$F_{\text{pulley3}} = F_{\text{pulley4}} = \frac{844.775}{SF} [N]$$

Pulley 2 and Pulley 3 are fixed on the same shaft. Thus,

$$\begin{aligned} F_{\text{pulley2}} &= \frac{F_{\text{pulley3}} * \frac{d_3}{2 * 1000}}{\frac{d_2}{2 * 1000}} = \frac{\frac{844.775}{SF} * \frac{14.32}{2 * 1000}}{\frac{85.94}{2 * 1000}} [N] \\ F_{\text{pulley2}} &= \frac{140.763}{SF} [N] \\ F_{\text{motor}} &= F_{\text{pulley2}} = \frac{140.763}{SF} [N] \end{aligned}$$

since $d_2 = 85.94$ mm and $d_3 = 14.32$ mm.

The peripheral force on belt 1 is within the safety limit as well.

Assuming an angular speed of 360 degrees/s (or 6.28 rad/s) during the stance phase, where torque is highest. The estimated speeds of the motor and shafts using the relation from Equation (4-8):

$$\omega_{motor} = 169.6 \text{ [rad/s]}$$

$$\omega_{shaft1} = 37.7 \text{ [rad/s]}$$

$$\omega_{shaft2} = 6.28 \text{ [rad/s]}$$

Assuming again 0.2 second per gait cycle is required for one particular phase, the angular acceleration of each shaft is calculated using Equation (4-13),

$$\alpha_{motor} = 848.2 \text{ [rad/s}^2]$$

$$\alpha_{shaft1} = 188.5 \text{ [rad/s}^2]$$

$$\alpha_{shaft2} = 31.4 \text{ [rad/s}^2]$$

The required torque to accelerate the pulley to the desired angular speed, determined by Equation (4-14) and from the moment of inertia values of Table 4.5.

$$\begin{aligned}\tau_{motor} &= (I_{motor} + I_{pulley1}) * \alpha_{motor} = (1430 + 4.128) * 10^{-7} * 848.2 \\ &= 0.0243 \text{ [Nm]}\end{aligned}$$

$$\begin{aligned}\tau_{pulley2} &= (I_{pulley2} + I_{pulley3}) * \alpha_{shaft1} = (2070 + 1.687) * 10^{-7} * 188.5 \\ &= 0.0391 \text{ [Nm]}\end{aligned}$$

$$\tau_{pulley4} = I_{pulley4} * \alpha_{shaft2} = 0.1825 * 10^{-3} * 31.4 = 0.00573 \text{ [Nm]}$$

The above inertial torques have to be overcome during acceleration of the pulleys and the motor. Another assumption is that the acceleration of the different pulleys occurs simultaneously. The result is that the peripheral forces along the belt at the pulleys are not the same throughout, however, the value of the inertial force is quite low compared to the actual force for an acceleration time of 0.2 s.

It still has an effect to what extent the belt and pulley system is back drivable. The detent torque is added together with $F_{inertial}$. This is discussed in the next subtopic 4.3.2.2.

The frictional torque at the rotating ends (bearings and bushes) are calculated using:

$$T_{bearing/bushing} = T_{shaft} * \mu$$

The following set of equations are used to do a summation of the resistive torques, with the radii in metres or millimeters ($r_n = \frac{d_n}{2}$) and assuming the belts do not undergo elastic deformation.

$$F_{pulley1} = F_{pulley2} = \frac{T_{motor} * (\frac{\mu_{motor_bearing} + \mu_{motor_encoder}}{2})}{r_1} \quad (I)$$

$$T_{pulley2} = T_{pulley3} = F_{pulley2} * r_2 \quad (II)$$

$$F_{pulley3} = F_{pulley4} = T_{pulley3} * (\frac{1 + \mu_{shaft1_bearing}}{r_3}) \quad (III)$$

$$T_{pulley4} = F_{pulley4} * r_4 * (1 + (\frac{\mu_{shaft2_bearing} + \mu_{shaft2_bush}}{2})) \quad (IV)$$

Substituting Equations (I), (II), (III) and (IV) into one another, we obtain the equation for final output torque with the resistive forces

$$T_{pulley4} = \frac{T_{motor} * (\mu_{motor_bearing} + \mu_{motor_encoder}) * r_2 * r_4}{2 * r_1 * r_3} * (1 + \mu_{shaft1_bearing}) * (1 + (\frac{\mu_{shaft2_bearing} + \mu_{shaft2_bush}}{2})) \quad (4-21)$$

A summary of the friction torques at peak output torque of 36.3 Nm is listed in Table 4.8 at each shaft. For a peak torque of $\frac{36.3}{SF}$ Nm, an approximate motor torque of $\frac{1.34}{SF}$ Nm is required if frictional forces are neglected at first. The frictional torques starting from the motor are amplified, similar to the active torque.

Bearing and bush position	Friction Torque [Nm]	Friction Torque [Nm] with SF = 1.5
Motor bearing (19 mm dia.)	$\frac{0.001}{SF}$	~ 0
Motor encoder (15mm dia.)	$\frac{0.168}{SF}$	0.112
Shaft 1 bearing (22 mm dia.)	$\frac{0.762}{SF}$	0.508
Shaft 2 bearing (22 mm dia.)	$\frac{2.29}{SF}$	1.53
Shaft 2 slotted bush (8 mm dia.)	$\frac{2.51}{SF}$	1.68

Table 4.8: Frictional forces

The actual peripheral force at each pulley is calculated again to account for the sum of resistive torques using the Equation (4-21). The resultant estimated torques considering resistive forces are listed in Table 4.9 for a peak output torque of 36.3 Nm, with SF = 1.5.

Parameter	Calculated Torques [N] neglecting frictional torques	Calculated Torque [Nm] with SF = 1.5 neglecting frictional torques	Estimated actual required Torque [Nm] with SF = 1.5 at 360 degrees/s, considering friction	Estimated actual required Torque [Nm] with SF = 1.5 during acceleration time of 0.2 s
Shaft 2	$\frac{36.3}{SF}$	24.2	27.4	27.4
Shaft 1	$\frac{6.05}{SF}$	4.03	4.54	4.61
Motor	$\frac{1.34}{SF}$	0.896	1.01	1.04

Table 4.9: Estimated resultant forces and torques

Hence to obtain the calculated torque of 24.2 Nm at the actuator output, an input motor torque of 1.01 Nm is required during constant speed operation, so as to overcome rotational friction. During acceleration and deceleration (braking), a motor torque of 1.04 Nm is required. There is a reduction in the safety factor SF from 1.5 to 1.32 in belt 2.

An efficiency factor η can be included in the torque increase mechanism during constant speed operation resulting in

$$T_{actuator} = \eta * T_{motor} * N \text{ [Nm]}$$

Where

$$\eta = \frac{T_{actual}}{T_{required}} = \frac{24.2}{27.4} * 100\% = 88.3\%$$

The efficiency can be increased by replacing the bushing at shaft 2 with a ball bearing, however, with the current design including the four-bar-linkage, this is not possible. The dimensions of the four-bar-linkage have to be changed to allow that considering the bushing only occupies about 10 mm diameter, while a ball bearing with bore diameter 8 mm, occupies 22 mm diameter of space which intersects with the pivot of the follower link.

Since the actuator is only responding to the knee movement and assisting the knee, it is safe to assume that the acceleration torque due to the inertia of the shank provided by the extensor and flexor muscles themselves, 30% of that torque which is

$$\tau_{knee\ acceleration} = 30\% * 31.4 * 0.139 = 1.31 \text{ [Nm]}$$

4.3.2.2 Passive Mode

In passive mode, the torque is exerted by the knee, while the brushless DC motor is spun freely. Thus, the detent torque of the motor, together with the frictional forces have to be overcome to allow any motion. Since the knee can provide a much larger torque than what is required, the limiting factor is thus the total power that the knee can exert, and hence, the peak angular speed. This affects the torque both during angular acceleration-deceleration, and in constant angular velocity operation.

Using the detent torque T_{detent} of the motor which is estimated at 0.05 Nm, the new peripheral forces in the belt can be calculated using [Equation \(4-9\)](#) together with the frictional forces with [Equation \(4-21\)](#) to estimate the backdrivable torque during constant speed. T_{motor} is replaced with T_{detent} . The acceleration torques are determined using [Equations \(4-14\)](#) and [\(4-15\)](#) similar for the calculation of active operation.

Additionally, for an angular speed of 500 degrees/s (or 8.73 rad/s) during the swing phase, the estimated speeds of the motor and shafts using the relation from [Equation \(4-8\)](#):

$$\omega_{shaft2} = 8.73 \text{ [rad/s]}, \omega_{shaft1} = 52.4 \text{ [rad/s]} \text{ and } \omega_{motor} = 235.6 \text{ [rad/s]}$$

Assuming again 0.2 second per gait cycle is required for one particular phase, the angular acceleration of each shaft is calculated using [Equation \(4-13\)](#),

$$\alpha_{shaft2} = 43.7 \text{ [rad/s}^2\text{]}, \alpha_{shaft1} = 196.7 \text{ [rad/s}^2\text{]} \text{ and } \alpha_{motor} = 1179.9 \text{ [rad/s}^2\text{]}$$

The required torque to accelerate the pulley to the desired angular speed, determined by [Equation \(4-14\)](#) and from the moment of inertia values of Table 4.5.

$$\tau_{motor} = (I_{motor} + I_{pulley1}) * \alpha_{motor} = (1430 + 4.128) * 10^{-7} * 1179.9 = 0.169 \text{ [Nm]}$$

$$\tau_{pulley2} = (I_{pulley2} + I_{pulley3}) * \alpha_{shaft1} = (2070 + 1.687) * 10^{-7} * 196.7 = 0.0408 \text{ [Nm]}$$

$$\tau_{pulley4} = I_{pulley4} * \alpha_{shaft2} = 0.1825 * 10^{-3} * 43.7 = 0.00798 \text{ [Nm]}$$

Table 4.10 lists the torque required to backdrive the actuator when it is not activated.

Parameter	Backdrive Torques [N] neglecting frictional torques	Estimated actual required Torque [Nm] at constant speed considering friction	Estimated actual required Torque [Nm] during acceleration time of 0.2 s to 360 deg/s	Estimated actual required Torque [Nm] during acceleration time of 0.2 s to 500 deg/s
Motor	0.05	0.0563	0.0806	0.250
Shaft 1	0.225	0.254	0.402	1.16
Shaft 2	1.35	1.60	2.42	6.97

Table 4.10: Backdrivable Torques

A nominal torque of 1.60 Nm is required from the user to backdrive the actuator. To rotate the actuator from rest to 360 degree/s, a torque of 2.42 Nm is required. For higher speeds, a larger acceleration occurs which results in an increase in the inertia, and thus, an increase in the acceleration torque. The maximum backdrivable torque is less than the peak permissible torque, hence, the safety of the actuator is confirmed when the backdrivable torque is applied.

4.3.2.3 Reaction force on pulley (Shaft Load)

This is the normal force acting directly at the centre of shaft where the pulley is fixed. It is the resultant of the forces present on both sides of the belt and is required to be able to determine the support needed in terms of ribs or material thickness in the Autodesk Inventor program. Additionally, the required bearing radial force is determined based on this property.

Given the following setup, the shaft load is:

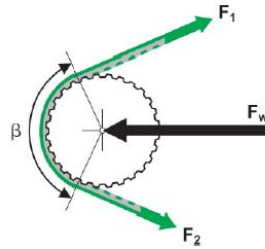


Figure 4.8: Shaft load description

For a belt moving at constant speed, the shaft load is the sum of the peripheral forces at the pulley. The direction of the shaft load is parallel to the bisector of the arc-of-contact angle and acts directly towards the shaft. Equation (4-22) defines the relation between the peripheral forces, the arc-of-contact and the shaft load.

$$F_{shaft} = F_w = \sqrt{F_1^2 + F_2^2 - 2 * F_1 * F_2 * \cos(\beta)} \quad (4-22)$$

Including the safety factor:

$$F_{shaft} = F_w = \frac{f(F_1, F_2)}{SF}$$

$$F_{shaft} * SF = f(F_1, F_2)$$

As the safety factor SF is increased, the torques at the shafts and the peripheral forces decrease. Thus, a safety factor SF of 1 for the load is set. Another safety factor is applied for the calculation of the shaft load and is denoted SF_{shaft}. The new safety factor SF_{shaft} is updated as follows

$$New SF_{shaft} = SF_{shaft} * SF$$

The shaft loads are thus determined and summarized Table 4.12. A coordinate system is used to identify the direction of the forces and to determine the resultant shaft loads, as shown in Figure 4.9. A scale of 1mm:1 unit is used for the coordinate grid. A simplified form is used where $F_1 = F_2$ since the difference between F_1 and F_2 is minimal due to low friction of the drives.

Shaft	Position	Arc angle $\beta [^{\circ}]$	$F_1 = F_2 [N]$	Shaft load [N]
Motor/Pulley 1	(0,0)	130	140.763	255.149
Pulley 2	(60.6, 49.8)	230	140.763	255.149
Pulley 3	(60.6, 49.8)	108	844.775	1366.87
Pulley 4	(95.2, 0)	252	844.775	1366.87
Shaft 1 resultant	(60.6, 49.8)	-	-	1410.3

Table 4.11: Pulley positions, angles, and shaft loads

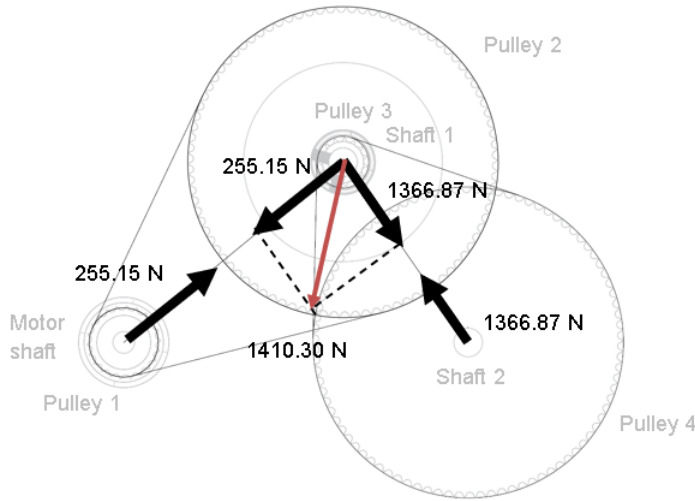


Figure 4.9: Actuator shaft loads enumerated

The resultant force is obtained by resolving the forces. It has a magnitude of 1410.3 N and acts at an angle of 66° to the horizontal line.

4.4 Four bar mechanism force calculation

In this section, the force calculations in the four-bar-linkage are carried out, as well as the determination of the proper lengths of the links.

The maximum permissible output torque from the belt and pulley system being known, a set of equations can be derived so as to determine the torque output from the four-bar-linkage. A simplified version which was as close as possible to the final desired design was created to facilitate the calculation process. The angles and lengths can be varied to match the final dimensions used.

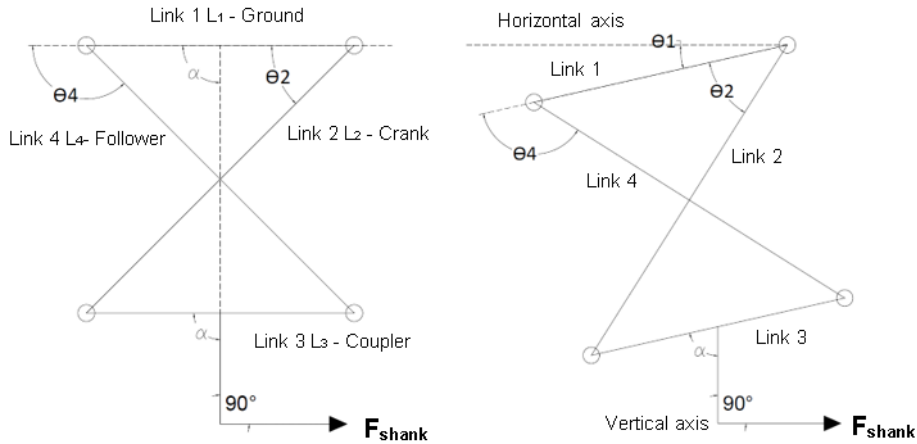


Figure 4.10: Four-bar-linkage description

The torque output of the four-bar mechanism is not constant and is not the same as the torque output of the belt and pulley system. Excluding frictional losses, which are minimal, the power input should be equal to the power output. Considering the design of the four-bar-linkage itself, there are four angles in particular: Θ_1 , Θ_2 , Θ_3 and Θ_4 and four links L_1 , L_2 , L_3 and L_4 represented in the schematic in Figure 4.10 above. The names of the links are: (link 1) L_1 = ground, (link 2) L_2 = crank, (link 4) L_4 = followers and (link 3) L_3 = coupler.

Θ_1 represents the offset of the ground link if it is not parallel to a horizontal line. In the case where ground is horizontal as shown in the left image in Figure 4.10, $\Theta_1 = 0$.

Θ_3 represents the angle between link 1 and link 3. In the case where both are parallel, $\Theta_3 = 180$.

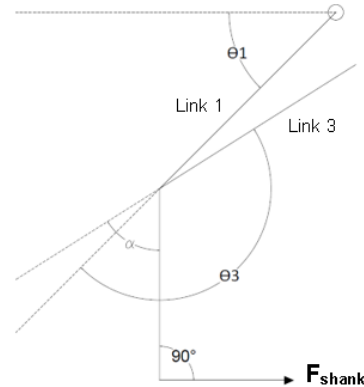


Figure 4.11: Angle Θ_3 between Link L_1 and Link L_3

Θ_1 is a constant, while Θ_2 , Θ_3 and Θ_4 are variable quantities, which are dependent on Θ_2 . The force acting on the shank is F_{shank} which is present at the connection to link 3.

To determine the output force and torque at the shank, a free body diagram has been constructed to break down the forces and to obtain an equation relating the input torque and output torque.

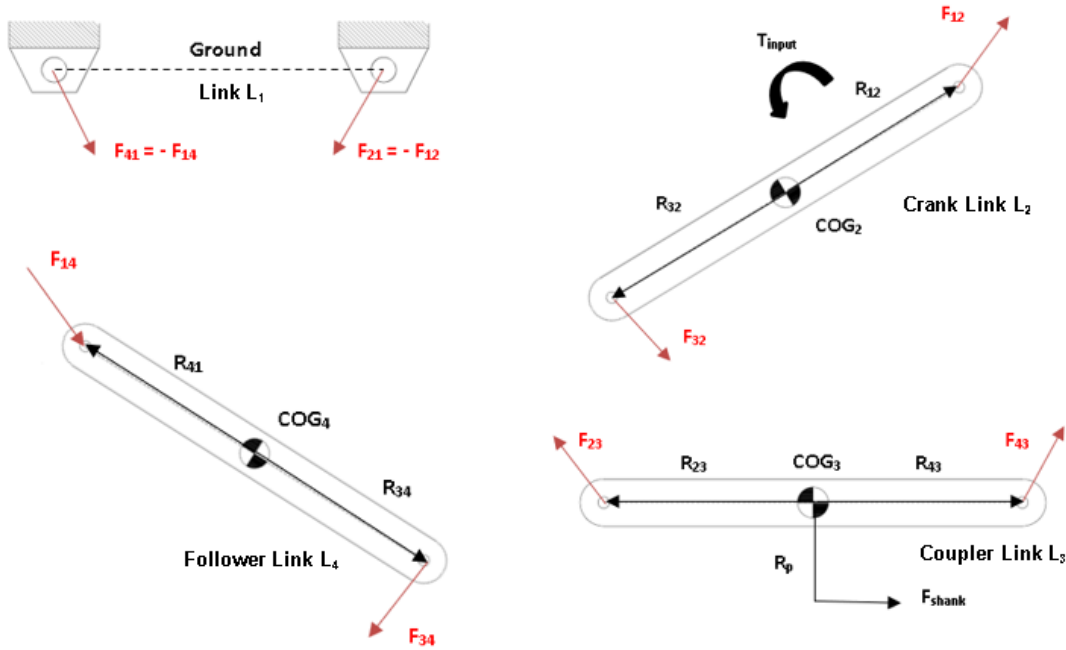


Figure 4.12: Four-bar-linkage force diagram

Points which were considered when formulating the force equations:

- There are no external direct forces are acting on the overall body. Static equilibrium is considered; hence, the resultant forces of each link are equal to 0. Equations for opposing forces are thus represented as $\mathbf{F}_{1x} + \mathbf{F}_{2x} = \mathbf{0}$ ($\sum F_x = 0, \sum F_y = 0$ and $\sum T = 0$)
- Only the input torque from the motor is considered. It is equivalent to the output of the belt and pulley series and denoted as T_{input}
- Only output force is the force acting on the shank. This is represented by the shank force on the coupler (link 3), denoted as $\mathbf{F}_{\text{shank}}$
- The **COG** (Centre of Gravity) of the links are represented, as well as the lengths from the link connection to the centre of gravity as \mathbf{R}_{nm} . For a uniform link with length L , $R = \frac{L}{2}$.
- \mathbf{R}_p is the length of the link connecting the shank to the coupler.

Based on the free body diagram, the vector forces are broken down into their scalar components x and y.

$$F: \{F_x, F_y\}$$

There are three equations for each link.

4.4.1.1 Calculations steps:

Starting from Link 2:

$$F_{12X} + F_{32X} = 0 \quad (4-23)$$

$$F_{12y} + F_{32y} = 0 \quad (4-24)$$

$$(R_{32x} * F_{32y} - R_{32y} * F_{32x}) + (R_{12x} * F_{12y} - R_{12y} * F_{12x}) - T_{input} = 0 \quad (4-25)$$

Link 3:

$$F_{43X} + F_{23X} + F_{shank\,x} = 0 \quad (4-26)$$

$$F_{43y} + F_{23y} + F_{shank\,y} = 0 \quad (4-27)$$

$$\begin{aligned} & (R_{43x} * F_{43y} - R_{43y} * F_{43x}) + (R_{23x} * F_{23y} - R_{23y} * F_{23x}) \\ & + (R_{px} * F_{shank\,y} - R_{py} * F_{shank\,x}) = 0 \end{aligned} \quad (4-28)$$

Link 4:

$$F_{14X} + F_{34X} = 0 \quad (4-29)$$

$$F_{14y} + F_{34y} = 0 \quad (4-30)$$

$$(R_{14x} * F_{14y} - R_{14y} * F_{14x}) + (R_{34y} * F_{34x} - R_{34x} * F_{34y}) = 0 \quad (4-31)$$

The nine equations obtained are represented in a matrix of the form:

$A \times B = C$, where A is the coefficients of the unknown forces, B represents the unknown force variables and C are the constants and known inputs. The output forces can be solved as such:

$$B = A^{-1} * C \quad (4-32)$$

Equation (4-32) is represented in its full matrix form in (4-33).

By normal convention, $F_{ab} = -F_{ba}$.

$$\begin{pmatrix} 1 & 0 & 1 & 0 & 0 & 0 & 0 & 0 \\ 0 & 1 & 0 & 1 & 0 & 0 & 0 & 0 \\ -R_{12y} & R_{12x} & R_{32y} & -R_{32x} & 0 & 0 & 0 & 0 \\ 0 & 0 & -1 & 0 & 1 & 0 & 0 & \cos(\Theta) \\ 0 & 0 & 0 & -1 & 0 & 1 & 0 & \sin(\Theta) \\ 0 & 0 & R_{23y} & -R_{23x} & -R_{43y} & R_{43x} & 0 & C \\ 0 & 0 & 0 & 0 & -1 & 0 & 1 & 0 \\ 0 & 0 & 0 & 0 & 0 & -1 & 0 & 0 \\ 0 & 0 & 0 & 0 & R_{34y} & -R_{34x} & -R_{14y} & R_{14x} \end{pmatrix} x \begin{pmatrix} F_{12x} \\ F_{12y} \\ F_{23x} \\ F_{23y} \\ F_{34x} \\ F_{34y} \\ F_{14x} \\ F_{14y} \\ F_{shank} \end{pmatrix} = \begin{pmatrix} 0 \\ 0 \\ T_{input} \\ 0 \\ 0 \\ 0 \\ 0 \\ 0 \\ 0 \end{pmatrix}$$

$$\begin{pmatrix} F_{12x} \\ F_{12y} \\ F_{23x} \\ F_{23y} \\ F_{34x} \\ F_{34y} \\ F_{14x} \\ F_{14y} \\ F_{shank} \end{pmatrix} = \begin{pmatrix} 1 & 0 & 1 & 0 & 0 & 0 & 0 & 0 \\ 0 & 1 & 0 & 1 & 0 & 0 & 0 & 0 \\ -R_{12y} & R_{12x} & R_{32y} & -R_{32x} & 0 & 0 & 0 & 0 \\ 0 & 0 & -1 & 0 & 1 & 0 & 0 & \cos(\Theta) \\ 0 & 0 & 0 & -1 & 0 & 1 & 0 & \sin(\Theta) \\ 0 & 0 & R_{23y} & -R_{23x} & -R_{43y} & R_{43x} & 0 & C \\ 0 & 0 & 0 & 0 & -1 & 0 & 1 & 0 \\ 0 & 0 & 0 & 0 & 0 & -1 & 0 & 0 \\ 0 & 0 & 0 & 0 & R_{34y} & -R_{34x} & -R_{14y} & R_{14x} \end{pmatrix}^{-1} x \begin{pmatrix} 0 \\ 0 \\ T_{input} \\ 0 \\ 0 \\ 0 \\ 0 \\ 0 \\ 0 \end{pmatrix}$$

(4-33)

Where,

$$F_{shank}: \{F_{shankx}, F_{shanky}\} = \{F_{shank} * \cos(\Theta), F_{shank} * \sin(\Theta)\}$$

$$C = R_{px} * \sin(\Theta) - R_{py} * \cos(\Theta)$$

R values are dependent on the link lengths and angles:

$$R_{12x} = \frac{L_2}{2} * \cos(\theta_2 + \pi), R_{12y} = \frac{L_2}{2} * \sin(\theta_2 + \pi)$$

$$R_{32x} = \frac{L_2}{2} * \cos(\theta_2), R_{32y} = \frac{L_2}{2} * \sin(\theta_2)$$

$$R_{23x} = \frac{L_3}{2} * \cos(\theta_3), R_{23y} = \frac{L_3}{2} * \sin(\theta_3)$$

$$R_{43x} = \frac{L_3}{2} * \cos(\theta_3 + \pi), R_{43y} = \frac{L_3}{2} * \sin(\theta_3 + \pi)$$

$$R_{34x} = \frac{L_4}{2} * \cos(\theta_4), R_{34y} = \frac{L_4}{2} * \sin(\theta_4)$$

$$R_{14x} = \frac{L_4}{2} * \cos(\theta_4 + \pi), R_{14y} = \frac{L_4}{2} * \sin(\theta_4 + \pi)$$

Irrespective of the angle between ground and the coupler, the force F_{shank} always has a component which is perpendicular to the shank direction.

Thus,

$$\theta = \theta_3 - 180 + \alpha - 90$$

The torque output is precisely defined as the product of F_{shank} with the distance from the instantaneous centre of rotation to the point of contact of the force. An estimation can be calculated from the product of the force F_{shank} and the distance from the centre of rotation of link 2 and the point of contact of the force.

4.4.1.2 Verification of equation set

The actual four bar linkage was designed following the data obtained during the research phase, so as to match the knee motion of the actuator with that of the wearer. The result was as follows. The lengths are in mm and angles in degrees.

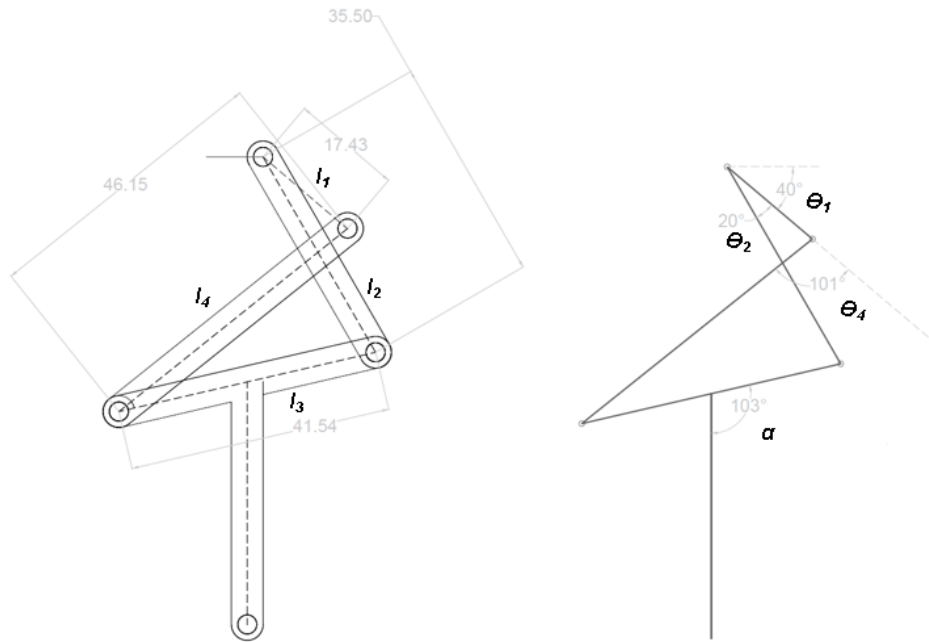


Figure 4.13: Four-bar-linkage dimensions

Figure 4.13 shows the four-bar-linkage. The lengths were chosen so as to fit the four bars within the actuator case and only allow the coupler link to protrude out, so that it can be connected to the shank support.

The matrices were implemented in a python script and by comparing the results of a similar four-bar-linkage development [21], its validity was checked. For an input torque of **36.3 Nm** and the following parameters:

$$l_1 = 17.43 \text{ mm}, l_2 = 35.50 \text{ mm}, l_3 = 41.54 \text{ mm}, \text{and } l_4 = 46.15 \text{ mm}$$

Since Θ_2 is variable, a starting value of $\Theta_2 = 20^\circ$ is used. The other angles are $\alpha = 103^\circ$, and $\Theta_4 = 101^\circ$

Θ_3 is estimated to be 127° for the initial value of $\Theta_2 = 20^\circ$.

Let R_p be in the range: $100 < R_p < 150$ mm, given a shank length of 300 mm.

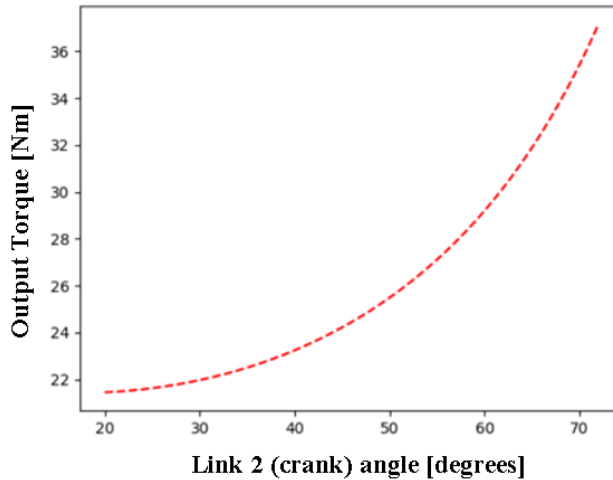


Figure 4.14: Shank torque variation with change in crank angle

From the graph in Figure 4.14, it can be observed that the effective torque transmission of the crossed four-bar mechanism is $\sim 60\%$ of the total output at its minimum. For a peak torque of 36.3 Nm, the minimum torque output is 21.75 Nm. This was confirmed during the implementation and testing phase.

4.4.2 Freudenstein's Equations for the variation in angle

The Freudenstein's Equations form a set of equations which are developed for the analysis of four-bar-linkages [21]. They are formulated based on the trigonometric relations between the linkages.

The Freudenstein's Equations used to solve the output angle of a crossed-four-bar-linkage is

$$\theta_3 = 2 * \tan^{-1} \left(\frac{-E + \sqrt{E^2 - 4 * D * F}}{2 * D} \right) \quad (4-34)$$

Where:

$$D = \cos(\theta_2) + K_2 * \cos(\theta_2) - K_1 + K_3$$

$$E = -2 * \sin(\theta_2)$$

$$F = (K_2 - 1) * \cos(\theta_2) + K_1 + K_3$$

$$K_1 = \frac{L_1}{L_2}, \quad K_2 = \frac{L_1}{L_3}, \quad K_3 = \frac{L_4^2 - L_1^2 - L_2^2 - L_3^2}{2 * L_2 * L_3}$$

The result of the first equation here is the angle between the coupler link (L_3) and the ground link (L_1), including the angular offset of the ground link. To obtain the angle relative to a vertical axis, that is, 0° being perfectly vertical:

$$\text{Relative to the ground link, } \theta_{shank} = \theta_3 - 180^\circ + \alpha$$

$$\text{Relative to a vertical axis, } \theta_{shank_true} = \theta_{shank} + \theta_1 - 90^\circ$$

This was confirmed with a simulation in Autodesk Inventor, for example, when the change in crank angle is equal to 20° , the output angle is 35° . Here, again Θ_2 is variable, but with a starting value of $\Theta_2 = 20^\circ$, due to the offset of the crank with the ground link. Hence, a change in crank angle of 20° results in an actual crank angle of 40° . The relation between the crank angle and shank angle is illustrated in the graph in Figure 4.16 below. The variation in angle occurs because when the crank L_2 moves, the point p_2 pushes the coupler link L_3 and the pivot point p_3 is constrained by the follower link L_4 . p_0 and p_1 are fixed pivot points. The centre of rotation is constantly changing, hence, denoted the Instantaneous Centre of Rotation (ICR). This is shown in Figure 4.15.

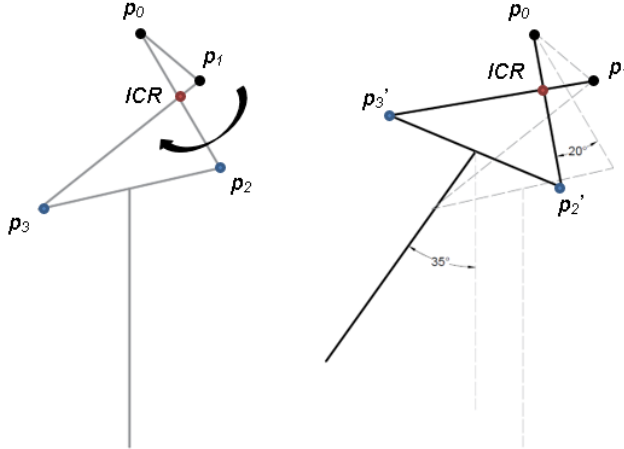


Figure 4.15: Change in pivot points and ICR

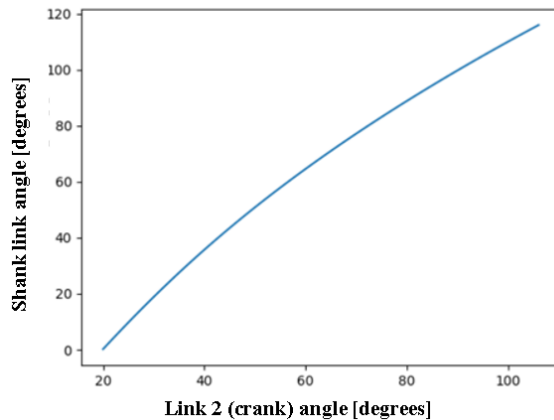


Figure 4.16: Shank angle variation with change in crank angle

4.5 Actuator Case

Now that the dimensional constraints have been analyzed, as well as the force constraints in terms of the shaft load and moment of the actuator about the knee, the actuator case can be designed. To perform an initial test, the case was created in layers, including the base and the top layer. Initially, a mechanical absolute encoder was used to monitor the angle of the actuator output.

4.5.1.1 Actuator Case Dimensioning

The dimensioning of the layer-based and inclined model is shown in Figures 4.17 to 4.20 below. The lengths are in mm and angles in degrees.

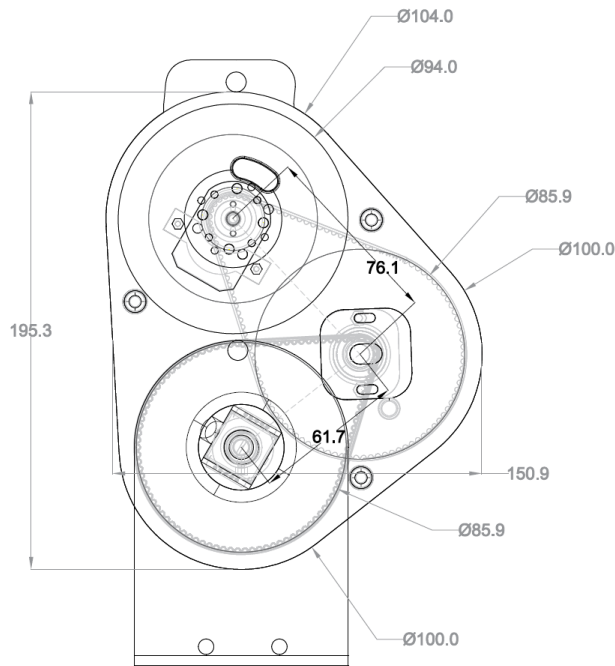


Figure 4.17: Dimensioning: Top-View of layer-based actuator

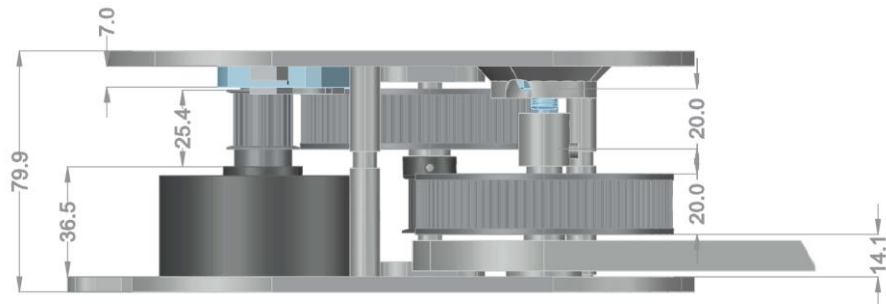


Figure 4.18: Dimensioning: Side-View of layer based actuator

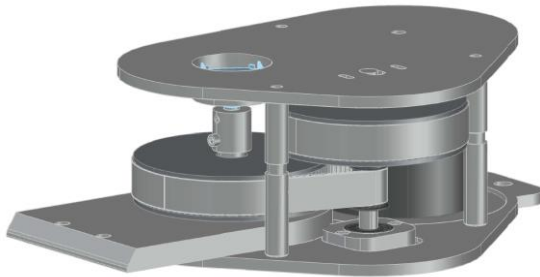


Figure 4.19: 3D Isometric Projection of layer-based actuator

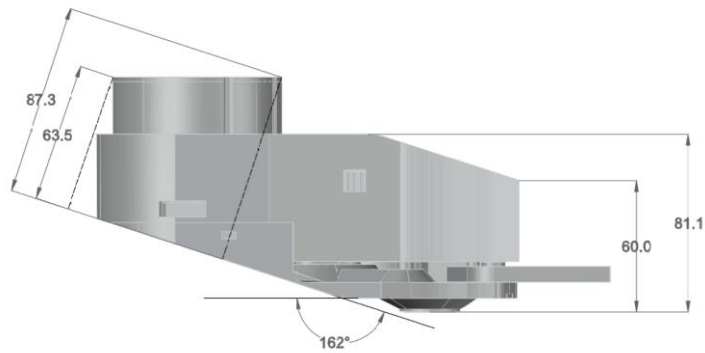


Figure 4.20: Dimensions: Side-View of inclined actuator

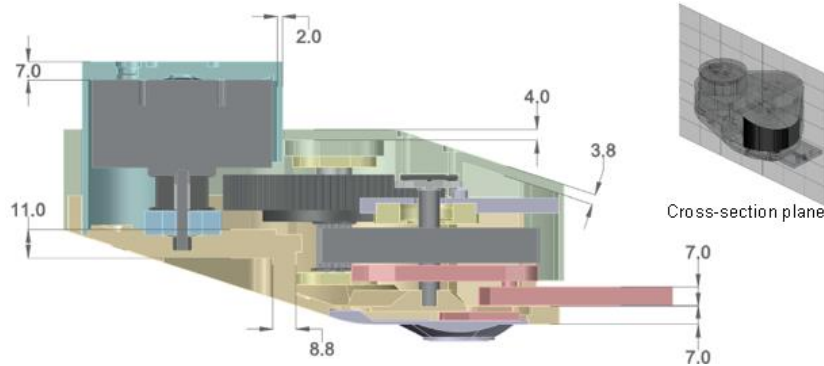


Figure 4.21: Dimensions: Cross-Section View of inclined actuator with wall thickness

In the inclined model, the dimensions from the top view remained the same, however, from the side, there is an inclination in the actuator. Overall, the same wall thickness was maintained as with the layer based model. After Finite Element Analysis (FEA), the thickness was adjusted to be as minimum as possible. Figure 8.2 in Appendix VI gives a detailed view of the parts.

In the layer based model in Figure 4.17 and 4.18, the four-bar-linkage has been excluded for the sake of simplicity, as well as the actual pulley models. Using Autodesk Inventor, an FEA was conducted. This set the base thickness which could withstand the required shaft loads from the pulley and belt system. Additionally, the motor and the four-bar-mechanism was implemented in the base part of the design.

The diameter of the actuator case was made about 14 mm greater, such that with a wall thickness of 5 mm for the sides, there is still a clearance of about 2 mm between the belt surface and the sides.

The total shaft load is distributed by the base and top layer. At the motor, the lateral forces are further distributed by the four motor support screws. As for the other shafts, they have bearing holders which are placed inside the main case.

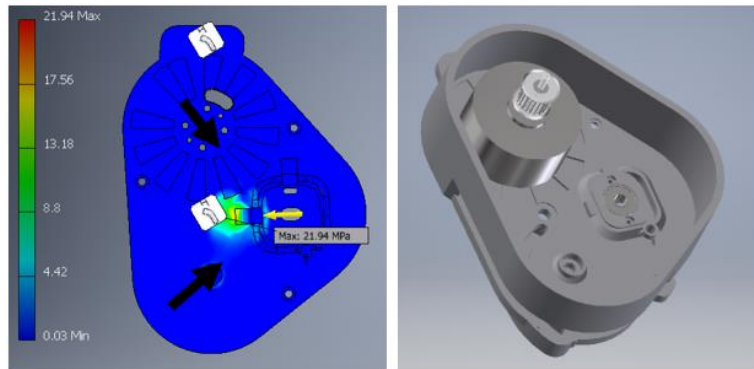


Figure 4.22: FEA on the actuator case and actual model used for FEA

In Figure 4.22, Autodesk Inventor's FEA was used as a tool to analyze the stresses in the parts made from additive manufacturing. The properties of PA 2200 or PA 12 (Polyamide 12), the material with which the parts were printed, were used with a yield strength of 53 MPa. In the first image, only the base plate with a thickness of 7 mm was tested with half of the shaft load values calculated in the previous sub-chapter. This gives the base by itself a safety factor of 2.42. The same results were obtained when the motor and the bearing holder was placed, which distributes the force over a larger area of contact.

The full exploded view of the primary design is shown in Figure 4.22. The yellow parts are the 3D-printed parts, while the blue parts represent the electronic parts. The same alignment of pulleys and centre distances are used in the final prototype model. The exploded view of the final prototype is shown in Appendix VI, Figure 8.2.

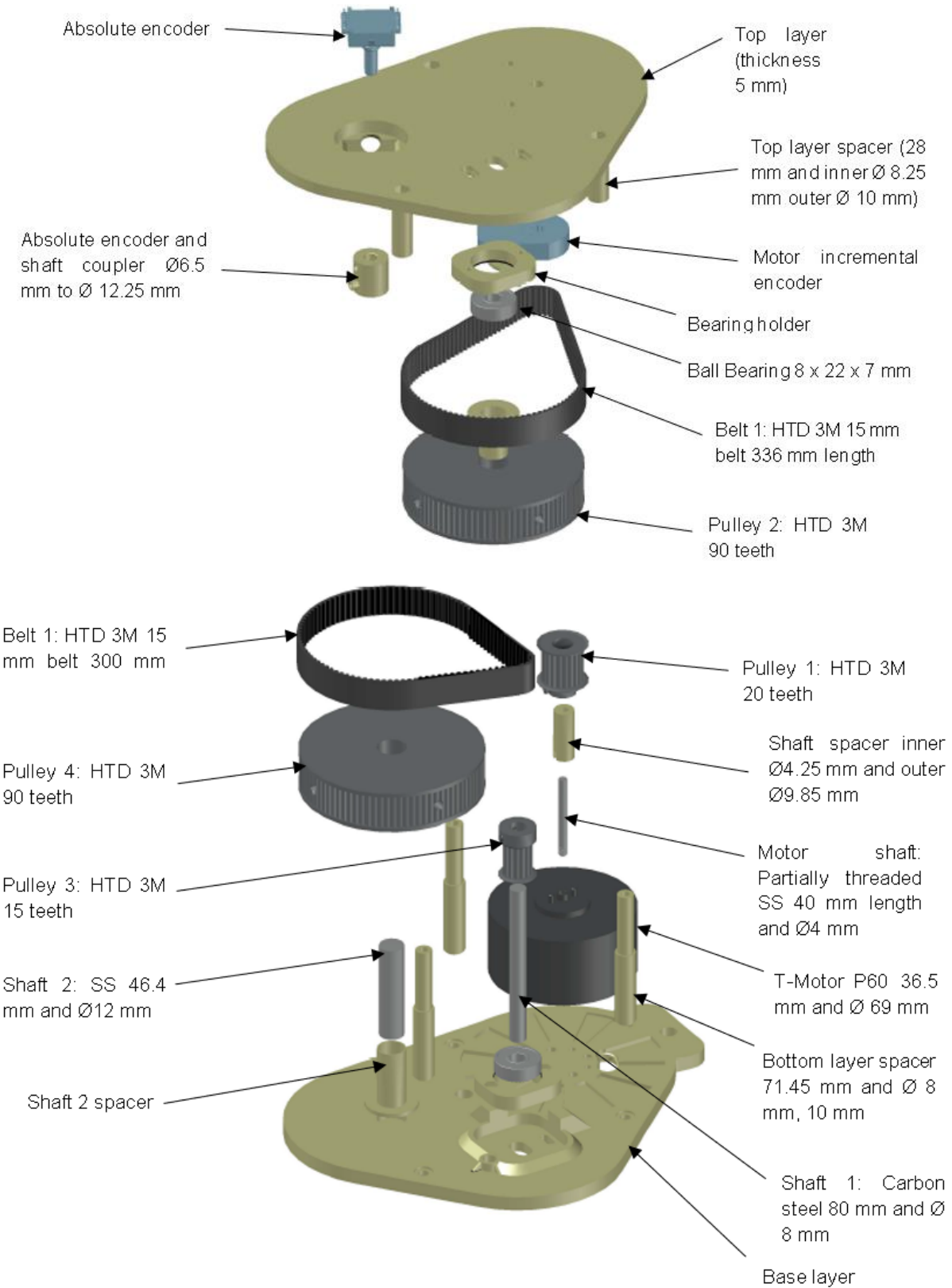


Figure 4.23: Exploded-View of layer based actuator

The placement and assembly setup for the four bar mechanism design is shown in the Figure 4.23 and Figure 4.24. The crank of the four bar was placed so as to be within the actuator case. Figure 4.25 demonstrates the rotation of the coupler link as simulated in Autodesk Inventor.

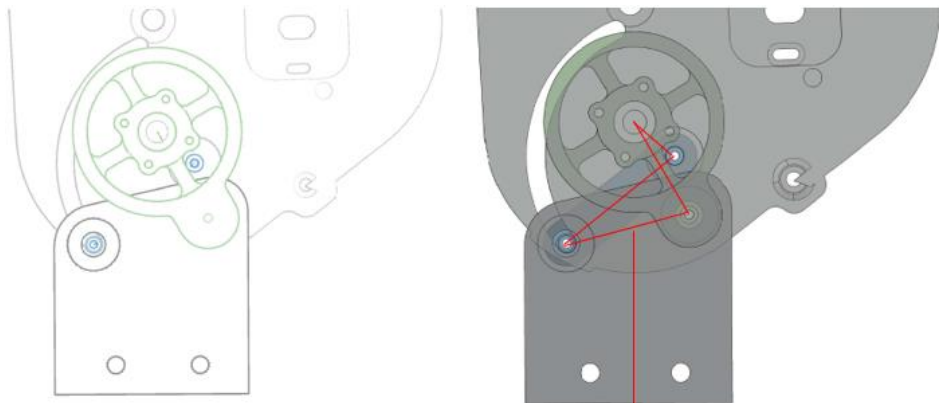


Figure 4.24: Four-bar-linkage integration in actuator case

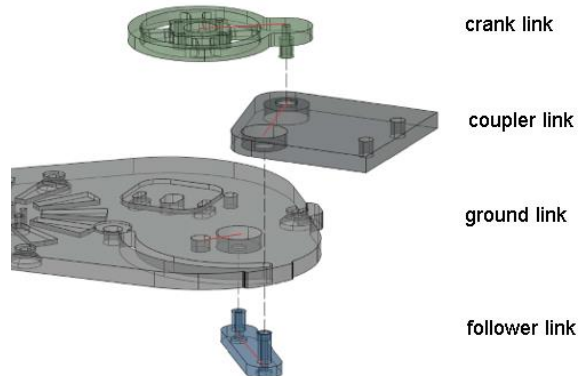


Figure 4.25: Assembly plan for four-bar-linkage and actuator case

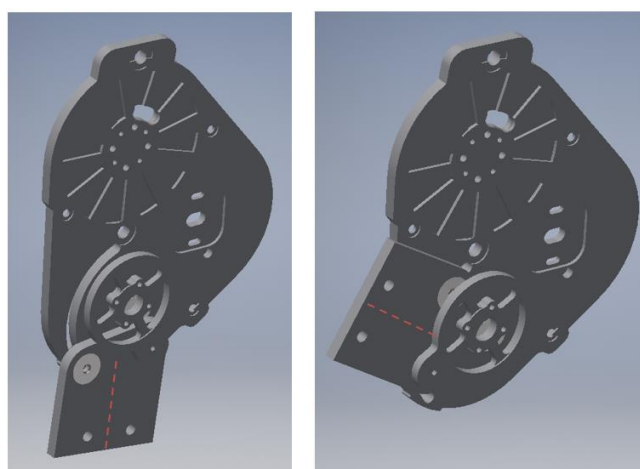


Figure 4.26: Four-bar-linkage rotation test in Autodesk Inventor

To test the strength of the four-bar-linkage, the setup was loaded on Inventor and constraints were set before a torque was applied at the crank link. The coupler link was fixed to simulate resistance. 318 lbf-in (pound-force-inch) is equal to 36.3 Nm. The maximum stress was in the connecting pins between the crank and the coupler links. However, this excludes the implementation of a stainless steel bolt which will strengthen the connection to a greater extent.

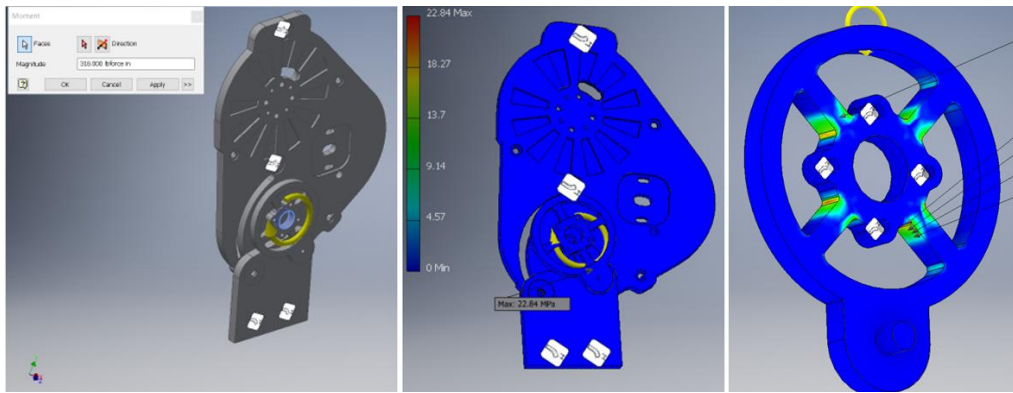


Figure 4.27: Four-bar-linkage and crank link FEA

The same torque was applied to the follower with the same results. The maximum ‘Von Mises’ stress was noted using a probe label and was about 20 MPa. Since the yield strength of PA 12 is 53 MPa, this gives a safety factor of 2.65. Generally, the four-bar-linkage is deemed safe. The maximum strain registered in the aluminum-6061 torque sensing element is 0.0027 with a minimum safety factor of 1.9.

To match the angular offset between the thigh and the shank, an inclined design had to be adopted which consisted of the same design elements of the straight design. The base of the motor was placed on the top plate so as to provide enough clearance for the inclined section.

Improvements from the primary design were resolved which as well includes:

- Replacing the absolute mechanical encoder with a magnetic frictionless encoder
- Implementing a bearing at the last link to hold the shaft load

This is discussed in the Implementation and Testing chapter as the new parts were only designed and modified in that phase of the project.

4.6 Electrical and Electronics Design

To power the motor and control its position, torque and velocity, a microcontroller is needed, together with a motor controller which will channel the current and voltage. Furthermore, the power requirements of the actuator should be determined. Therefore, electrical design is divided into the following subtopics:

- The electrical schematic
- Power requirements
- Microcontroller
- Motor controller
- Electronic components: Angle sensor and encoders

4.6.1 Electrical schematic

A full schematic of the circuit to control the motor is represented in the Figure 4.28. A complete electrical schematic with the detailed pin connections is shown in the Appendix V Figure 8.1.

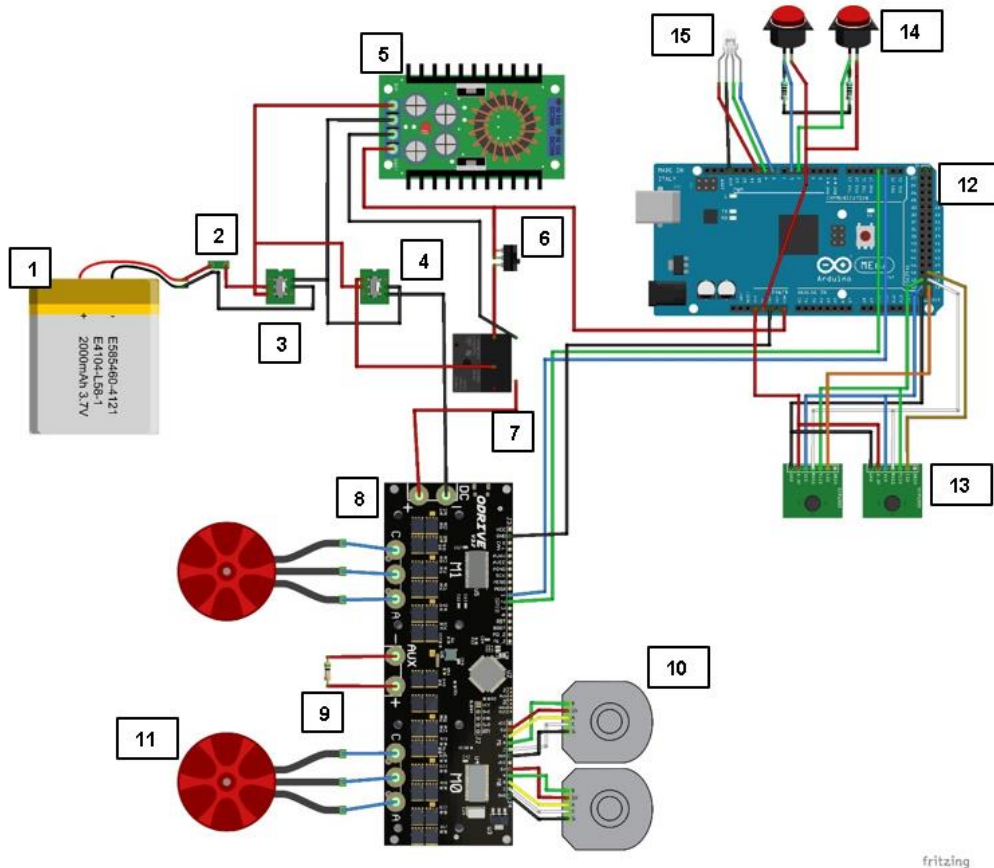


Figure 4.28: Electrical schematic for the actuator

Key:

Part Number	Part Name	Part Description
1	Battery	22.2 V, ~5000 mAh LiPo Battery
2	Fuse Holder	Fuse rating > 8 A
3	On/Off Switch	DPST or DPDT Switch rated at 10 A
4	Emergency Switch	DPST Emergency Switch at 10 A
5	DC-DC Step Down Converter	22.2 V to 5 V, 4A XL4016 Converter
6	Emergency Push Button	Latching Push Button rated at 2 A
7	Mechanical Relay	Relay rated at 10A
8	ODrive Motor Controller	ODrive v3.6 Dual BLDC Motor Controller (24V,6A)
9	Braking resistor	50W 0.5Ω Braking resistor
10	Motor Encoder	AMT-102V CUI Incremental Encoder
11	BLDC Motor	T-Motor P60 340KV BLDC Motor
12	Microcontroller	Arduino Mega 2560 Microcontroller (12V,2A)
13	Angle Sensor	AS5048A Magnetic Angle Sensor
14	Push Button	Latching Push Button (2A)
15	RGB LED	Common Anode RGB LED

Table 4.12: Electrical part names and descriptions

An Arduino microcontroller was chosen to control the ODrive controller, as well as to measure the angle sensor values. The analog sensor values can be read by the Arduino microcontroller itself or it could be fed from the Raspberry Pi or any other processing unit. While the other elements utilize the digital pins of the microcontroller, communication between the Arduino and the ODrive microcontroller is achieved by UART (Universal Asynchronous Receiver Transmitter) protocol, using the RX (receive) and TX (transmit) lines and a common ground wire. Each of the electrical components serves a specific purpose and this is discussed in the following subtopics, together with the specific parameter requirements. The motor has already been discussed in the previous mechanical design section.

4.6.2 Power requirements

The power requirement of the actuator is divided into that of the microcontroller and that of the ODrive which powers the motor. Furthermore, a 5V relay also is operated to act as a secondary emergency switch in the system.

4.6.2.1 Arduino Microcontroller

The Arduino Microcontroller operates at 5 to 12V and the current intake should not exceed 2A, depending on the number of components connected to the microcontroller. The microcontroller itself is set to be used for low current applications, since its digital pins can only output up to 40mA and its 5V V_{cc} pin can output up to 200 mA.

Since there is already a voltage regulator present inside the Arduino Microcontroller, the angle sensor is powered directly from the Arduino itself. The angle sensor AS5048A operates at 3.3 V and has an input current of 15 to 100 mA. Since two angle sensors are being used by the microcontroller, the maximum input current is just enough for the two angle sensors from the Arduino.

4.6.2.2 ODrive Controller

The ODrive motor controller operates at 24 V peak, however, lower voltages can be adopted too if required. This affects the peak speed of rotation of the motor, following the relation between speed constant and voltage. The ODrive supplies only 70% of the input voltage to the motor, thus the peak angular speed can be estimated as such:

$$\omega_{motor_peak} = 0.70 * \frac{K_v * \pi}{180} * 60 * V_{supply} \quad (4-35)$$

Where V_{supply} is the voltage input from the power supply. The speed can be limited by the controller. This is discussed later in software design.

While the current generated inside the motor windings can reach up to a permissible value of 120 A for the ODrive, the intake current is limited at 5A. There is no direct relation between the motor windings current and the intake current, however, this can be estimated by reading the power supply current or by the use of a current sensor or an ammeter at the input terminals of the ODrive controller.

An estimation of the current usage of the ODrive can be carried out based on the gait cycle of a person which lasts for one second. The peak torque requirement of the motor will only be reached for less than about 30% of the gait cycle. Hence, during that time, the current draw from the supply will reach near the peak value, while for the rest of the 70%, the current draw can be averaged at a median value 1.67 A, much lower than the peak value, as in the swing phase which last 20% of the gait cycle, there is almost no current draw that would be required. Thus, for a 1 second gait cycle, assuming continuous walking at a pace of 1 m/s:

For a peak current of 4.8 A is drawn for 0.3 seconds, while a nominal current of 1.67 A is drawn for 0.7 seconds. An estimation for the total Amp-hours can be done using:

$$Average\ current\ drawn = (4.8 * 0.3) + (1.67 * 0.7) = 2.609[A]$$

Thus, on average, the ODrive is drawing 2.609 A at 24 V. This would apply for normal walking, unless a sustained motion is maintained for longer periods of time, then the ODrive controller will draw higher average currents. Thus, to last one hour with a battery as a power supply, a battery pack of 2.609 Ah would be required. Alternatively, if a battery pack of 5 Ah is available, the actuator could operate continuously for about 2 hours.

4.6.3 Microcontroller

The microcontroller stores the main program or code which will allow the actuator to run through sequentially. The different pin out connections from the Microcontroller to the other devices are listed in Table 4.14 below. Components such as the angle sensor and the push buttons are connected to the V_{CC} of the Arduino. An Arduino Mega 2560 was used as the main microcontroller due to its higher speed and compatibility with the ODrive controller.

Component	Pin connection
ODrive Motor controller	D18 (TX1)
	D19 (RX1)
Angle Sensor	D50 (MISO – Master In, Slave Out)
	D51 (MOSI – Master Out, Slave In)
	D52 (SCK – Serial Clock)
	D53 (CS – Chip Select)
Push buttons	D5
	D6
RGB LED	D8
	D9
	D10

Table 4.13: Circuit connections of electronic components

The angle sensor was connected via SPI (Serial Peripheral Interface) protocol to the Arduino. With SPI communication, there can be several devices connected to the same MISO and MOSI pins which will be used as a bus line for data transfer. The CS_n (Chip Select n) pin is used to select which device to communicate with at any instant. In this application, the Arduino communicates with 2 angle sensors, one in each knee at any instant. SPI is chosen over I²C (Inter-Integrated Circuit) protocol since it is faster and more robust.

As for the push buttons, they are simply used as an interface when using the actuator without any other devices connected to it such as wirelessly or through RS232. The RGB LED is used for feedback if the actuator is being used stand-alone, that is, without a Serial Monitor.

4.6.4 Bourns ACE Absolute Encoder and AS5048A Angle sensor

To determine the actual position of the motor, an angle sensor is required. The motor encoder AMT CUI-102 gives positional feedback to the ODrive for precise control of the motor. However, the actuator itself requires an angle sensor to know the position of the actuator link. Without such a sensor, the output angle cannot be monitored, and the motor will spin continuously without any exterior feedback.

In this case, two types of encoders have been selected. In the final design, the AS5048A angle sensor was selected due to its improved functionality and design.

The Bourns ACE Absolute Encoder is a mechanical contacting encoder which relies on an internal contacting surface. It has a simple design which makes it easier to use, and less prone to failure. Each contacting surface has a pin out connection which connects to a digital pin of the Arduino. Alternatively, an 8 bit multiplexer was used to reduce the number of pins required on the microcontroller. The 8-bit data from the mechanical encoder is then compared to a table provided by the manufacturer to know the position. It does not require any power, and thus, it can immediately give position feedback without any initialization on power-up. The only downside is the friction since it has to be coupled to the output shaft of the actuator. It is lengthy and requires more space as opposed to the AS5048A. With 128 positions, it has a resolution of 2.81° per rotation.

The AS5048A angle sensor is a 14-bit sensor which uses hall-effect to read the position of a neodymium magnet placed on the shaft of rotation. It uses both I²C and SPI communication and has the possibility to send specific data on command. Furthermore, it has the ability to measure up to 16375 positions per rotation, about 0.02° resolution, and also provide feedback in case of errors. It has a much more complex design, and the tolerances have to be respected to get proper results. The neodymium magnet has to be placed a distance of 0.5 to 3 mm from the centre of the AS5048A chip. Furthermore, while it has the ability to set the error bits, this can also happen if there is too much noise around the data cables or even if there is a slight shift in magnetic field around the sensor. Overall, the AS5048A is much smaller and thin compared to the Bourns ACE mechanical encoder and since there is no coupling that is required, it completely eliminates the frictional resistance on the output shaft.

4.6.5 ODrive Controller

The most important part of the electrical schematic is the motor controller. The ODrive motor controller is produced by the ODrive Robotics Team, and it allows dual brushless DC motor control. It has an onboard microcontroller which stores the firmware and also allows communication via serial ports to a computer or external device so that it can be programmed and tuned. The microcontroller on the ODrive board is by STMicroelectronics (STM32F405RGT6) and it allows further communication protocols such as CAN, I²C, SDIO, SPI and UART. It has 51 GPIO pins, the majority of which is connected to the motor encoders and the motor drivers. It has an inbuilt thermistor which monitors the temperature, as well as a hall current sensor which is used to measure the motor current.

The AMT CUI-102 encoder connects to the ODrive board, which uses its pulse increments to monitor the position of the motor. In terms of the hardware, the only other additional element required is a 0.5 Ohms braking resistor which is rated at high power due to the heat dissipation. This allows the currents due to back-emf produced when the motor decelerates to flow through without flowing through the MOSFET gates and the STM32 chip. It has a fuse as well which protects the ODrive from short circuits and high currents.

A common issue called Ground Loops was encountered which will be discussed later in the implementation and testing section.

The ODrive microcontroller uses 6 MOSFET gates for the motor control. This is represented in the available schematic in Figure 4.29.

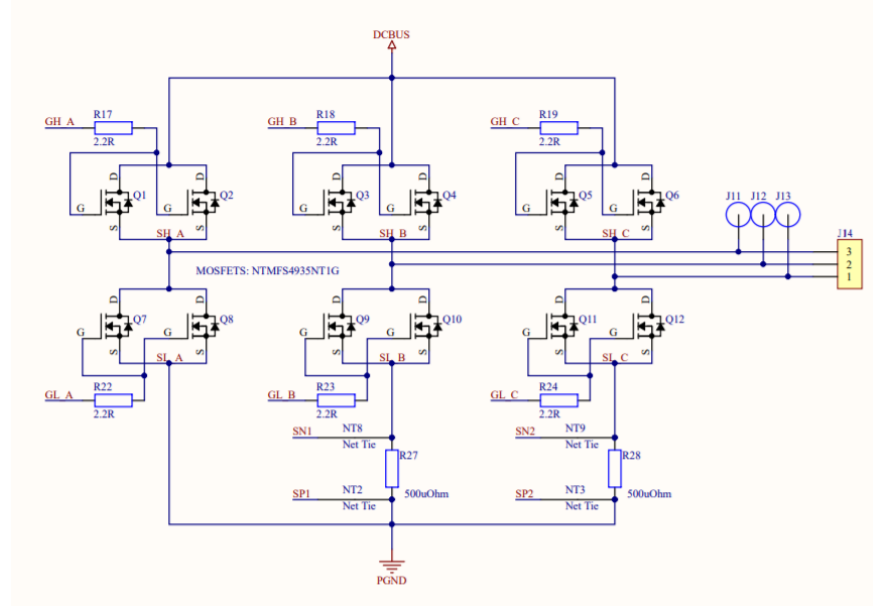


Figure 4.29: MOSFET Gates circuit in ODrive Controller (Source: ODrive Robotics)

4.6.6 AMT102-V CUI Motor encoder

The motor position encoder being used is the AMT102-V CUI. It has a high resolution of 2048 Pulses per Revolution (PPR) and can support high rotational speeds of up to 7500 rpm. It has one index pulse and two phase pulses A and B, the pinout connection of both of which are clearly indicated. The pulse signals of A lead B for clockwise rotation and are represented as follows in Figure 4.30.

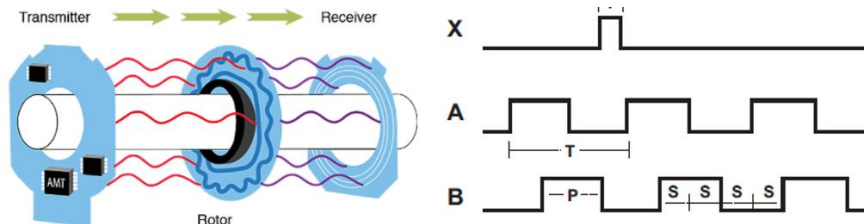


Figure 4.30: AMT capacitance based incremental encoder and signal waveform (Source: AMT CUI datasheet)

Whereby the T, P, I, and S clearly indicates the pulse waveform properties: period, pulse width, index, and state respectively. The pulses are read by a patented capacitive ASIC (Application Specific Integrated Circuit) technology. Unlike magnetic and optical encoders, they are immune to factors from the environment such as dust or magnetic fields. This is because the pulses are created by detecting the changes in capacitance through a high frequency reference signal. The capacitance changes as a rotor, which is inscribed with a specific sinusoidal pattern, spins and the transmitter is placed on one side, while the receiver on the other. This is represented in the left image in Figure 4.30 above. The signals A and B occur in the particular pattern due to the capacitance change. The encoder operates at 5V and 6mA, which is supplied by the ODrive. Its output signal is at 2 mA.

4.7 Software Design

Before the actuator can be operated, it has to be coded. The coding for the actuator consists of two different parts: the Arduino Microcontroller code, and the ODrive parameter setup. This is to be carried out through a computer with Windows OS, and in this chapter, the different programs and documentations that can be used are mentioned. It is also to be understood that while the microcontrollers operate at the machine level, codes written will be carried out by high-level languages such as C and Python. The Arduino code is broken down into:

- Sequence of operation
- Communication
- Sensor reading

The ODrive coding is categorized in:

- ODrive parameter setup
- ODrive Motor tuning

For the sake of simplicity, snippets of the actual code are displayed and the whole code is represented in terms of flowcharts throughout where possible.

4.7.1 ODrive parameter setup

The ODrive controller is delivered with the firmware pre-installed. There is the possibility to upgrade or install a new firmware and this is achieved by using the device in DFU (Device Firmware Update) mode or using the ST-LINK V2 which allows communication via USB ports to the STM32 chip on the ODrive. The language in which the ODrive can be programmed in is dependent on the device being used and there are several protocols that can be used. On Windows OS, Python is used, thus an existing Python program is required on the OS. ASCII and CAN protocol are available for communication too.

Through the ‘ODrive tools’ utility, the ODrive can be accessed via the command prompt or a terminal. Additionally, the ‘odrive’ library has to be installed for Python. From there, there is the possibility to write Python commands through the command line interface (CLI). The full documentation of ODrive commands is available online.

Since it uses Python, it has classes and objects which are installed together with the ‘ODrive tools’ utility and there are several methods also which can be used. An example of the command line from ODrive is explained so as to give a brief overview of how it works.

Considering the command:

```
odrv0.axis0.motor.config.torque_constant = 0.07
```

For example, the motor torque constant has to be identified and this is done by first creating the object ‘odrv0’ which is identified by the ‘ODrive tools’ utility. If an own script is written in Python,

when the ‘odrv0’ can be replaced by another variable name. This object has attributes such as ‘axis0’, ‘motor’, ‘config’, and ‘torque_constant’. In this case, the two motors are referred to as axis0 and axis1. And when motor parameter has to be changed, then the ‘motor’ attribute is invoked, together with ‘config’. Then finally, the torque constant attribute is changed.

Certain commands input floating point values, while others only accept known attributes or integers. For example, the first command that has to be sent to the ODrive to calibrate the motor is:

```
odrv0.axis0.requested_state = AXIS_STATE_FULL_CALIBRATION_SEQUENCE
```

and in this case, the ‘requested_state’ attribute only recognizes the known values which are all listed on the ODrive documentations page. They also have the integer values assigned to each state. For example, calibration state is ‘3’, while idle state is ‘1’. There is also a function which can be called to state the current state in which the ODrive is in.

Every time the actuator is started, the following sequence of codes are run to ensure that the proper limits are set, and the actuator runs properly:

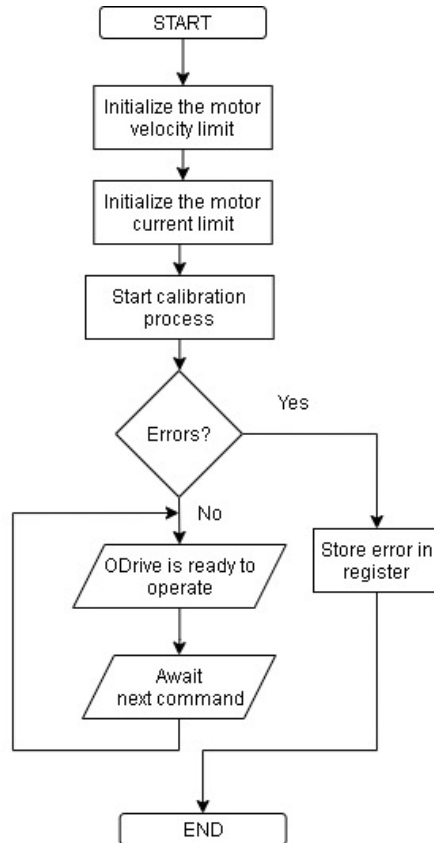


Figure 4.31: Flowchart: Actuator startup sequence

All the errors can be accessed only via the Python utility, but only some specific error codes can be retrieved using the Arduino microcontroller. Further commands are sent from the Arduino for

the actuation of the knee exoskeleton. To obtain data during testing phase, a Python script was written which reads the data over a period of time and saves it in a ‘csv’ file with timestamps spaced between 20 to 60 ms apart.

4.7.2 ODrive Motor tuning

Another positive aspect of the ODrive is that it has a built-in PID (Proportional-Integral-Derivative) control and tuning facility. The feedback loop is represented in Figure 4.32, with the motor encoder providing position feedback and the current sensor, the current or torque feedback. There is thus the possibility to also input velocity and current as shown with the velocity and current feedforward in the diagram.

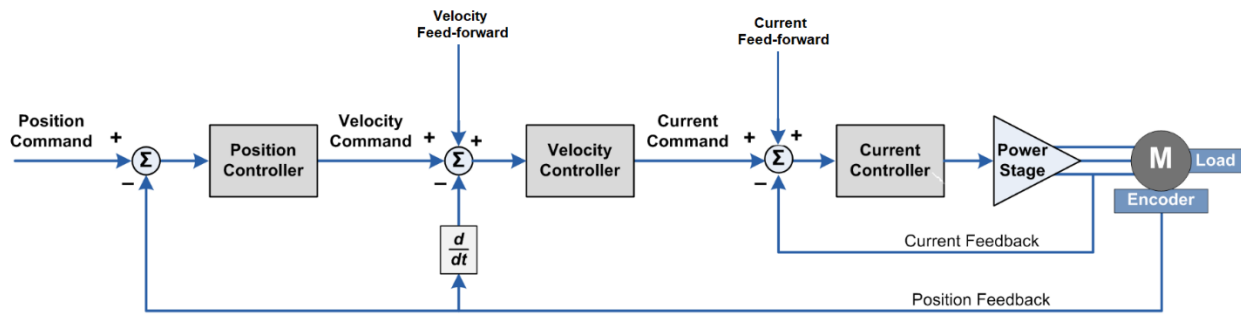


Figure 4.32: ODrive motor controller control interface (Source: ODrive Robotics)

The control mode can be selected and based on that selection, only a certain loop is activated. Some of the commands for the PID control are already set automatically, and the motor will turn smoothly when the frequency response $[\frac{1}{s}]$ is changed. A higher value means a faster and more aggressive response. This can be adjusted to obtain the desired motion. In this particular case, the tuning has to be implemented again once it is on the wearer, so as to make the motion more compliant. It can also be tested, by checking the plotted values of the position and well it adapts to an external resisting torque.

The position loop is governed by the Proportional loop (P gain) which is recognized as the ‘pos_gain’ in the ODrive tool utility. As for the velocity and the current, they include an integral gain (I gain) also. Tuning is achieved following the basic Ziegler-Nichols method.

4.7.3 Arduino Coding

The code for the Arduino is written in C using the Arduino IDE program. The Arduino libraries ‘odrivearduino’ and ‘as5048a’ were installed before any code could be written. The most critical part of the Arduino coding is decreasing the latency in the code which is easy to verify since the code loops over time and each loop has an accumulated delay. In total, there is 55 ms of delay in every code which is required. 5 ms for sending the position command and 50 ms for sending the input filter bandwidth and input mode to the ODrive.

4.7.3.1 Communication between Arduino and ODrive

One vital aspect was the communication line between the Arduino and the ODrive controller. Since UART was used, the commands `serial.write()` and `serial.read()` to send the commands via the UART lines and read data from the ODrive. The baud or bitrate defines the speed and amount of data sent to and from the Arduino. The highest baud for Arduino is 115200 bits per second or bps. And additionally, a delay of about 5 to 50 ms was set after every data transmission, so as to allow the full bits (data packet) to be transmitted and have a valid data packet sent back. There is a parity bit which is contained in the data packet and the Arduino microcontroller checks for errors by comparing the number of 1's with the parity bit. Each command byte is transferred to a series of bits which is then sent as a packet to the ODrive and the same happens in the opposite way.

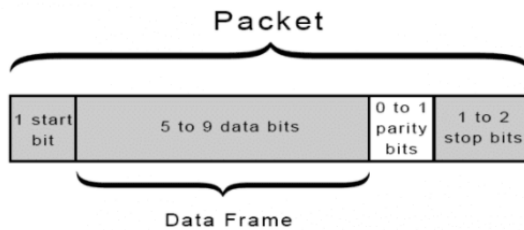


Figure 4.33: Packet description for UART communication

4.7.3.2 Reading sensor data

The angle sensor transmits the raw value which is an unsigned long value through SPI communication to the Arduino microcontroller. This value ranges from 0 to 16375, however, since only a small range of actuation is measured (0 to 90°), the values are 13070 to 16375. This is read from the line `angleSensor.getRawRotation();` where `angleSensor` is the object name attached to the chip select pin on the Arduino. This means that any data corresponding to that pin will be assigned to ‘`angleSensor`’. ‘`getRawRotation()`’ is a built-in function in the library for the AS5048A angle sensor. Since whole number integers are desired for the angle, the raw value is converted to the angle value with the map function using the line:

```
int angle = map(val,13070,16375,0, 90);
```

0° to 90° represents the crank angle. The actual shank link angle is estimated using the Freudenstein’s Equation (4-34).

4.7.3.3 Sequence of Operation

The code for the actuator to move with respect to a change in an analog input data such as a joystick was created so as to test whether the actuator could work standalone without being connected to an external device such as a computer. The Arduino code has been created to work with position control in this application, thus the motor will map the analog input value linearly.

It is represented in the flowchart in Figure 4.34 and 4.35. PB1 represents the push button to start the actuator, while PB2 is the push button to switch states. Due to the RGB led not displaying the colours well, the (r, g, b) values are noted for complex secondary colours.

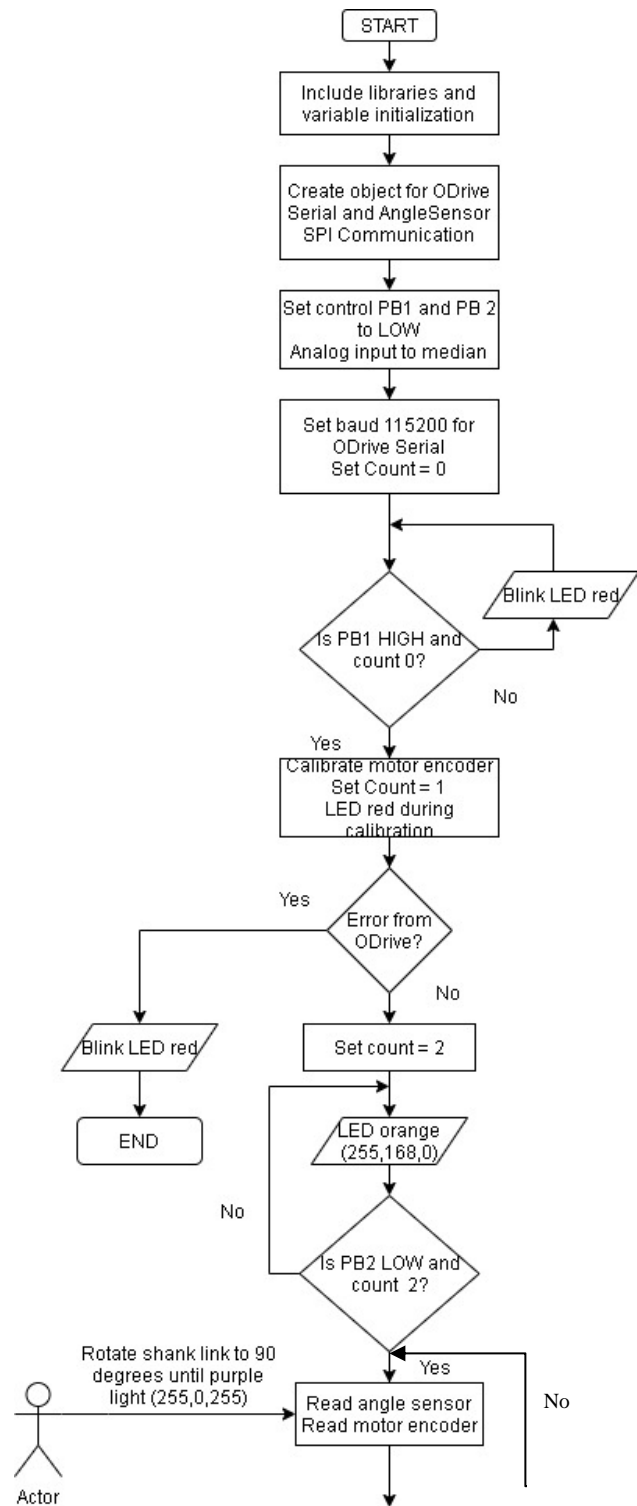


Figure 4.34: Flowchart: Actuator Sequence of operation part 1

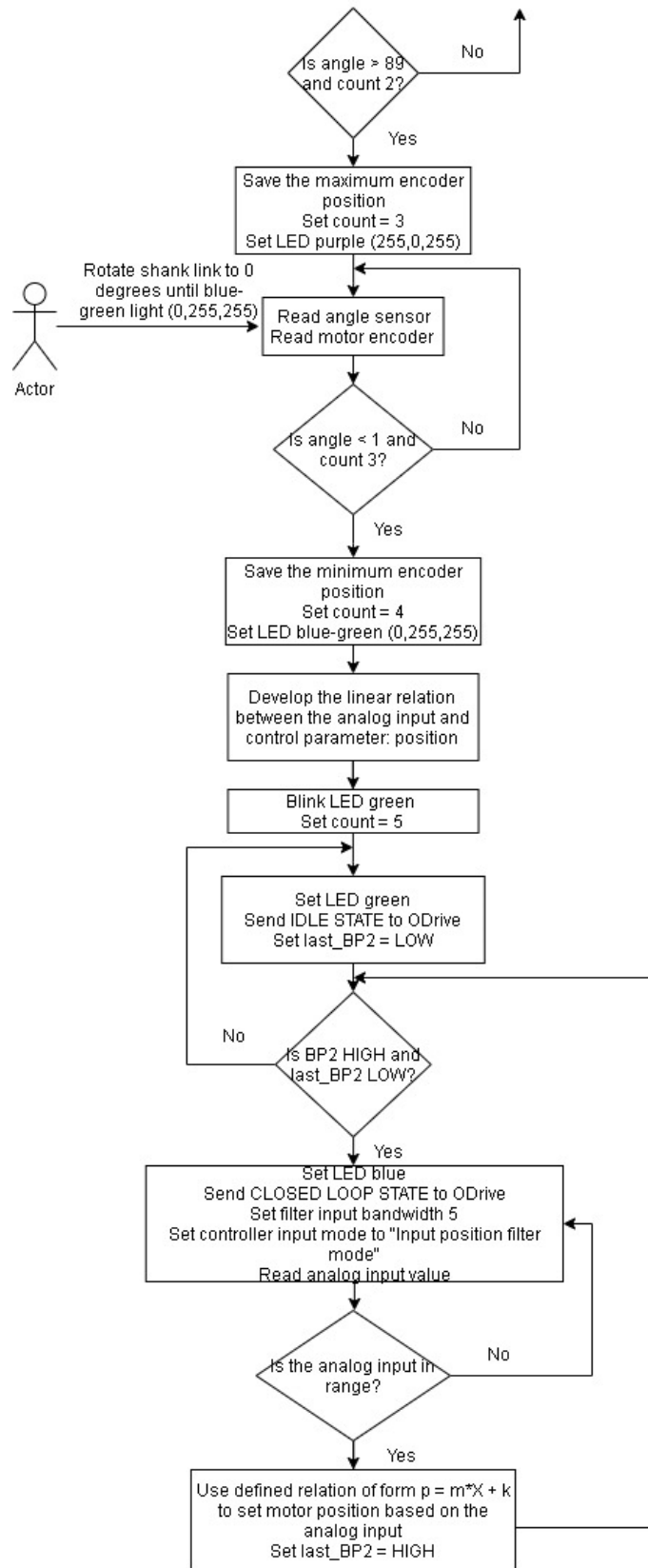


Figure 4.35: Flowchart: Actuator sequence of operation part 2

4.8 Overall final actuator

A CAD model of the overall actuator for the exoskeleton was thus achieved. This model represents certain changes which were brought about in the implementation phase, such as including push buttons for control and for emergency stop. Furthermore, the edges were fileted to give a smoother finish.

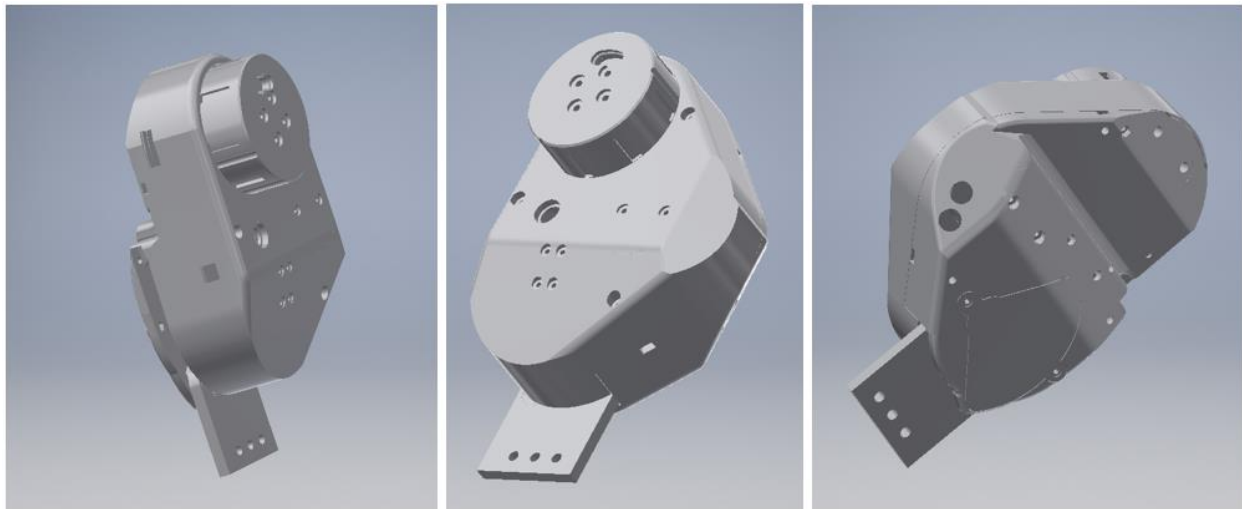


Figure 4.36: Final actuator CAD models

The actuator was designed such that it could be fitted with the exoskeleton frame. This was performed in an iterative manner to ensure a perfect fit between the actuator and the frame. A connector was designed to fit the output link of the actuator to the shank link. The exoskeleton frame was designed by student Patrick Hensel from Campus Huttthurm.



Figure 4.37: Actuator on the prosthetic exoskeleton frame

5 Implementation, Testing and Evaluation

In this chapter, the assembly of the knee exoskeleton actuator is discussed, after which test data is collected and reviewed. The implementation was carried out in different stages, primarily starting with a layer-based test model until an actuator which could be fitted to the knee exoskeleton frame was created. Similarly, for the testing, different sub parts and components were tested to check if the requirements are met. The limitations and proposed improvements as well are listed at each step in this section. In the evaluation part, the results obtained are compared with the requirements and specifications that were defined in the conceptual design phase. Furthermore, the results are justified based on the process of designing and assembling the actuator for the knee exoskeleton.

5.1 Implementation and testing

The implementation is described based on the chronological sequence in which the actuator was assembled, and not based on which part it belongs to (mechanical, electrical and software). The testing of each step is included with the implementation so as to keep the description coherent. The implementation part is broken down into the following subtopics:

- List of components
- Knee model
- ODrive and Arduino setup
- Layer based open actuator
- Inclined closed actuator models
- Actuator and prosthesis
- Active and passive test

The material used for the implementation of the test prototype is PA 2200 or PA 12 (Polyamide 12) and the process used were SLS and MJF (Selective Laser Sintering and Material Jet Fusion) respectively. The printers used were the HP Jet Fusion 4200 and the EOS P100/P110. Some related parameters are described in Table 5.1.

Parameter	EOS P100/P110	HP Jet Fusion 4200
Process	SLS	MJF
Printing space	200 x 250 x 330 [mm ³]	389 x 284 x 380 [mm ³]
Layer thickness	0.1 mm	0.08 mm
Material	PA 2200	PA 12

Table 5.1: Additive Manufacturing process and material

The surface finish of MJF is much better than SLS due to the lower layer print height. Tighter tolerances can be achieved too, however, for each printer the dimensions have to be readjusted for fitting parts with tight tolerances. With reference to the images in this section, the darker coloured parts are from MJF, while the lighter ones are from PA 2200 made by SLS.

5.1.1 List of components

A summary list of all the components used for the test prototype assembly is included Table 5.2, together with their quantity, cost, and total mass.

This list accounts for one knee, as the test prototype was created for one knee only. Parts highlighted in grey do not form part of the final test prototype.

Electrical and Electronics Parts				
No.	Part Name	Quantity	Mass [g]	Cost [EUR]
	Arduino Mega2560 Microcontroller	1	52	38.00
1	ODrive Motor Controller	1	81	159.00
2	CUI AMT102-V Incremental Motor Encoder	1	20.5	39.00
3	T-Motor P60 340 KV BLDC Motor	1	369	75.50
4	ams AS5048 absolute encoder	1	12.3	13.87
5	T-Motor P80 III 120 KV BLDC Motor	1	635	200.00
6	ACE Bourns Absolute encoder	1	18	7.66
7	Battery	1	565	132.00
8	ADUM1201 Digital Isolator	1	15	6.28
9	Emergency Push Button	1	55.3	9.78
10	ON/OFF switch	1	20	4.80
11	Fuse Connector	1	-	8.00
12	Push buttons	2	-	1.40
13	RGB LED	1	-	5.00
14	XT 90 and latching 4-pin connectors	-	-	12.00
15	DC-to-DC Buck Step Down converter	1	80	9.00
16	Battery Voltage level indicator	1	60	13.00
Mechanical Parts				
No.	Part Name	Quantity	Mass [g]	Cost [EUR]
1	20 teeth 9 mm width 3M HTD Pulley 1	1	10.4	8.61
2	Pulley1 shaft	1	3.00	-
3	Cylindrical bush slotted version 5 x 7 x 5 mm	1	0.700	0.42
4	608 ZZ ball bearing (8mm bore)	3	36.6	3.75
5	90 teeth 9 mm width 3M HTD Pulley 2	1	179.7	24.97
6	90 teeth 15 mm width 3M HTD Pulley 3	1	11.0	6.55
7	Pulley2-3 shaft	1	23.5	5.11
8	90 teeth 9 mm width 3M HTD Pulley 4	1	141.1	24.97
9	Neodymium magnet	1	-	-
10	Pulley4 shaft	1	17.5	-
11	626 ZZ ball bearing (6mm bore)	3	23.7	3.48
12	HTD Belt 3M 15mm 300 mm length	1	13.2	6.23
13	HTD Belt 3M 9mm 336 mm length	1	9.00	4.59
Additive Manufacturing Parts				
No.	Part Name	Quantity	Mass [g]	Volume [mm ³]
1	Actuator top cover	1	140.1	150679.26
2	Middle plate	1	28.8	30927.51
3	Motor holder	1	52.1	56029.79
4	Bearing holder 1	2	5.00	5391.38
5	Bearing holder 2	1	4.20	4469.99
6	Actuator base	1	204.8	220250.56
7	Actuator base follower link cover	1	6.90	7418.39
8	Actuator crank link	1	10.7	11546.82
9	Actuator shank link	1	25.5	27398.86
10	Actuator follower link	1	2.90	3160.17
11	Angle adapter (testing)	1	56.2	60431.3
12	Shank adapter (testing)	1	52.0	55895.36

Table 5.2: Summary list of components used

The cost for the components for one actuator itself is 230 EUR, excluding the printing costs and shipping costs. The cost for the control and power supply is about 400 EUR. The total mass of one actuator alone is 1352 g, excluding fastening elements. The mass can be rounded off to 1375 g. Including the peripheral devices, control and power, the calculated mass is 928 g.

The total price is an approximate due to shipping cost and the purchase quantities having been single units which is higher than if parts are purchased in larger orders. Fastening elements and connecting wires were also not included in the list.

5.1.2 Knee model

Prior to the implementation of the knee exoskeleton actuator, the mechanical calculations have been outlined, including the fact that the knee actuator rotates based on the profile of the four-bar-linkage mechanism. Nonetheless, to test the basic movement of the actuator, a normal hinge could still be used. However, the pivot point on the shank part translates as the knee rotates.

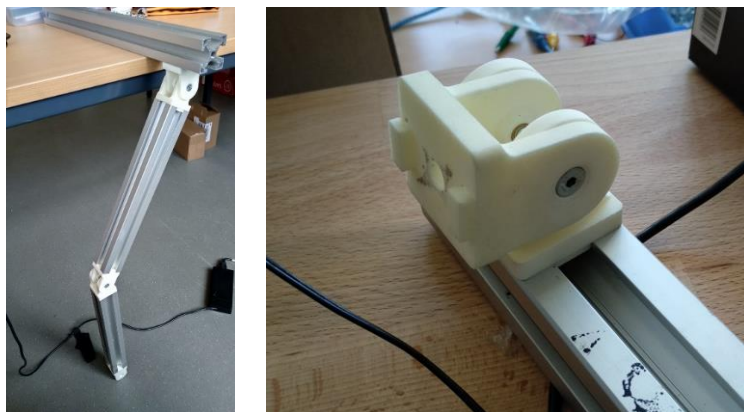


Figure 5.1: Knee model with aluminum extrusion and single axis hinge

This was developed with an aluminum extrusion, together with a 3D printed one-axis hinge. The lengths of the thigh and shank were both 30 cm. The primary purpose of this model was to test not only the motion of the knee, but also to measure the torque output.

5.1.3 ODrive and Arduino setup

The ODrive controller was connected directly to a computer with Windows OS so as to set up the parameters for the motor.

Prior to testing the ODrive with the first version of the actuator, the motor was already connected, and some parameters were set. These include setting the maximum motor current to 40 A, and the maximum motor velocity to 10 turns/s (3600 degree/s or 600 rpm). This ensured that the motor does not spin too fast and could also be controlled based on its position. Additionally, the mechanical encoder was tested in to ensure that a proper reading was being registered by the Arduino microcontroller.

The ODrive and Arduino UART connection through the RX and TX lines were tested successfully. However, after several operation cycles, the ODrive did not respond at all. This was due to the fact that the UART pins of the ODrive had been damaged or the STM32 microcontroller had experienced a fault which resulted in the boot process not to occur as it should. Operation using the Device Firmware Update (DFU) mode was possible and a new firmware was loaded on the ODrive. In normal operation, the ODrive could still be communicated with.

The issue arose because of ground loops which happened between the Arduino and the ODrive. Ground loops occur due to a potential difference between the supply voltage's negative terminal and that of the other peripheral device, such as the Arduino. It could also occur with the ground wire of the USB cable connected to a computer. The potential difference exists if the power supply leads are too long which gives rise to unwanted inductances, hence, changing the voltage level of that ground lead connecting to the negative terminal of the ODrive. The ground lead connecting to the other device has a different voltage level. Since a ground connection is required between the Arduino and the ODrive for UART communication, this potential difference causes a current to flow in the ground wire. If it surpasses the minimum tolerable current, it damages or disrupts the UART interface.

The solution is to use shorter lead wires if that is permitted or to use digital isolators which can cope with the high speed data transfer between the Arduino and the ODrive. One such isolator is produced by Analog Devices and is the ADUM series (ADUM 1201). Texas Instruments supplies digital isolators as well which are more robust.

5.1.4 Layer based actuator

A layer based actuator was developed with the sides open so as to provide an aid for visual inspection of parts during motion. It would help identify errors as well as improvements in the design of the actuator.

The parts of the actuator were created as a base and top layer, which hold the bearing holders and the shaft for the pulleys. The top part holds the absolute encoder for angle determination and the motor encoder. The base layer holds the motor and the four-bar-linkage. Initially a middle layer was included in the design which was discontinued in the implementation due to redundancy. The three layers were made with PA12 and were sturdy with a 5 to 7 mm thickness.

The motor was fixed first, together with the axle which was a partially thread M4 screw with the head sawed off. Since the bore diameter for the smaller 20 teeth pulley was larger, a printed spacer was used. The encoder is coupled tightly with the shaft using the appropriately sized sleeve which they provide. This sleeve clips onto the encoder shaft to reduce slippage and errors. The base plate, top plate and the encoder sleeve are labelled in Figure 5.2.

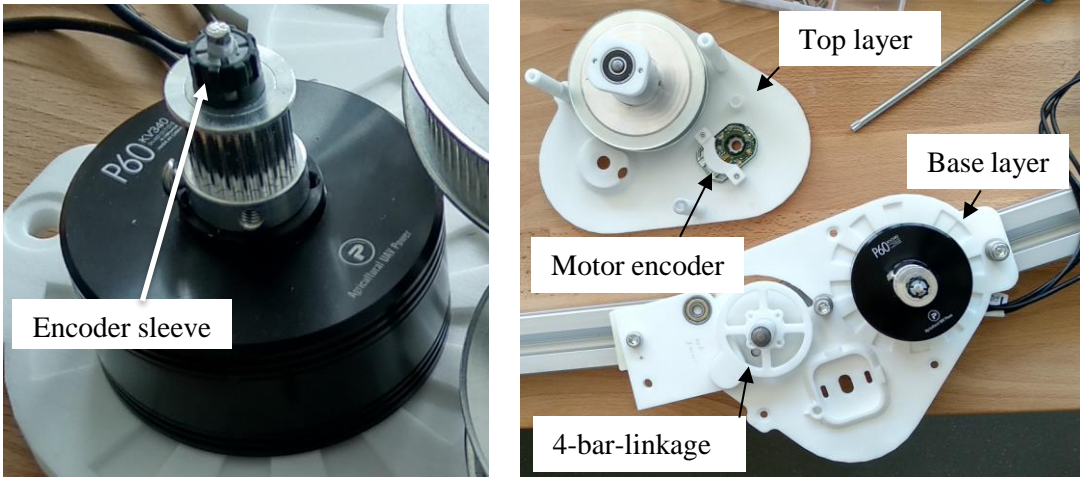


Figure 5.2: Motor with pulley and encoder sleeve on base-plate

Other components on the base plate include the bearing holder for the first 8 mm shaft, and that of the second 8 mm shaft. Initially an 12 mm shaft was used to account for the larger bore diameter of the larger 90 teeth pulley. The alternative was to use a spacer to bridge the gap in the diameter. Given that the pulleys had an extended support around the bore, there was no need for a spacer.



Figure 5.3: Pulley and shaft assembly on base-plate

The bearing holder was placed at the position to allow a loose belt initially, which was then pushed further to increase the centre distance and belt tension. Figure 5.3 shows the motor and pulley assembly on the base layer. Figure 5.5 shows the top layer and the complete assembly.

The four-bar-linkage elements which consists of the ground link, crank link, coupler link and the follower link were all 3D-printed. The ball-bearings were fitted inside the printed parts by press-fitting them with a bench-vice.

The crank link was fitted first onto the pulley, which is then slided onto the shaft 2. The pin of the crank link was press-fitted inside the bore of the bearing of the coupler link. The follower link was then fitted from the back. Figure 5.4 shows the installed four-bar-linkage.

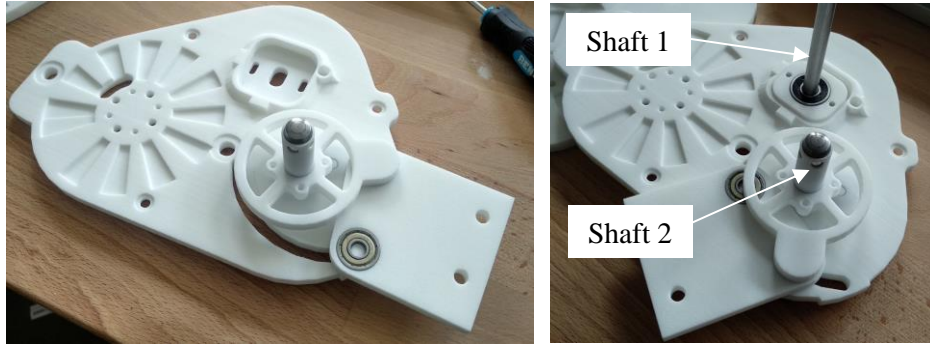


Figure 5.4: Four-bar-linkage at extended(left) and flexed(right) position



Figure 5.5: Top-plate with motor and absolute encoder and shaft coupler of absolute encoder

In the top layer, the mechanical absolute encoder was placed, as well as the coupler to connect to the shaft as shown in Figure 5.5. The motor encoder was also fitted in the debossed area. Three printed spacers were used to maintain a proper clearance between the base and top plates. An 80 mm M4 screw was used to tighten the two layers. When fitting the two plates together, the encoder sleeve was ensured to properly mesh with the holding teeth on the encoder bore.

The first step was completed, and the electrical wiring was done. The motor encoder connects with a latching pin connector to the ODrive board, and the motor leads are screwed onto the ODrive board. As the power source for the ODrive, a power supply set at 24 V and 4 A was used. Figure 5.6 below provides another view of the completed layer-based model.



Figure 5.6: Layer-based actuator prototype

5.1.5 ODrive and actuator testing

5.1.5.1 First tests – Speed and jerkiness

Initially, based on the motor encoder position, position values were sent to measure the absolute encoder angles. This allowed the testing of the four-bar-linkage to verify that the rotation occurs without any hindrances. Additionally, the belt-and-pulley system was inspected the same way.

The first motion test was performed by connecting the actuator to the knee model and clamping the hip part of the knee fix to the laboratory table. Thus, the angle of rotation could be measured, and it was achieved using the absolute encoder and the Python code which determines the output angle based on the crank angle.



Figure 5.7: First prototype model position and speed test

Figure 5.7 above shows the different rotation angles of the actuator. The speed was tested by setting the input filter bandwidth for the PID which varied the response time of the system. Greater accelerations increased the reluctance of rotation due to the higher inertia of the larger pulleys. This was adjusted by varying the PID gains set by ODrive, and by measuring the current spikes that resulted because of braking. The end goal was a faster acceleration, and lower deceleration to lower the effects of inertia. Based on the data of the peak speed obtained, together with the timestamps, the peak acceleration was estimated at 1772 degree/s². With a smaller response time, the acceleration and current change rate was greater as shown in Figure 5.8. (Orange line is motor velocity and blue line is motor current).

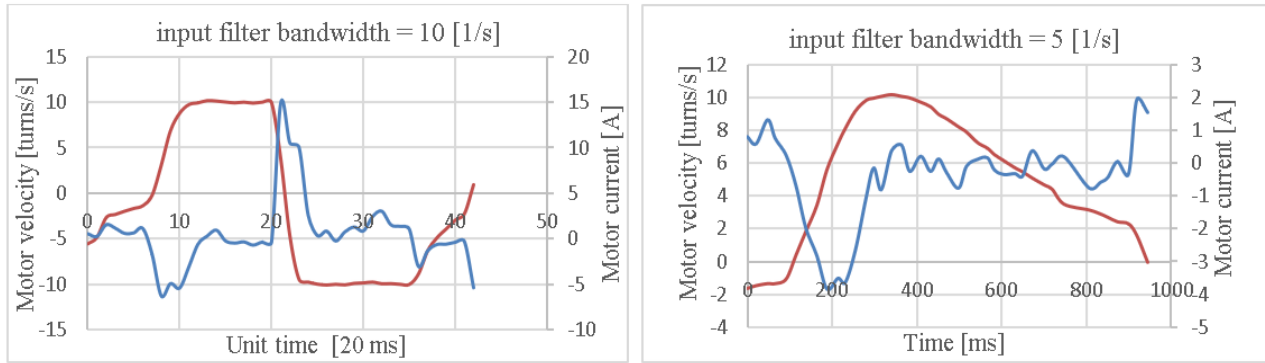


Figure 5.8: Motor speed and current at different filter bandwidth

At each instant braking occurs and there is a change in direction, there is a current change in the opposite direction which occurs because of the inertia that the pulley has. This process has to be repeated continuously until the actuator is tested with a better model, such as the human knee to obtain better results as the inertia of the knee model affects it too. In this case, the knee model spins freely without any positive or negative torques on the shank link.

The gains in ODrive can be adjusted with the following commands and they have been set with the following values:

Position gain: `odrv0.axis1.controller.config.pos_gain = 10.0`

Velocity gain: `odrv0.axis1.controller.config.vel_gain = 0.24`

Acceleration gain: `odrv0.axis1.controller.config.vel_integrator_gain = 0.36`

This was adjusted with the popular Ziegler-Nichols method and depending on the type of motion that is required or the weight of the shank, it can be adjusted, since the inertia of not only the gears, but that of the shank of the wearer affects the output motion. An added 420 g to the shank link also yielded desirable results. In Figure 5.9, a 7 moving point average shows the motor velocity in red, while the motor current is represented by the solid blue line. The velocity change is smooth, depicting a smooth acceleration.

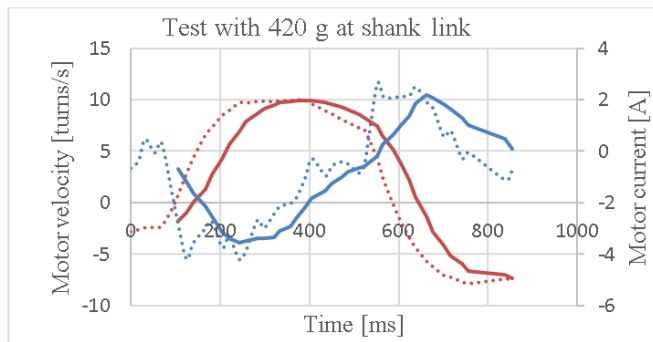


Figure 5.9: Test with a 420 g weight added to the shank link

With the ODrive controller, there is also the possibility of using trajectory control, shown in Figure 5.10, which sets predefined motions with a certain position, velocity, and torque command. The output is something similar to this, where the orange line is the velocity, and the blue line is the position change.

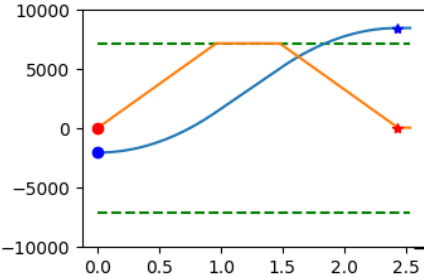


Figure 5.10: Trajectory control by ODrive controller

The following commands were used during testing and can be adapted to a sensor value which will change the parameters listed, namely the velocity limit, acceleration limit, deceleration limit and the inertia.

```
odrv0.axis1.trap_traj.config.vel_limit = 14.0
odrv0.axis1.trap_traj.config.accel_limit = 2.0
odrv0.axis1.trap_traj.config.decel_limit = 1.10
odrv0.axis1.controller.config.inertia = 1.0
```

The inertia configuration changes with the load and mass of the system and was changed sparingly in relation to the inertia calculations of the belt and pulley design from Detailed Design. Another benefit of trajectory control is that the position can be moved not only with a basic position input command, but in increments from a previous position using:

```
odrv0.axis1.controller.move_incremental(pos_increment, from_goal_point)
```

The only downside with trajectory control is the control from the Arduino and the sensor, as the sensor parameters have to be defined properly so it can be used well. For example, if an EMG sensor identifies that the muscle contraction demands a certain position, or torque level, then the motor position or torque setpoint can be applied relative to a previous command, such that there is no median value or average value. The previous sensor value becomes the old set point or goal point. This can be achieved with a C code via Arduino as well but was not implemented due to time constraints.

The peak speed of 360 degrees/s at the output link was confirmed. The motor encoder AMT-CUI 102 can record the approximate velocity of rotation. A simulated swing action of the shank was thus recorded which is shown in Figure 5.11. The peak speed was 27 turns per second (or 1620

rpm) at the motor. With a 27:1 speed reduction, it amounts to 360 degrees/s. However, the average speed was not constant since the speed is varied due to the variation in the four-bar-linkage.

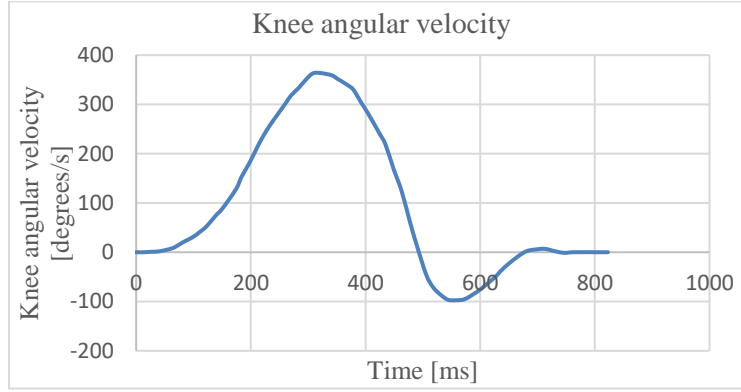


Figure 5.11: Peak knee angular velocity

5.1.5.1.2 Torque test:

Another test which was performed was the peak torque measurement. For this setup, besides the current sensing element in the ODrive, an electronic scale was used. Since the peak estimated torque is about 20 Nm, and the aluminum link was 30 cm or 0.3 m in length from the axis of rotation to the point of contact, an estimated maximum $\frac{20}{0.3} = 66.6 \text{ N}$ or 6.79 kg of weight force was expected. A scale with a resolution of 0.001 kg and which can withstand up to 20 kg was used.

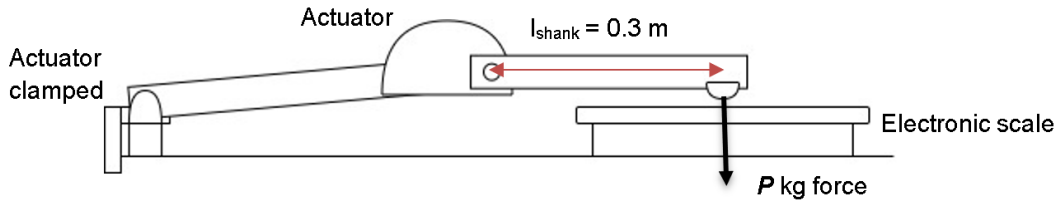


Figure 5.12: Actuator torque test schematic

The torque of the actuator is measured using:

$$\text{Torque } T_{\text{actuator}} = l_{\text{shank}} * P * 9.81 \text{ [Nm]}$$

Where $l_{\text{shank}} = 30 \text{ cm}$ or 0.3 m and P is the measured force in kilogram force.

The thigh part of the knee model was clamped securely to the table, while the end of the shank link was placed on a scale which was zeroed out. The torque was tested by increasing the set position of the motor values further from the actual values which following the PID loop from ODrive should increase the current set point further as well, hence, increasing the torque.

Alternatively, the torque set point could have been changed, but the ODrive does not have a closed loop position control in the torque control mode, hence only an impulse is given which cannot be recorded with the scale. The actual setup for the test is shown in Figure 5.13.



Figure 5.13: Actuator torque test with electronic scale

The command to set the position through ODrivetool utility:

```
odrv0.axis0.controller.input_pos = 1
```

The position value was determined at scale value being zero to be 1 turn. It was then increased in increments. A torque at peak power was obtained by setting a value of 10 turns.

The current measurement was achieved with the command:

```
odrv0.axis0.motor.current_control.Iq_measured
```

The torque of the motor is measured using Equation (4-1):

$$Torque T_{motor} = I_{motor} * 0.03 [Nm]$$

The torque of the actuator is then

$$T_{actuator} = f_{four-bar-linkage}(T_{motor} * 27) [Nm] \quad (5-1)$$

Where 0.03 [Nm/A] is the K_T value. The value of the motor torque constant is calculated from the speed constant (340 KV or 35.6 rad/s) to be about 0.0281 Nm/A. However, tests and measurements showed that this value is higher. The source could be an error or noise in the current measurement from ODrivetool. It could also be the thigh link not being grounded properly. Hence, the torque constant is adjusted to be approximately 0.03 Nm/A.

$f_{four-bar-linkage}$ (*Torque*) in Equation (5-1) is the function for the four-bar-linkage to calculate the actual output from the torque at the fourth pulley. It is derived from the equations' matrix (4-32).

The scale readings were then measured, together with the current values from the current sensor in the ODrive. These were then compiled and compared to deduce if the actual torque increase was effective. The result is displayed in Table 5.3 for the two instances where torque was measured.

Angle position of knee [degrees]	Measured Motor Current [A]	Motor Torque Value [Nm]	Calculated Actuator Torque [Nm]	Measured Actuator Torque [Nm]	Difference in Actual vs Calculated value [Nm]
Close to 0 (20)	6.90	0.2070	2.891	2.980	0.089
Close to 90 (70)	5.77	0.1731	4.427	4.680	0.258

Table 5.3: Current and torque measurement

The graphs in Figure 5.14 represent the function $f_{\text{four-bar-linkage}}(\text{Torque})$ with the calculated actuator torque with respect to the crank angle.

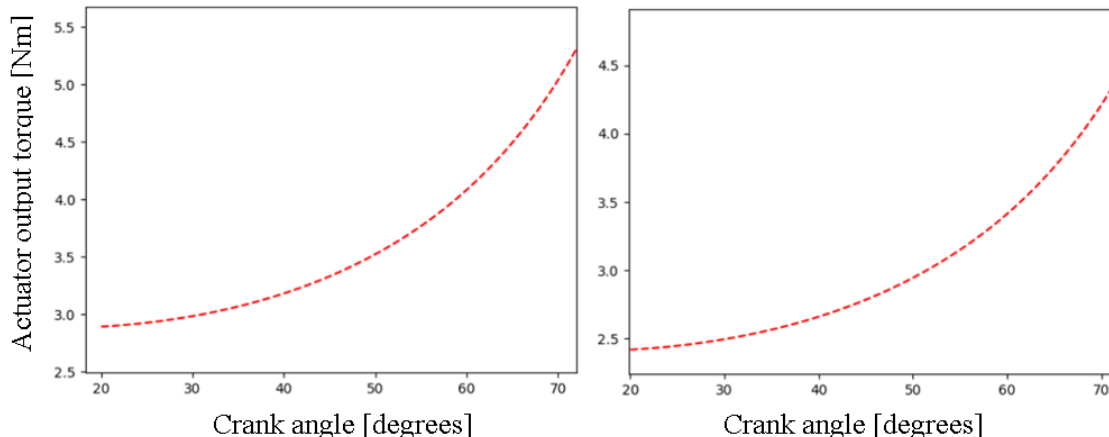


Figure 5.14: Change in four-bar-linkage torque (peak current 6.90 A left and 5.77 A right)

Hence, this confirms that the peak torque could be applied. The decreased in the output torque is also because of the elasticity of the belt at higher peripheral forces which causes the elongation of the belt. Furthermore, in the first model, belt slippage occurred, hence the true current value could not be measured.

The torque reduction because of the four bar mechanism was confirmed as well. The scale test was performed at a knee angle of 0 degrees; thus, the total torque was about 65% of the actual torque output. To confirm that there is an increase in torque, close to 90 degrees of crank angle was tested which resulted in a higher torque of about 94% of the supposed peak torque. The setup is shown in Figure 5.15.



Figure 5.15: Torque test at an angle close to 90°

Initially, the four bar elements were not fastened at the pivot points to decrease the friction between the SLS parts. However, in the design improvement, a 6 mm bore washer was used which reduced the coefficient of friction between the contacting parts. Furthermore, it allowed a bolt and nut to be used to fasten the pivot points, hence, there was almost no sideways translation and twisting of the links, in particular the follower link. The follower link was also exposed which could pose a hazard as a pinch point, or even endanger the actuator's operation.



Figure 5.16: Exposed follower link underneath the base plate and damaged absolute encoder

Another issue was the mechanical encoder which was initially supporting the half of the secondary shaft's radial and axial loads. After some time, there were errors in the encoder reading and eventually, the base of the encoder which holds the contacting plates were broken. The middle layer which was part of the first model was fitted, however the tolerance was wrongly determined and there was contact between the pulleys and the 3D-printed part. An additional bearing had to be installed which would further increase the height of the actuator, hence, the mechanical encoder was excluded from the design and replaced with the AS5048A angle sensor. These were improved in the next design – inclined closed actuator.

5.1.6 Inclined closed actuator

Once the actuator with the open model was tested and confirmed values for the torque and speed were obtained, the next iteration was to implement the inclined actuator. This test prototype model represents the same design which could be used for the final prototype of the actuator as it eliminates any openings, making it safer for the user as there is no access to the moving belt and pulley inside. It is also more robust since the sides are lined with a wall of 5 minimum thickness, unlike spacers in the first version.

The new inclined design had the following assembly procedure and improvements. The base of motor being fixed on the other side of the actuator, a motor holder was designed which was fitted with the proper tolerance. The first belt was installed first, before the motor is installed. Screws were used, together with nuts to fasten the motor in place and there are three teeth on the circumference of the motor holder to hold it in place and prevent it from moving. The four-bar-linkage was installed, and the follower link has a cover which prevents it from being a hazard.

Similar to the layer-based model, the belt and pulley, together with the shafts were then fitted inside the bearing, which is held by a bearing holder. The larger pulleys were machined with a lathe to remove any excess material so as to reduce its overall weight.

The mechanical encoder, with the shaft coupler were replaced by the AS5048A angle sensor. It was fitted with the four bolts, and a spacer is placed on the shaft which effectively keeps a clearance of 2 mm to the magnet found on the second shaft. Another bearing press fitted in a bearing holder is used to provide a smooth rotation of the shaft. 6 mm bore washers were used as spacers to ensure there is no additional friction between the four-bar-linkage pivot points and between the actuator case.

Figure 5.17 shows the change from the layer-based model to the inclined model. The motor rotation also can be seen.

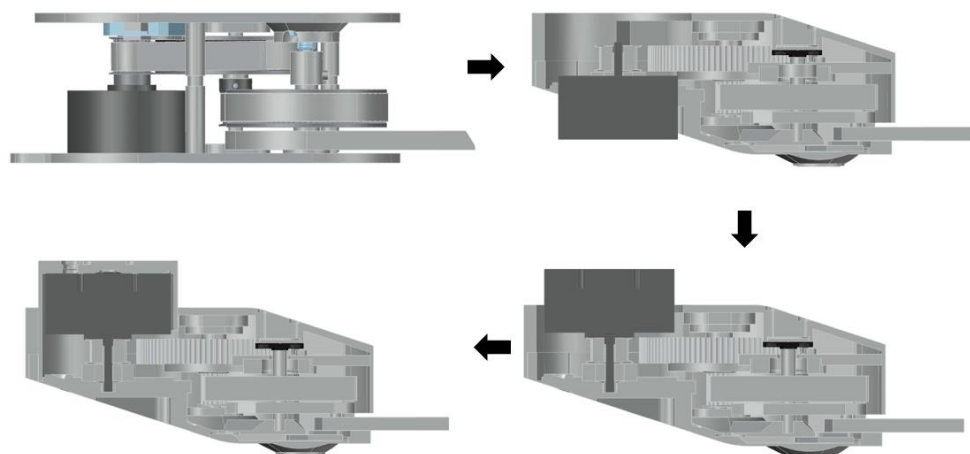


Figure 5.17: From layer-based to inclined actuator

Figure 5.18 and Figure 5.19 on the next pages shows some key elements of the final test prototype during the implementation phase. The total height of the sensor for angle measurement was reduced from 27 mm to roughly 10 mm. The angle sensor is also fitted inside the actuator which reduces its susceptibility to external magnetic noise.



Figure 5.18: Key aspects of inclined actuator assembly

A weight reduction from 259 g to 179.7 g and 141.1 g for pulley 2 and pulley 4 respectively was achieved. Washers were placed in between the crank (torque sensing element) and the larger pulley which were secured together using two screws as shown in Figure 5.18(h).



Figure 5.19: Middle and top layer with support bearing for shaft 2 Final Actuator prototype

5.1.6.1 Actuator testing

The same tests as with the opened layer-based model was done, both with and without the knee model. During this stage, the code was written to match the motor encoder with the angle sensor since the angle data was more accurate, had less errors and were obtained faster through SPI. Nonetheless, due to the backlash in the pulley, there was a small change in the angle sensor and motor encoder values. It was minimal but could pose a risk if an algorithm is the only method of determining this relation. Thus, during implementation, to map the motor encoder and angle sensor properly, the shank link is rotated manually to its extremities to confirm that the angle sensor and motor encoder have the same lower and upper bounds.

To test the actuator with the knee test model, an inclined mount was designed and made with SLS. It supports the inclination of the actuator, while at the shank link, the same free moving pivot support was kept. The same tests were performed, and the results were confirmed as with the layer-based model.

5.1.6.2 Actuator with exoskeleton frame

Eventually, the exoskeleton frame from student Patrick Hensel from Campus Huththurm was printed using MJF. The actuator was installed onto the thigh part with four bolts and nuts. As for the shank link, a connector was proposed. Initially to allow flexible sideways and twisting motion, the connector was printed with TPU (Thermoplastic polyurethane), a flexible filament. However, the increased flexibility did not allow the transmission of torque to the shank link. Thus, the same connector design was printed with MJF with better results.

The passive rotation was first tested with the motor inactive, and the connector obstructs the full rotation. One solution is to make a filleted edge. Nonetheless, it allowed ample rotation from 0 to 90 degrees to perform some tests. The whole build was sturdy enough and had a good aesthetic finish. Straps were used to secure the prosthesis to the leg. In terms of ergonomics, the prosthesis fits perfectly well with the thigh and the shank, as it follows the contour of the leg. Furthermore, the inclination of the actuator matched that of the leg perfectly. There might be less than 20 mm gap between the frame and the leg, depending on the person wearing it, but this could be resolved by using a padded support which will also increase comfortability. Figure 5.20 shows the outcome of the completed knee exoskeleton actuator and exoskeleton frame.

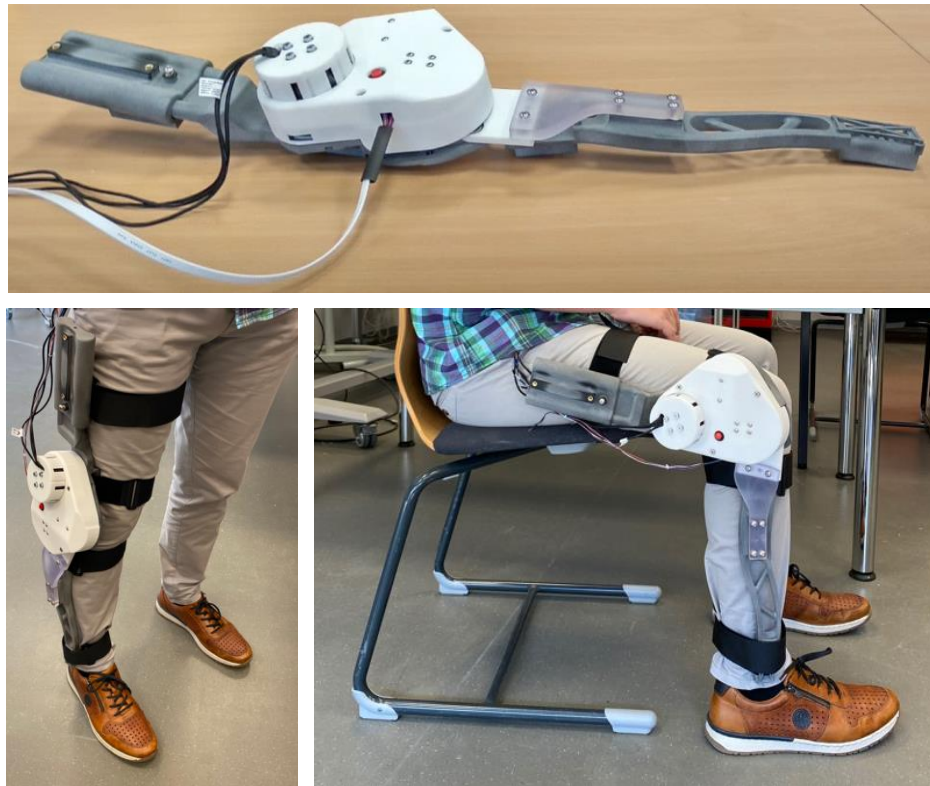


Figure 5.20: Knee exoskeleton actuator with exoskeleton frame

5.1.6.3 Active and Passive Tests

Due to safety concerns, in the beginning, only a passive test was carried out where the actuator was unpowered, and the knee was moved with the actuator on the wearer. This was also a test to determine if the backdrivability of the actuator is comfortable enough which is confirmed by the fact that the user does not have to apply much effort to move the knee. Furthermore, the four bar mechanism is confirmed as well as there is not much translation in the shank link as the knee rotates. A better way to confirm this is to test the actuator with a anatomically precise dummy which would be able to replicate the four-bar-linkage motion due to the ACL and PCL ligaments. Certain motion, such as walking around and sitting were achieved and tested without any issue.

To perform the active tests, certain elements of the safety features were implemented, including the emergency push button which controls the connection between the power supply and the ODrive. A fused was used which was rated at 8A since the peak current from the supply is already 5A and trips when that is reached, however with the battery there is no limitations to the current supplied. A contacting relay was connected to the emergency push button on the actuator which further secures the connection between the power supply and the ODrive.

To drive the actuator, an analog input was required which was achieved via a joystick providing analog values from 0 to 1023. The joystick, as well as the other connection to the push button and the UART communication with the ODrive was made robust by soldering the cables and using latching connectors. This resulted in less noise and fewer anomalous signals which could cause the actuator to respond erratically. The latching connectors can be seen in the third image in Figure 5.19.

The code displayed in Software Design was implemented and the whole actuator with the exoskeleton frame was worn by the user. After a successful calibration, the actuator responded in position control mode which moved the actuator with respect to the analog input device. The leg was relaxed and made free to be moved by the actuator. This corresponds to a sensor signal, such as a conditioned signal from an EMG or EEG, or a flex sensor.

One limitation was the transfer of torque from the shank link which could be improved by adding a back and front support to the prosthesis. As for the actuator, the response time to the analog input was good enough and showed good compliance. However, another algorithm should be implemented to switch between closed-loop and open-loop control so that the person can move the leg passively in case the torque level in the shank goes beyond a certain limit. This could be achieved as an improvement in the design, by using an actual torque sensing element in the knee. A preliminary design was created to include the torque sensor as the crank link of the four-bar-linkage. The push button to switch states works really well and passive and active mode could be chosen at will.

Specific motions were performed to obtain a valid result for the knee motion. These include standing up and flexing the knee and sitting and extending the knee. The images for the test and the results are displayed in Figures 5.21 to 5.24 below. The graphs in Figures 5.25 to 5.27 also compare the position, speed, current and thus torque in response to the analog input of the joystick.

The backplate in Figure 5.21 below to hold the electrical components and other electronics were designed by student Florian Neumann from Technologie Campus Huththurm. Further implementations include a fully supported backplate in the form of a backpack and a hip support to hold the knee exoskeleton frame.

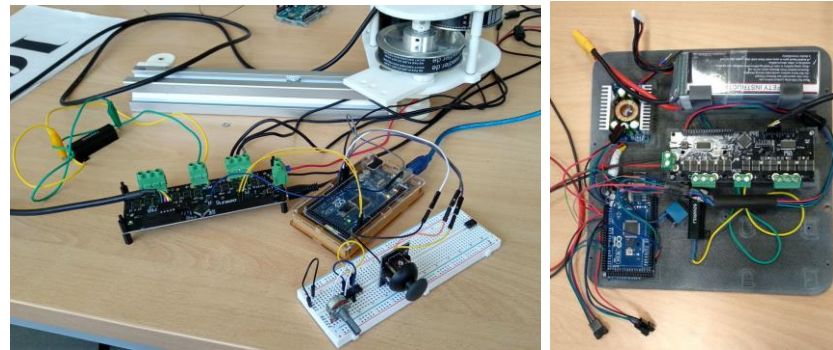


Figure 5.21: First model test and new backplate to hold all control and power components

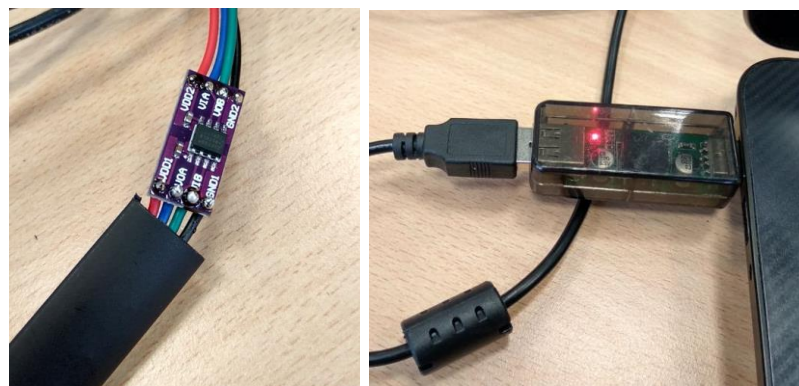
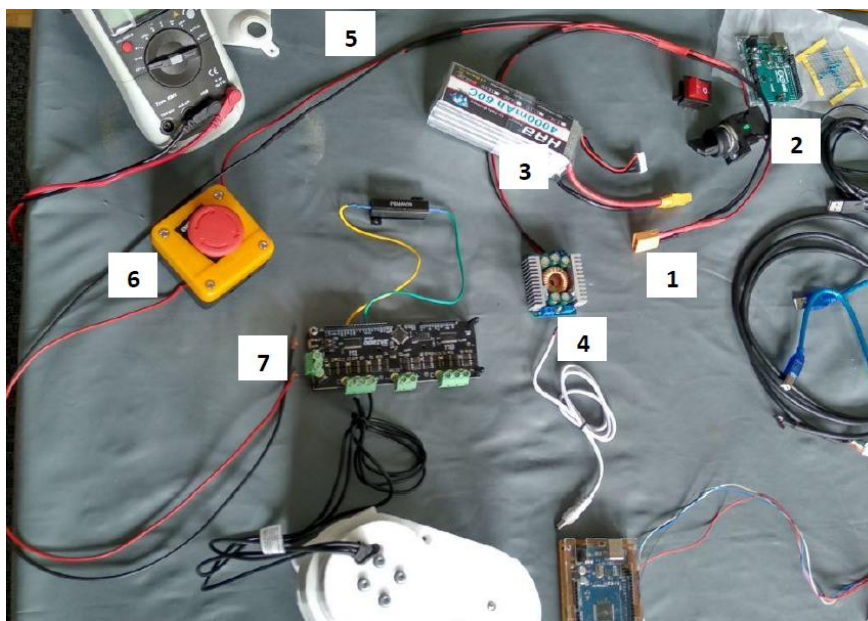


Figure 5.22: GPIO Digital Isolator and USB Isolator by Analog Devices



- 1:** power supply connection
- 2:** ON/OFF Main switch
- 3:** Leads to Arduino and Relay
- 4:** DC-DC Step-Down Converter
- 5:** Leads to emergency switch and ODrive controller
- 6:** Emergency Switch
- 7:** ODrive power connection

Figure 5.23: Description of Electrical connection of actuator

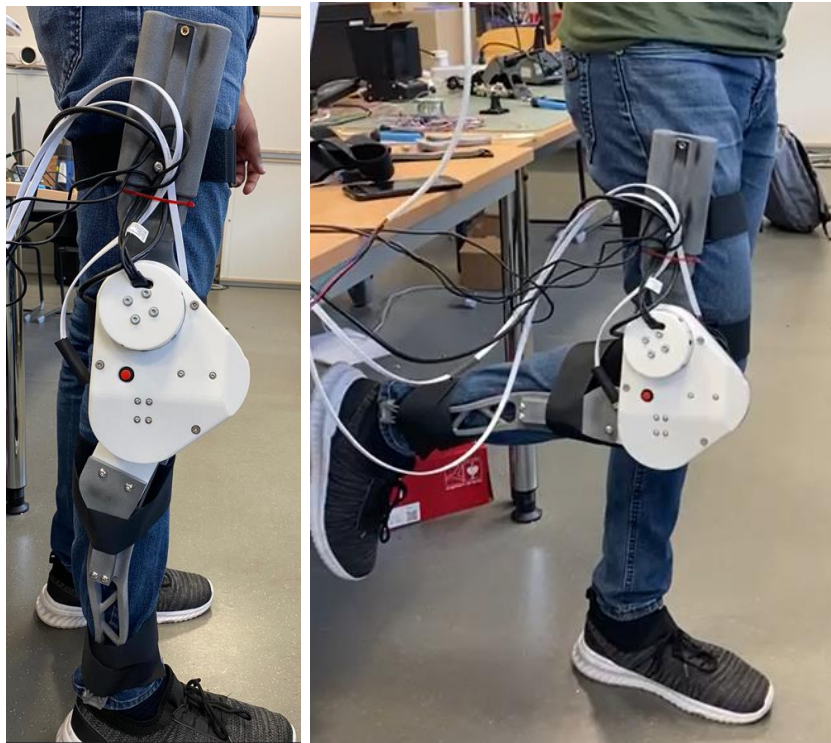


Figure 5.24: Knee exoskeleton on wearer during active test

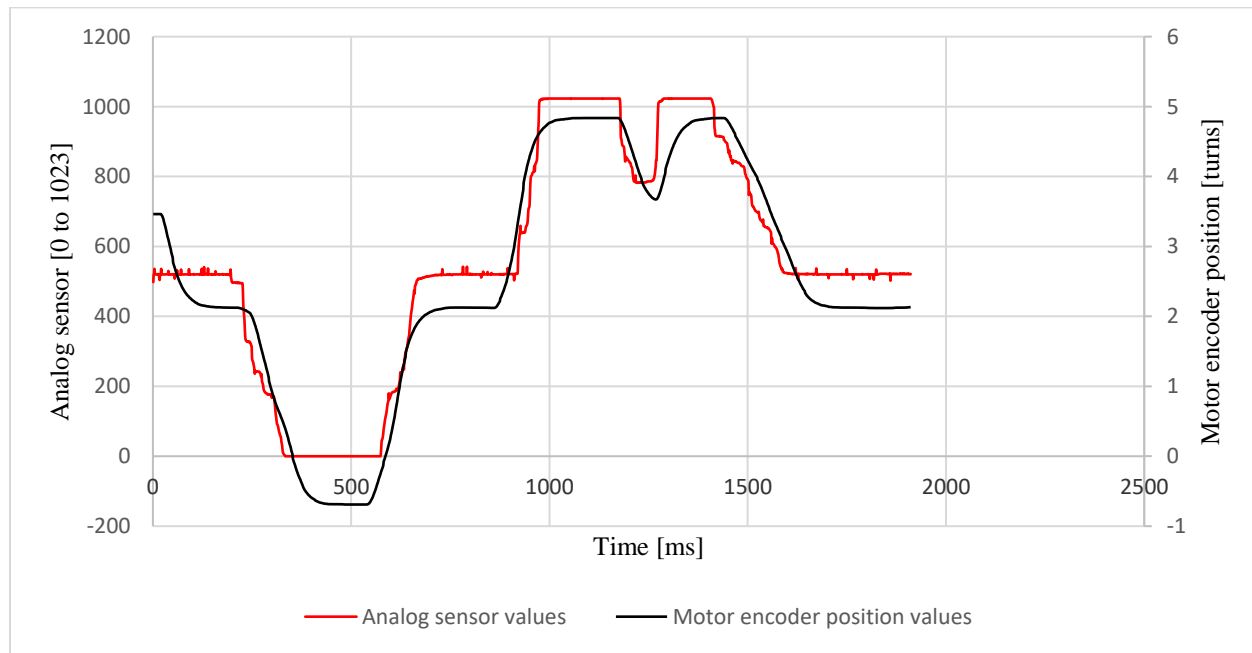


Figure 5.25: Analog Sensor vs. Encoder position

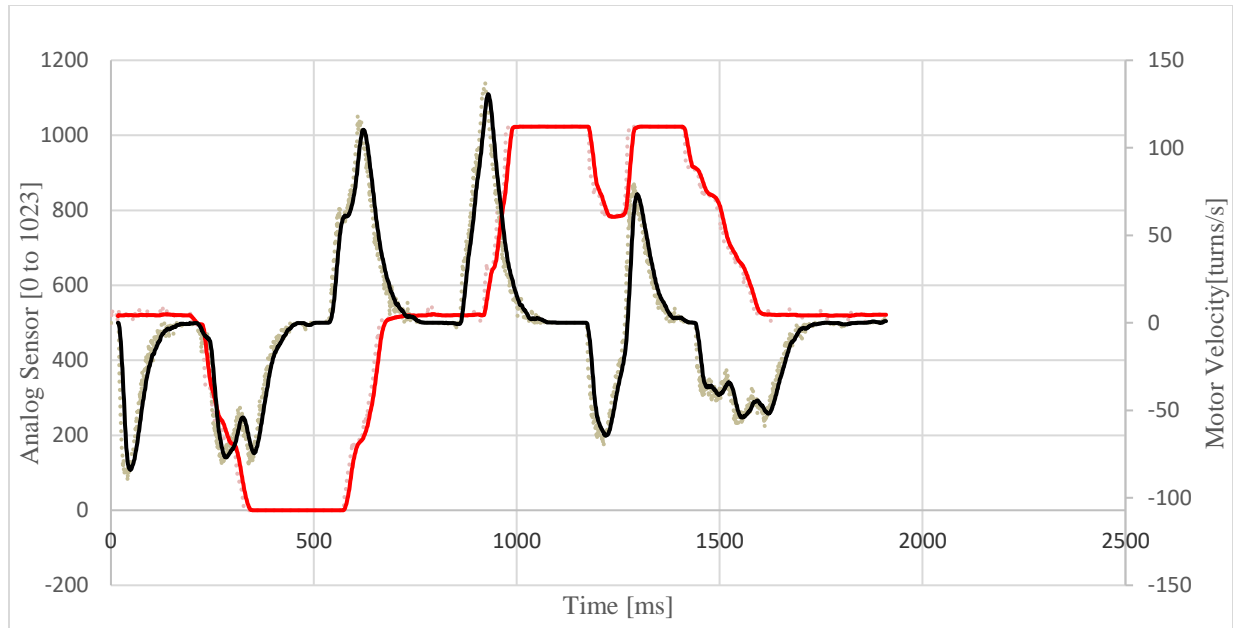


Figure 5.26: Analog Sensor vs. Motor velocity

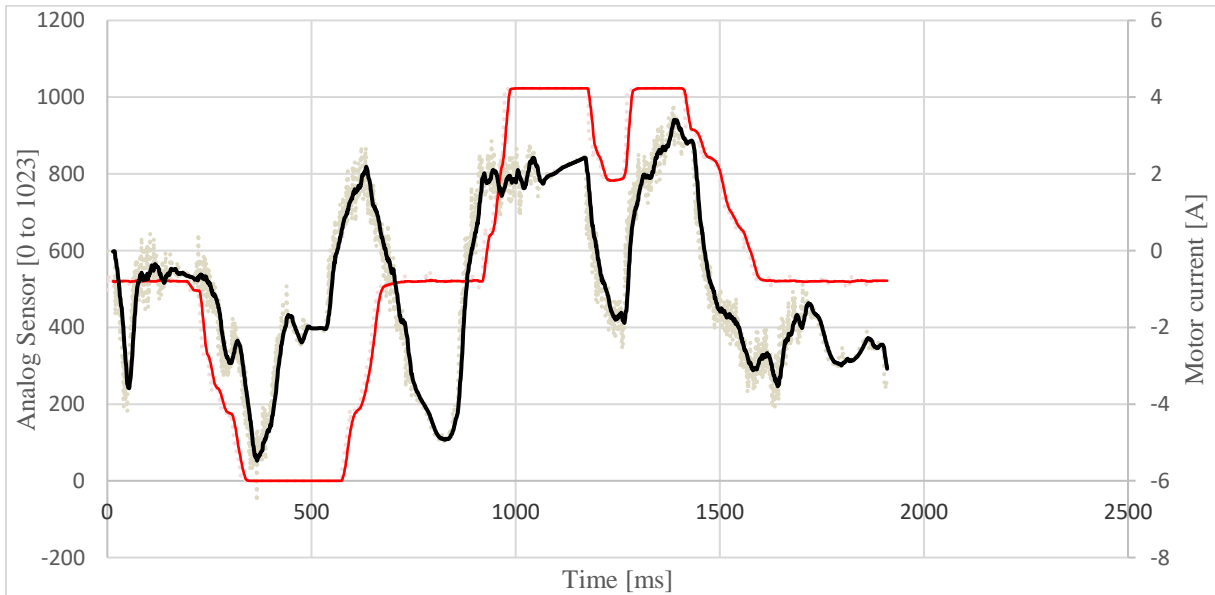


Figure 5.27: Analog Sensor vs. Motor Current

In the graphs above, the red line represents the analog sensor values, while the thick black line represents the motor current as a 15 point moving average. The grey points represent the actual value of the current, which is measured, hence, sustained noise. The set current provided a smoother curve. The current spikes still occurred even after the inertia and PID parameters were adjusted. This is because it depends on the speed at which the knee rotates. For example, between time units 500 and 1000, there is a drastic change in the velocity, and the velocity curve smooths out to zero due to the low deceleration gain, however, the user's knee kept moving forward due to inertia, so a higher current setpoint was set for braking.

Additionally, since the motor is set in closed-loop-control for position control, the current-setpoint is almost never plateauing at zero as the motor is always providing a holding torque.

The values were measured with a timestamp with delay ranging from 16.66 ms to 60 ms.

5.2 Evaluation

In this subsection, the results obtained are evaluated by summarizing and comparing them with the requirements of the system set in conceptual design phase. A comparison between the detailed design calculations and the actual test prototype is also conducted. Both the user operation and technical requirements were evaluated. The user requirements from Table 3.1 and technical requirements from Table 3.3 are used as reference.

5.2.1 Angular displacement range

The designed angular displacement range was from 0 degrees to 135 degrees for the rotation of the knee from the fully extended to the fully flexed position. This was obtained based on the constraints of the knee, and that the knee is following a motion profile similar to the four-bar-linkage movement. This holds true as the ACL and PCL (ligaments) inside the knee provides the roll and slide motion which was tested by three users. If the actuator is tested with a larger number of people, there might be a slight mismatch as the size of the knee varies, and thus the lengths and orientation angles of the ACL and PCL vary too. The actuator has to be adjusted based on the user to ensure the axes of rotation align.

The user operation requirements 1, 2 and 4 are thus fulfilled. To evaluate if the actuator is comfortable, a larger number of people have to test the comfortability of the actuator.

5.2.2 Peak torque range

A range for the peak torque was provided to cater for the need of the user, depending on what type of application is required. The percentage of assistance was initially selected at 30% which is what is appropriate for rehabilitation purposes. The final value obtained was 36.30 Nm, due to the restriction in the belt strand forces, which is further reduced to about 20 Nm due to the four-bar-linkage when the knee is fully extended. This was the confirmed value obtained after testing. The same applies for the peak power of the actuator. Initially, the power required was set at 616.41 W. While the motor can deliver up to 1500 W of power, the belt and pulley system restricts this value to up to 551 W. This is achieved by restricting the speed of the motor to 2630 rpm (or 43.83 turns/s), so that the total power is not exceeded at peak torque which is 1.97 Nm with the T-Motor P60 motor. However, since the total torque output is 36.3 Nm at the fourth pulley, with a safety factor of about 1.32, the motor torque is restricted at 1.1 Nm, slightly higher than the 1.04 Nm required torque. The peak speed limit is also 2250 rpm (or 37.5 turns/s). With the limited speed and torque, the actual power output from the motor is then about 260 W. This value lies in the range of peak power at 30% assistance.

Thus, comparing with Table 3.2 and Table 3.3 in Section 3.1 for the percentage assistance, the resulted torque would satisfy the following requirements with 30% assistance:

- Basic stationary knee flexion and extension
- Sit-to-stand with an additional support for a requirement of 0.9 Nm/kg by the knee
- Walking with a speed of up to 0.9 m/s
- Stair climbing

These satisfy the basic requirements for rehabilitation purposes only, where the user provides only 70% of the knee torque. This is allowable, as the user still has control over their body motion and are less likely to lose balance and fall. Generally, in cases where higher percentage assistance is available, the user has to use crutches to keep their balance. Actions such as vertical jumping or running are thus not supported by the actuator, only with decreased assistance level which is not recommended. The user requirements 2, 3 and 6 are fulfilled.

5.2.3 Peak angular speed

During the conceptual design phase, the peak angular speed was set at 500 degrees/s which is less than the peak unrestrained knee speed of 680 degrees/s as a means of safety since higher speeds would result in higher power and thus the teeth-in-mesh factor would not apply, causing the belt to slip. This was successfully achieved with a recorded speed of 360 degree/s. The peak acceleration is 1772 degrees/s², which is close to 2000 degrees/s². The user requirements 1, 2, 4, and 5 were fulfilled. The back drivable torque, which was calculated as 2.42 Nm, is deemed acceptable given that in this case, we accept the fact that the user's knee can generate up to 0.9 Nm/kg. The back drivable torque for the actuator is thus 0.0285 Nm/kg or 3% of the user's knee capability when the person is moving their knee unrestrained up to a peak angular speed of 360 degrees/s.

5.2.4 Maximum weight

The maximum weight of the whole actuator, including the backplate to hold the battery and components was set at 5 kg. This requirement was respected as the maximum weight of each actuator is at 1.375 kg.

In terms of comfort, this weight is distributed throughout the hip support and the backplate support, hence, it is not acting at a single point on the leg. Furthermore, the centre of mass of the heaviest component, the motor which weighs about 0.369 kg, is at a distance of approximately 0.08 m from the leg surface which results in a moment of 0.290 Nm. The centre of gravity of the whole actuator is obtained from AutoCAD and is at approximately 0.05 m from the surface of the leg. Given that the weight of the actuator is 1.375 kg, the maximum moment because of the actuator is about 0.675 Nm. There is no ideal value for comparison – the smaller the moment is, the more comfortable the exoskeleton is while being worn.

As for the backplate with the control and power components, it was measured as 1.58 kg, including the wires and switches. The exoskeleton frame weighs 0.685 kg. Thus, the total effective weight of the portable exoskeleton, with the battery, is 5.7 kg. This is slightly higher than the 5 kg threshold, however, it can be reduced by using a lower capacity battery for a lower operation time.

5.2.5 Overall actuator

5.2.5.1 Dynamic operation

The actuator was successfully tested with an analog input. A joystick provided an analog value to the Arduino ranging from 0 to 1023. Position, velocity, and torque control were achieved, and admittance control was implemented where the value of the analog input matches a specific position in the actuator.

5.2.5.2 Feedback

Both the angle sensor and the motor encoder provided feedback in terms of the angular position of the knee movement. When timestamps are used in the code, the position can be mapped respectively with the sensor value. This is demonstrated in the graph in Figure 5.28 where the angle sensor matches the analog sensor input profile almost perfectly.

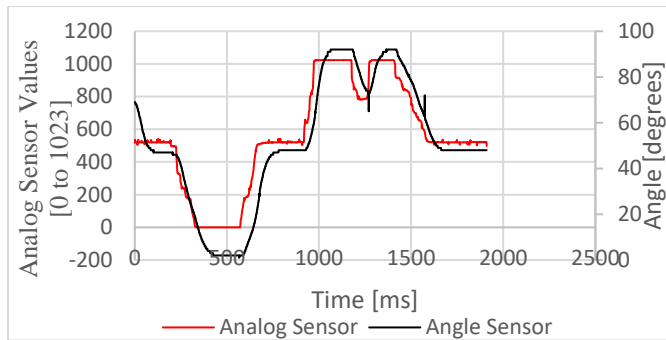


Figure 5.28: Angle sensor variation with change in analog input

Space has been allocated within the four-bar-linkage such that a torque sensing element can be implemented to obtain impedance control. This was achieved in this project due to time constraints.

5.2.5.3 Portable operation

Portable operation was achieved by placing all the control elements on a backplate, as well as the power supply in terms of a Lithium Polymer (LiPo) battery rated at 5000 mAh which could deliver power to the actuator for about 2 hours maximum. The wires from the actuator to the backplate can be incorporated in the leg prosthesis as an improvement. It makes the actuator less cumbersome and ensures that there are no extra tensions on the wire.

5.2.5.4 Safety

From an electrical point of view, two emergency safety switches and a fuse provided a reliable system which could be stopped in case there is an erratic behaviour or a failure of the controllers or sensor. In addition, the ODrive controller has current and velocity limits which switches off the applied torque in case they are exceeded. As for the mechanical aspect, the whole actuator case

and four-bar-linkage ensure a safe operation, as it was tested with FEA on Autodesk Inventor. The belt peripheral forces were calculated, and so was the peak force that the belt can withstand. The datasheet from the belt supplier, Maedler, states a value with a very high safety factor. This value was lowered to allow for a higher torque output, given that the conditions of operation involve low speeds and power.

6 Conclusion and further works

The aim of this project was to create an actuator for a knee exoskeleton, with two specific features: namely, a four-bar-linkage and a belt-driven speed reduction mechanism. These two features were selected after conducting a thorough research on the types of available actuating methods and human biomechanics. The four-bar-linkage serves the purpose of replicating the knee ACL and PCL ligaments, such that, the exoskeleton is more comfortable for the wearer. The torque requirements of the knee also were analyzed, and a proper assistance torque was decided upon. As for the belt-driven system, it provides an increase in torque, while maintaining a lower shear force by increasing the damping effect. The effects due to inertia also is decreased by using a brushless DC motor which provides an ‘flexible’ holding torque. With PID tuning, the rate of response of the motor is adjusted by adjusting parameters such as the torque rate and the peak velocity of the motor.

Through the course of this master thesis, a concept was created which was further detailed by assigning proper dimensions and by selecting the proper components. With the help of additive manufacturing and CAD modelling, an actuator case was created which could fit the wearer to a more comfortable level. During the implementation phase, initial tests were done with a layer-based actuator model so that the interior functioning of the components could be visually inspected and improved. Parameters such as the speed, the acceleration and the torque of the motor were continually adjusted so as to obtain an actuator which could rotate smoothly when a varying signal is provided. As interface, a Raspberry Pi and an Arduino microcontroller are available to which the respective sensors can be connected. The conditioned sensor signal can be adapted to control the position, speed and torque of the actuator using the ODrive motor controller commands. A 14-bit angle sensor provides accurate feedback on the position of the knee joint.

Besides an aesthetic prosthetic frame which adapts perfectly to the human leg, the exoskeleton’s peripheral components such as the battery and the controllers are mounted on a backplate. The belt-driven actuator was successfully tested and sets the basis for a rehabilitation exoskeleton which can help patients, for example with a knee injury to regain their ability to walk in a compliant manner due to the four-bar-linkage and the belt-driven system. Part of a future work is the integration of a torque sensing element to provide a true torque feedback at the four-bar-linkage. The position of the pulleys can be changed, so as to make the actuator slimmer and fit better with the exoskeleton frame. Additionally, a more robust communication protocol such as CAN protocol can be used to obtain more reliable data exchange between the sensor and the actuator.

7 Bibliography

- [1] V. Kumar, Y. Hote and S. Jain, "Review of Exoskeleton : History, Design and Control", in *International Conference on Recent Developments in Control, Automation & Power Engineering (RDCAPE)*, Noida, India, 2019. doi: 10.1109/RDCAPE47089.2019.8979099
- [2] M. Lyu, W. Chen, X. Ding, J. Wang, Z. Pei and B. Zhang, "Development of an EMG-Controlled Knee Exoskeleton to Assist Home Rehabilitation in a Game Context", *Frontiers in Neurorobotics*, vol. 13, 2019. doi: 10.3389/fnbot.2019.00067.
- [3] Z. Tang, K. Zhang, S. Sun, Z. Gao, L. Zhang and Z. Yang, "An Upper-Limb Power-Assist Exoskeleton Using Proportional Myoelectric Control", *Sensors*, vol. 14, no. 4, pp. 6677-6694, 2014. doi: 10.3390/s140406677
- [4] J. Zhang, C. Yang, Y. Chen, Y. Zhang and Y. Dong, "Modeling and control of a curved pneumatic muscle actuator for wearable elbow exoskeleton", *Mechatronics*, vol. 18, no. 8, pp. 448-457, 2008. doi: 10.1016/j.mechatronics.2008.02.006.
- [5] J. Varghese, A. V.M., R. P.K. and S. K.S., "A rotary pneumatic actuator for the actuation of the exoskeleton knee joint", *Theoretical and Applied Mechanics Letters*, vol. 7, no. 4, pp. 222-230, 2017. doi: 10.1016/j.taml.2017.08.002.
- [6] P. Heo and J. Kim, "Power-Assistive Finger Exoskeleton With a Palmar Opening at the Fingerpad", *IEEE Transactions on Biomedical Engineering*, vol. 61, no. 11, pp. 2688-2697, 2014. doi: 10.1109/TBME.2014.2325948.
- [7] Z. Tang, D. Shi, D. Liu, Z. Peng, L. He and Z. Pei, "Electro-hydraulic servo system for Human Lower-limb Exoskeleton based on sliding mode variable structure control," *2013 IEEE International Conference on Information and Automation (ICIA)*, pp. 559-563, 2013. doi: 10.1109/ICInfA.2013.6720360
- [8] X. Ouyang, S. Ding, B. Fan, P. Li and H. Yang, "Development of a novel compact hydraulic power unit for the exoskeleton robot", *Mechatronics*, vol. 38, pp. 68-75, 2016. doi: 10.1016/j.mechatronics.2016.06.003.
- [9] Y. Jung and J. Bae, "An asymmetric cable-driven mechanism for force control of exoskeleton systems", *Mechatronics*, vol. 40, pp. 41-50, 2016. doi: 10.1016/j.mechatronics.2016.10.013.
- [10] D. Popov, K. Lee, I. Gaponov and J. Ryu, "Twisted Strings-based Elbow Exoskeleton", *The Journal of Korea Robotics Society*, vol. 8, no. 3, pp. 164-172, 2013. doi: 10.7746/jkros.2013.8.3.164.
- [11] D. Serrano, D. Copaci, L. Moreno and D. Blanco, "SMA based wrist exoskeleton for rehabilitation therapy*", *2018 IEEE/RSJ International Conference on Intelligent Robots and Systems (IROS)*, pp. 2318-2323, 2018. doi: <https://doi.org/10.1109/IROS.2018.8593987>

- [12] C. Mavroidis, "Development of Advanced Actuators Using Shape Memory Alloys and Electrorheological Fluids", *Research in Nondestructive Evaluation*, vol. 14, no. 1, pp. 1-32, 2002. doi: 10.1007/s00164-001-0018-6.
- [13] O. Gomis-Bellmunt, *Design Rules for Actuators in Active Mechanical Systems*, 1st ed. Springer London, 2014.
- [14] J. Wojtusch and O. von Stryk, "HuMoD - A versatile and open database for the investigation, modeling and simulation of human motion dynamics on actuation level," *2015 IEEE-RAS 15th International Conference on Humanoid Robots (Humanoids)*, pp. 74-79, 2015. doi: 10.1109/HUMANOIDS.2015.7363534
- [15] N. Hamilton, W. Weimar and K. Luttgens, *Kinesiology*. New York, NY: McGraw-Hill, 2012.
- [16] T. Vail, J. Lang and C. Van Sikes, "Surgical Techniques and Instrumentation in Total Knee Arthroplasty", *musculoskeletalkey.com*, 2016. [Online]. Available: <https://musculoskeletalkey.com/surgical-techniques-and-instrumentation-in-total-knee-arthroplasty-2/>. [Accessed: 05- May- 2021].
- [17] H. Aguilar-Sierra, W. Yu, S. Salazar and R. Lopez, "Design and control of hybrid actuation lower limb exoskeleton", *Advances in Mechanical Engineering*, vol. 7, no. 6, 2015. doi: 10.1177%2F1687814015590988.
- [18] Y. Pai and M. Rogers, "Speed variation and resultant joint torques during sit-to-stand", *Archives of Physical Medicine and Rehabilitation*, vol. 72, no. 11, pp. 881-885, 1991. doi: 10.1016/0003-9993(91)90004-3.
- [19] S. Bhardwaj, A. Khan and M. Muzammil, "Knee torque estimation in sit to stand transfer", *Journal of Physics: Conference Series*, vol. 1240, 2019. doi: 10.1088/1742-6596/1240/1/012153.
- [20] C. Tunca, N. Pehlivan, N. Ak, B. Arnrich, G. Salur and C. Ersoy, "Inertial Sensor-Based Robust Gait Analysis in Non-Hospital Settings for Neurological Disorders", *Sensors*, vol. 17, no. 4, p. 825, 2017. doi: 10.3390/s17040825.
- [21] J. Kim et al., "Design of a Knee Exoskeleton Using Foot Pressure and Knee Torque Sensors", *International Journal of Advanced Robotic Systems*, vol. 12, no. 8, p. 112, 2015. doi: 10.5772/60782.
- [22] M. Grimmer, M. Eslamy and A. Seyfarth, "Energetic and Peak Power Advantages of Series Elastic Actuators in an Actuated Prosthetic Leg for Walking and Running", *Actuators*, vol. 3, no. 1, pp. 1-19, 2014. doi: 10.3390/act3010001.

- [23] G. Caldwell, W. Adams III and M. Whetstone, "Torque/Velocity Properties of Human Knee Muscles: Peak and Angle-Specific Estimates", *Canadian Journal of Applied Physiology*, vol. 18, no. 3, pp. 274-290, 1993. doi: 10.1139/h93-024.
- [24] B. Siciliano, O. Khatib and T. Kröger, *Handbook of Robotics*. Berlin: Springer, 2016.
- [25] D. Ponce, D. Martins, R. Carlos, R. Fabiola and M. Ari, "Modeling Of Human Knee Joint In Sagittal Plane Considering Elastic Behavior Of Cruciate Ligaments", in *COBEM*, Ribeirão Preto, São Paulo, Brasil, 2013. doi: 10.13140/2.1.5077.9847
- [26] M. Grimmer, A. Elshamahory and P. Beckerle, "Human Lower Limb Joint Biomechanics in Daily Life Activities: A Literature Based Requirement Analysis for Anthropomorphic Robot Design", *Frontiers in Robotics and AI*, vol. 7, 2020. doi: 10.3389/frobt.2020.00013.
- [27] H. Lakany, "Requirements Specifications For A Wearable Robotic Exoskeleton For Rehabilitation", *Human-Centric Robotics*, pp. 605-612, 2017. doi: 10.1142/9789813231047_0073
- [28] J. Wang et al., "Comfort-Centered Design of a Lightweight and Backdrivable Knee Exoskeleton", *IEEE Robotics and Automation Letters*, vol. 3, no. 4, pp. 4265-4272, 2018. doi: 10.1109/LRA.2018.2864352.
- [29] M. Milewski, J. Hart and M. Miller, "Sports Medicine", *musculoskeletalkey.com*, 2016. [Online]. Available: <https://musculoskeletalkey.com/sports-medicine-3/>. [Accessed: 16- Oct- 2021].
- [30] J. Mitchell, M. Mahfouz and N. Battaglia, "Accurate Length Measurements Of ACL And PCL Of A Healthy Patient During Weightbearing Deep Knee Bend", in *ORS 2012 Annual Meeting*, 2012. Available: <http://www.ors.org/Transactions/58/2282.pdf>
- [31] *Smarthost.maedler.de*. [Online]. Available: http://smarthost.maedler.de/datenblaetter/zahnriemenantriebe_EN.pdf. [Accessed: 01- Oct- 2021].
- [32] S. Fu, B. Lauke, E. Mäder, C. Yue and X. Hu, "Tensile properties of short-glass-fiber- and short-carbon-fiber-reinforced polypropylene composites", *Composites Part A: Applied Science and Manufacturing*, vol. 31, no. 10, pp. 1117-1125, 2000. doi: 10.1016/S1359-835X(00)00068-3.
- [33] A. Dollar and H. Herr, "Design of a Quasi-Passive Knee Exoskeleton to Assist Running", in *IEEE/RSJ International Conference On Intelligent Robots And Systems*, 2008. Available: https://www.eng.yale.edu/grablab/pubs/dollar_IROS08.pdf
- [34] D. Jessop and M. Pain, "Maximum Velocities in Flexion and Extension Actions for Sport", *Journal of Human Kinetics*, vol. 50, no. 1, pp. 37-44, 2016. doi: 10.1515/hukin-2015-0139.
- [35] P. de Leva, "Adjustments to Zatsiorsky-Seluyanov's segment inertia parameters", *Journal of Biomechanics*, vol. 29, no. 9, pp. 1223-1230, 1996. Available: 10.1016/0021-9290(95)00178-6.

- [36] M. Sanchez-Villamañan, J. Gonzalez-Vargas, D. Torricelli, J. Moreno and J. Pons, "Compliant lower limb exoskeletons: a comprehensive review on mechanical design principles", *Journal of NeuroEngineering and Rehabilitation*, vol. 16, no. 1, 2019. doi: <http://doi.org/10.1186/s12984-019-0517-9>.
- [37] D. S. Pieringer, M. Grimmer, M. F. Russold and R. Riener, "Review of the actuators of active knee prostheses and their target design outputs for activities of daily living," *2017 International Conference on Rehabilitation Robotics (ICORR)*, pp. 1246-1253, 2017. doi: [10.1109/ICORR.2017.8009420](https://doi.org/10.1109/ICORR.2017.8009420)
- [38] X. Jin, Y. Cai, A. Prado and S. K. Agrawal, "Effects of exoskeleton weight and inertia on human walking," *2017 IEEE International Conference on Robotics and Automation (ICRA)*, pp. 1772-1777, 2017. doi: [10.1109/ICRA.2017.7989210](https://doi.org/10.1109/ICRA.2017.7989210)
- [39] M. S. Islam, S. Mir and T. Sebastian, "Issues in reducing the cogging torque of mass-produced permanent-magnet brushless DC motor," in *IEEE Transactions on Industry Applications*, vol. 40, no. 3, pp. 813-820, May-June 2004, doi: [10.1109/TIA.2004.827469](https://doi.org/10.1109/TIA.2004.827469)
- [40] H. Crowell III, A. Boynton and M. Mungiole, *Exoskeleton Power and Torque Requirements Based on Human Biomechanics*. Army Research Laboratory, pp. 25 – 28, 2002. [Online]. Available: <https://apps.dtic.mil/sti/pdfs/ADA408684.pdf> [Accessed: 05-May-2021]
- [41] M. Kadaba, H. Ramakrishnan and M. Wootten, "Measurement of lower extremity kinematics during level walking", *Journal of Orthopaedic Research*, vol. 8, no. 3, pp. 383-392, 1990. doi: [10.1002/jor.1100080310](https://doi.org/10.1002/jor.1100080310)

8 Appendix

Appendix I - List of Figures and Tables

List of Figures:

Figure 2.1: Classification of Actuators	2
Figure 2.2: DC Motor powered lower limb exoskeleton with	3
Figure 2.3: Fluid power actuator with curved cylinder [4]	3
Figure 2.4: Fluid power linear	4
Figure 2.5: Principles of rotation of belt and Bowden cable [9].....	4
Figure 2.6: Bowden Cable upper-limb actuator setup [9].....	4
Figure 2.7: Belt driven knee exoskeleton	4
Figure 2.8: Pneumatic pistons for articulate	5
Figure 2.9: Hydraulic pistons for lower.....	5
Figure 2.10: Principle of operation of PAM [3]	6
Figure 2.11: Pneumatic Artificial Muscle (PAM) for upper-limb exoskeleton [3]	6
Figure 2.12: Shape Memory Alloy (SMA) for wrist movements [11]	6
Figure 2.13: Review list of actuators for upper-limb exoskeletons	7
Figure 2.14: Review list of actuators for lower-limb exoskeletons	7
Figure 2.15: Planes of motion in the body: a) Sagittal/median, b) frontal/coronal and c) transverse/horizontal planes [14]	9
Figure 2.16: Description of the Degrees of Freedom (DoF) in the body [15]	9
Figure 2.17: Rotation limits of the lower limbs (Hip, Knee and Ankle) [15].....	10
Figure 2.18: Possible positions of the knee	11
Figure 2.19: Kinematic diagram of the lower limbs showing 1 DoF of the knee.....	11
Figure 2.20: Inclination of the femur with respect to the tibia [16].....	12
Figure 2.21: Roll and glide motion of the knee	12
Figure 2.22: Four-bar-linkage in knee	12
Figure 2.23: ACL and PCL with instantaneous centre of rotation (IC) [29]	13
Figure 2.24: Approximate ratio of body parts [17].....	13
Figure 2.25: Force diagram for static knee flexion torque calculation	14
Figure 2.26: Basic Sit-to-Stand motion [19].....	15
Figure 2.27: Different phases of gait cycle [20]	16
Figure 2.28: Torque requirements per kilogram of body weight for walking and running [22] ..	16
Figure 3.1: Classification of the sub-sections of the knee exoskeleton	23
Figure 3.2: Description of the chosen concept of the knee exoskeleton.....	24
Figure 4.1: Mechanical schematic of the actuator	30
Figure 4.2: Description of belt tensile forces.....	31
Figure 4.3: Primary dimensions from concept model.....	33
Figure 4.4: Lateral force due to actuator weight.....	34
Figure 4.5: Belt tensioning forces	37
Figure 4.6: Description of teeth-in-mesh	39

Figure 4.7: Actuator and external torque representation	42
Figure 4.8: Shaft load description.....	48
Figure 4.9: Actuator shaft loads enumerated	49
Figure 4.10: Four-bar-linkage description	50
Figure 4.11: Angle Θ_3 between Link L ₁ and Link L ₃	50
Figure 4.12: Four-bar-linkage force diagram.....	51
Figure 4.13: Four-bar-linkage dimensions.....	54
Figure 4.14: Shank torque variation with change in crank angle	55
Figure 4.15: Change in pivot points and ICR	56
Figure 4.16: Shank angle variation with change in crank angle	56
Figure 4.17: Dimensioning: Top-View of layer-based actuator	57
Figure 4.18: Dimensioning: Side-View of layer based actuator.....	57
Figure 4.19: 3D Isometric Projection of layer-based actuator	58
Figure 4.20: Dimensions: Side-View of inclined actuator.....	58
Figure 4.21: Dimensions: Cross-Section View of inclined actuator with wall thickness.....	58
Figure 4.22: FEA on the actuator case and actual model used for FEA	59
Figure 4.23: Exploded-View of layer based actuator	60
Figure 4.24: Four-bar-linkage integration in actuator case.....	61
Figure 4.25: Assembly plan for four-bar-linkage and actuator case	61
Figure 4.26: Four-bar-linkage rotation test in Autodesk Inventor	61
Figure 4.27: Four-bar-linkage and crank link FEA	62
Figure 4.28: Electrical schematic for the actuator	63
Figure 4.29: MOSFET Gates circuit in ODrive Controller (Source: ODrive Robotics)	68
Figure 4.30: AMT capacitance based incremental encoder and signal waveform (Source: AMT CUI datasheet)	68
Figure 4.31: Flowchart: Actuator startup sequence	70
Figure 4.32: ODrive motor controller control interface (Source: ODrive Robotics)	71
Figure 4.33: Packet description for UART communication	72
Figure 4.34: Flowchart: Actuator Sequence of operation part 1	73
Figure 4.35: Flowchart: Actuator sequence of operation part 2	74
Figure 4.36: Final actuator CAD models	75
Figure 4.37: Actuator on the prosthetic exoskeleton frame	75
Figure 5.1: Knee model with aluminum extrusion and single axis hinge.....	78
Figure 5.2: Motor with pulley and encoder sleeve on base-plate	80
Figure 5.3: Pulley and shaft assembly on base-plate	80
Figure 5.4: Four-bar-linkage at extended(left) and flexed(right) position.....	81
Figure 5.5: Top-plate with motor and absolute encoder and shaft coupler of absolute encoder ..	81
Figure 5.6: Layer-based actuator prototype	81
Figure 5.7: First prototype model position and speed test	82
Figure 5.8: Motor speed and current at different filter bandwidth	83

Figure 5.9: Test with a 420 g weight added to the shank link	83
Figure 5.10: Trajectory control by ODrive controller	84
Figure 5.11: Peak knee angular velocity	85
Figure 5.12: Actuator torque test schematic	85
Figure 5.13: Actuator torque test with electronic scale	86
Figure 5.14: Change in four-bar-linkage torque (peak current 6.90 A left and 5.77 A right)	87
Figure 5.15: Torque test at an angle close to 90°	87
Figure 5.16: Exposed follower link underneath the base plate and damaged absolute encoder...	88
Figure 5.17: From layer-based to inclined actuator	89
Figure 5.18: Key aspects of inclined actuator assembly	90
Figure 5.19: Middle and top layer with support bearing for shaft 2 Final Actuator prototype ...	91
Figure 5.20: Knee exoskeleton actuator with exoskeleton frame	92
Figure 5.21: First model test and new backplate to hold all control and power components.....	94
Figure 5.22: GPIO Digital Isolator and USB Isolator by Analog Devices	94
Figure 5.23: Description of Electrical connection of actuator	94
Figure 5.24: Knee exoskeleton on wearer during active test	95
Figure 5.25: Analog Sensor vs. Encoder position.....	95
Figure 5.26: Analog Sensor vs. Motor velocity	96
Figure 5.27: Analog Sensor vs. Motor Current.....	96
Figure 5.28: Angle sensor variation with change in analog input	99
Figure 8.1: Actuator electrical connection schematic	xii

List of Tables:

Table 2.1: Summary of the general properties of actuators	8
Table 2.2: Range of limits of motion of the hip, knee and ankle.....	10
Table 2.3: Summary of the torque requirements for different motions	17
Table 3.1: Numbered list of requirements for the knee exoskeleton	18
Table 3.2: Torque requirements based on 30% assistance	19
Table 3.3: Parameters for the technical requirements of the knee exoskeleton.....	19
Table 4.1: Summary and comparison of motor types	27
Table 4.2: Comparison of commercially available motors	28
Table 4.3: Comparison of commercially available motor controllers	29
Table 4.4: Coefficients of friction.....	36
Table 4.5: Moment of inertia of motor and pulley.....	38
Table 4.6: Coefficients for permissible belt power 1	40
Table 4.7: Coefficients for permissible belt power 2.....	41
Table 4.8: Frictional forces	45
Table 4.9: Estimated resultant forces and torques	46
Table 4.10: Backdrivable Torques	47
Table 4.11: Pulley positions, angles, and shaft loads	49

Table 4.12: Electrical part names and descriptions	64
Table 4.13: Circuit connections of electronic components.....	66
Table 5.1: Additive Manufacturing process and material.....	76
Table 5.2: Summary list of components used.....	77
Table 5.3: Current and torque measurement.....	87
Table 8.1: Detailed comparison on the research conducted on available actuators.....	x
Table 8.2: Detailed comparison between BLDC motors	xi

Appendix II - List of Abbreviations

Abbreviation	Description
EMG	Electromyography
BLDC	Brushless DC Motor
SEA	Series Elastic Actuator
PAM	Pneumatic Artificial Muscle
DoF / df	Degrees of Freedom
ACL	Anterior Cruciate Ligament
PCL	Posterior Cruciate Ligament
STS	Sit-to-Stand
IMU	Inertial Measurement Unit
FOC	Field Oriented Control
L _n	Link 'n'
FEA	Finite Element Analysis
LiPo	Lithium Polymer (battery)
UART	Universal Asynchronous Receiver -Transmitter
RX, TX	Receive, Transmit
SPI	Serial Peripheral Interface
CAN	Controller Area Network
SDIO	Secure Digital Input-Ouput
PID	Proportional-Integral-Derivative
IDE	Integrated Development Environment
PB	Push Button
SLS	Selective Laser Sintering
MJF	Material Jet Fusion
PA (PA 2200)	Polyamide
TPU	Thermoplastic Polyurethane

Appendix III - Detailed comparison of available actuating methods

Actuators	Details	Suitable for	Power-to-Weight Ratio	Advantages (+)	Disadvantages (-)
DC Motor	Series DC motors provide both high torques at set speeds. A harmonic drive can provide the required torque for an exoskeleton.	Upper, lower limbs, wrist motion assistance and rehabilitation. <i>Portable application.</i>	Good. Lower compared to hydraulic and SMA.	Easy variable positioning, load rating and speed control possible. Affordable and easy to setup.	Harmonic drives can be costly. Conventional gearing will increase the weight of the motor. Higher power consumption.
Linear mechanical actuator	Max. Force: upto 10 kN. Also provides lower forces of 70 N with great accuracy.	Wrist, hand and fingers motion assistance. <i>Portable application.</i>	Good	High accuracy in motion control, low inertia, reduced component count (simple build), relatively lightweight	Prone to wear for high-speed uses. Cannot be moved manually due to the inbuilt high reduction gear. (for a passive-mode in the exoskeleton)
Pneumatic	Max. σ : 0.5 – 0.9 MPa, E: $5 - 9 \times 10^{-4}$ GPa Equivalent to 50 – 90 N/cm ²	Upper limbs, lower limbs motion assistance and rehabilitation. <i>Tethered application.</i>	Low	Compliant since air is compressible. Safe and reliable.	Requires an onboard compressor, filter for continuous use. Air compressors decreases the power/weight ratio of pneumatic systems and are noisy. Difficult to achieve variable position accurately.
PAM	High tensile forces of up to 28 kN. (at 4 MPa) (for a 40mm diameter and 700 mm length PAM)	Upper limbs motion assistance and rehabilitation. <i>Tethered application.</i>	Good. Higher than conventional pneumatic cylinders and DC Motors	Lightweight, flexible, and compliant, non-linear control. Safe and not prone to damage.	Requires an onboard/tethered compressor or air tank.
Hydraulic	Max. σ : 20 - 70 MPa, E: 2 – 3 GPa Equivalent to 2 – 7 kN/cm ²	Lower limbs motion assistance and augmentation. <i>Tethered application.</i>	High	Operates over a larger range of speeds and has good response to position control	Requires an onboard pump and oil reservoir for continuous use, which lowers the power/weight ratio of the system. Noisy, leaks and low compliance.
SMA	Max. σ : 100 – 700 MPa, E: 30 – 90 GPa Equivalent to 10 – 70 kN/cm ²	Small displacements for upper, lower limbs. For medical rehabilitation. Wrist and hand exoskeleton <i>Portable application.</i>	Very High	Compact, lightweight, and fewer moving parts. Increases comfort due to its highly flexible geometry. Low operational voltage.	Only restricted to small displacements. Relatively lower operational speed and complex thermo-mechanical control required. Relatively expensive.
Cable driven	Dependent on the DC Motor used.	Upper, lower limbs and wrist. <i>Portable application.</i>	Good	Lightweight. Provides a stable system by placing motor at a base.	-

Twisted strings	Requires a low input torque from a DC Motor. Requires a load attached at the actuating end. This setup has been tested with a maximum load force of 31.5N. (Claims of tensile forces of up to 900N)	Upper limbs, wrist. Motion assistance and rehabilitation. <i>Portable application.</i>	High	Low cost and lightweight. Intrinsic compliance.	A complex mathematical model, which is highly dependent on the string type used. Continuous adjustment is necessary over long term use due to wear of the string.
SEA	Corresponds to the main actuator being used. The work done by the actuator changes. Usually, the torque does not have a set limit and varies with the spring constant.	Upper, lower limbs and wrist. For motion assistance and mostly rehabilitation. <i>Portable application.</i>	-	High compliance.	Additional construction and complex design. Has to be modelled properly. Can lead to added weight.
Human Muscle	Max. σ : 0.1 – 0.4 MPa, E: 5×10^{-3} – 2×10^{-2} GPa	-	-	-	-

Table 8.1: Detailed comparison on the research conducted on available actuators

Appendix IV - Comparison between different BLDC Motors

No.	Motor	Nominal Voltage	Speed Constant Kv	Torque Constant Kt	Peak Current	Winding resistance	Peak Power	No. of pole pairs	Weight	Dimensions	Price	Remark (+/-)
1	Maxon EC 90 Flat ^[1]	18 V	118 rpm/V	0.0807 Nm/A	183 A	0.0692 Ohms	260 W	11	985 g	90 mm dia x 39.9 mm	217 EUR	High lead time and requires Maxon controller
2	GARTT ML 8318 ^[2]	22.2 - 44.4 V	100 rpm/V	0.0955 Nm/A	62 A	0.226 Ohms	3000 W	21	635 g	92 mm dia x 38.3 mm	179 EUR	High power 'pancake' motor. High lead time and unconfirmed manufacturer
3	T-Motor P60 ^[3]	22.2 - 30 V	340 or 170 rpm/V	0.0308 Nm/A	65 A	0.035 Ohms	1550 W	14	347 g	69 mm dia x 36.5 mm	75 EUR	Compact moderate torque motor, low lead time. Low power loss.
4	T-Motor P80 III ^[4]	22.2 - 44.4 V	120 rpm/V	0.0795 Nm/A	70 A	0.041 Ohms	3600 W	21	635 g	91.6 mm dia x 43 mm	200 EUR	Compact high power motor, low lead time. Relatively low power loss.

Table 8.2: Detailed comparison between BLDC motors

Web-shop links:

[1] <https://www.maxongroup.com/maxon/view/product/500269>

[2] <https://de.aliexpress.com/item/32254102153.html>

[3] <https://www.premium-modellbau.de/t-motor-p60-340kv-multicopter-brushless-motor-6s-8s-379g>

[4] <https://www.premium-modellbau.de/t-motor-p80-iii-120kv-multicopter-brushless-motor-6s-12s-635g-ohne-pin>

Appendix V - Electrical Connection Schematic

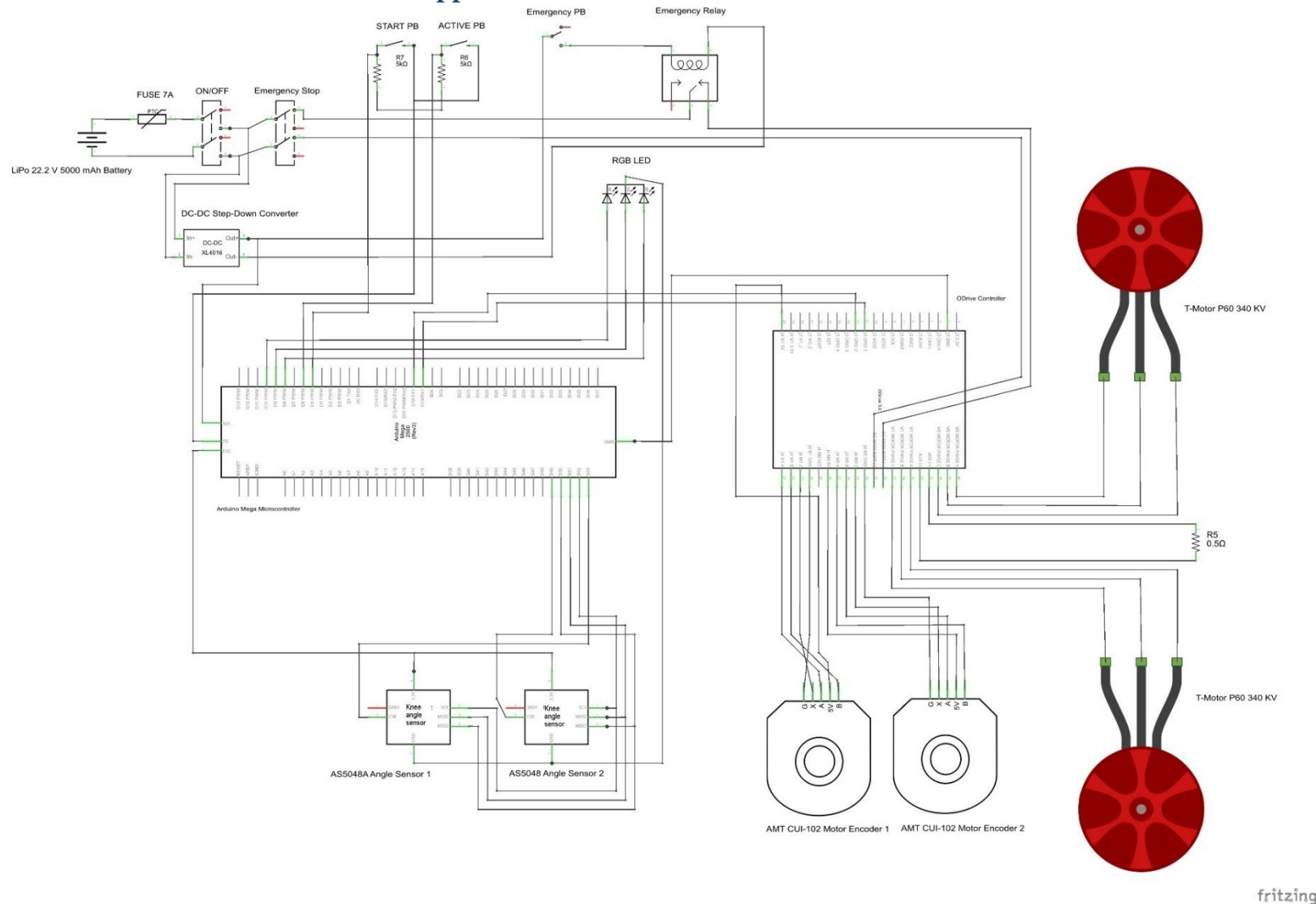


Figure 8.1: Actuator electrical connection schematic

Appendix VI - Exploded View of final prototype model

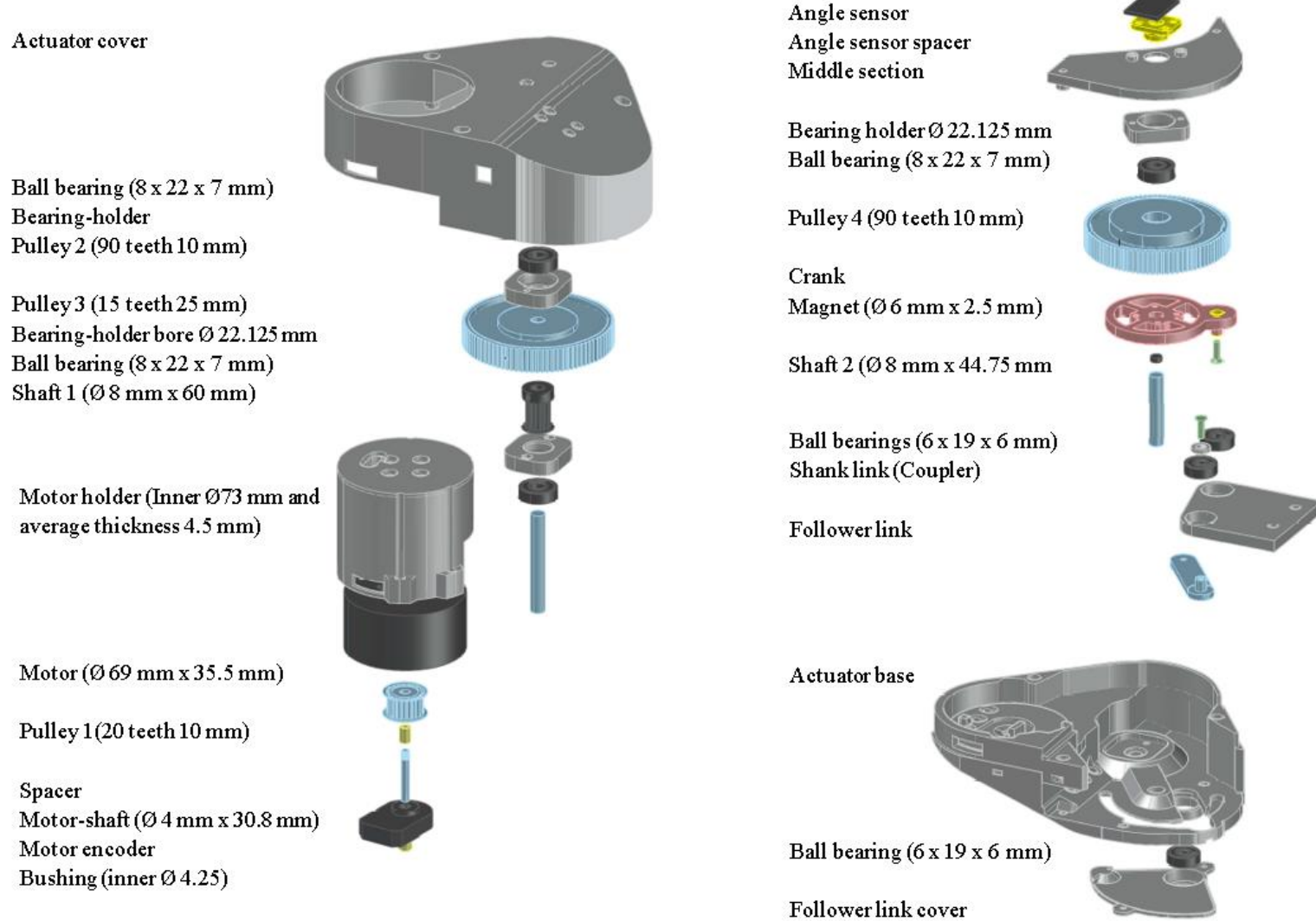


Figure 8.2: Exploded View of Final Prototype